

IB-RM-OP-2019-227

**Design of a low-cost sensor matrix
for use in human-machine
interactions on the basis of
myographic information**

Masterarbeit

Konrad Fründ



DLR

**Deutsches Zentrum
für Luft- und Raumfahrt**

MASTERARBEIT

DESIGN OF A LOW-COST SENSOR MATRIX FOR USE IN HUMAN-MACHINE INTERACTIONS ON THE BASIS OF MYOGRAPHIC INFORMATION

Freigabe:

Der Bearbeiter:

Unterschriften

Konrad Fründ



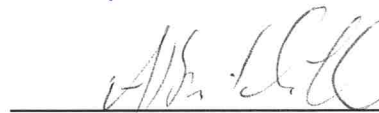
Betreuer:

Bernhard Vodermayr



Der Institutsdirektor

Prof. Alin Albu-Schäffer



Dieser Bericht enthält 149 Seiten, 72 Abbildungen und 5 Tabellen



JUSTUS-LIEBIG-UNIVERSITÄT GIESSEN

FB06 - PSYCHOLOGIE UND SPORTWISSENSCHAFT

INSTITUT FÜR SPORTWISSENSCHAFT

BIOMECHANICS - MOTOR SKILL - HUMAN MOTION ANALYSIS (MSc)

SUPERVISOR: PROFESSOR DR. HERMANN MÜLLER

Design of a low-cost sensor matrix for use in human-machine interactions on the basis of myographic information

MASTER-THESIS

Author:

KONRAD FRÜND

Supervisor DLR:

BERNHARD VODERMAYER

In cooperation with:

GERMAN AEROSPACE CENTER (DLR)

Institute of Robotics and Mechatronics

Münchener Straße 20

82234 Weßling - Oberpfaffenhofen

Submission Date: November 28, 2019

Studiengang: Biomechanik - Motorik-Bewegungsanalyse

Name: Konrad Fründ

Matrikel-Nr.: 2010693

Erklärung zur Abschlussarbeit (Thesis)

Ich erkläre hiermit, dass ich die Thesis selbständig verfasst und keine anderen als die angegebenen Hilfsmittel benutzt habe. Die Stellen der Arbeit, die anderen Werken im Wortlaut oder dem Sinn nach entnommen sind, sind durch Angaben und Quellen kenntlich gemacht. Dies gilt auch für Zeichnungen, Skizzen, bildliche Darstellungen und dergleichen.

Weiterhin erkläre ich, dass die Abschlussarbeit (Thesis) noch nicht im Rahmen einer staatlichen oder anderen Prüfung (z. B. als Magister-, Diplom- oder Staatsexamensarbeit) eingereicht wurde.

Mit der Überprüfung meiner Abschlussarbeit mittels einer Anti-Plagiatssoftware bin ich einverstanden und reiche die Abschlussarbeit auch in digitaler Form ein.

(Ort, Datum)

(eigenhändige Unterschrift)

Abstract

Myographic sensor matrices in the field of human-machine interfaces are often poorly developed and not pushing the limits in terms of a high spatial resolution. Many studies use sensor matrices as a tool to access myographic data for intention prediction algorithms regardless of the human anatomy and used sensor principles. The necessity for more sophisticated sensor matrices in the field of myographic human-machine interfaces is essential, and the community already called out for new sensor solutions. This work follows the neuromechanics of the human and designs customized sensor principles to acquire the occurring phenomena. Three low-cost sensor modalities (Electromyography, Mechanomyography, and Force Myography) were developed in a miniaturized size and tested in a pre-evaluation study. All three sensors comprise the characteristic myographic information of its modality. Based on the pre-evaluated sensors, a sensor matrix with 32 exchangeable and high-density sensor modules was designed. The sensor matrix can be applied around the human limbs and takes the human anatomy into account. A data transmission protocol was customized for interfacing the sensor matrix to the periphery with reduced wiring. The designed sensor matrix offers high-density and multimodal myographic information for the field of human-machine interfaces. Especially the fields of prosthetics and telepresence can benefit from the higher spatial resolution of the sensor matrix.

Contents

List of Abbreviations	IV
List of Figures	VIII
List of Tables	XIII
1 Introduction	1
2 Background	3
2.1 Human-Machine Interface	3
2.2 Motor Pathway	5
2.3 Target group and use case	6
2.4 Intention prediction	8
2.5 State of the Art	10
2.6 Conclusion	15
3 Objective	17
3.1 Design principles	18
4 Muscle architecture	21
4.1 Muscle physiology	21
4.2 Forearm anatomy	26
5 Myography	29
5.1 Electromyography	30
5.2 Force Myography	37
5.3 Mechanomyography	42
5.4 Tomography	48
5.5 Further techniques	49
5.6 Discussion	50

6	Sensors	51
6.1	Force Myography	51
6.2	Electromyography	57
6.3	Mechanomyography	65
6.4	Further sensors	68
6.5	Discussion	69
7	Sensor Pre-Evaluation	71
7.1	Standardized myographic protocol	71
7.2	Force Myography	72
7.3	Electromyography	77
7.4	Mechanomyography	81
7.5	Conclusion	83
8	Sensor module	85
8.1	Microcontroller	86
8.2	Components	86
8.3	Setups	87
8.4	Discussion	88
9	Sensor Matrix	91
9.1	Master Module	91
9.2	Data Transfer	92
9.3	Wristband/Bracelet	94
9.4	Discussion	96
10	Discussion	97
11	Conclusion/Outlook	103
	Appendix	XVII
	Bibliography	XX

List of Abbreviations

ADC	Analog-to-Digital Converter
API	Application Programming Interface
ATP	Adenosine Triphosphate
CPU	Central Processing Unit
CS	Chip Select
DAQ	Data Acquisition System
DC	Direct Current
DLR	Deutsches Zentrum für Luft- und Raumfahrt (German Aerospace Center)
DOF	Degree of Freedom
EEG	Electroencephalography
EMG	Electromyography
ESD	Electrostatic Discharge
FFT	Fast Fourier Transformation
FMG	Force Myography
FSR	Force Sensing Resistor
HMI	Human-Machine Interface
HVQFN	Heatsink Very-thin Quad Flat-pack No-leads
I ² C	Inter Integrated Circuit
IC	Integrated Circuit
IMU	Inertial Measurement Unit

MEMS	Microelectromechanical Systems
MISO	Master-In-Slave-Out
MMG	Mechanomyography
MOSI	Master-Out-Slave-In
MUAP	Motor Unit Action Potential
PCB	Printed Circuit Board
PSD	Power-Spectral Density
RMS	Root Mean Square
SCL	Serial Clock
SMD	Surface-Mounted Device
SPI	Serial Peripheral Interface
UART	Universal Asynchronous Receiver Transmitter
USB	Universal Serial Bus

List of Figures

2.1	Human-Machine Interface	3
2.2	Motor Pathway	5
2.3	Intention Prediction Software	10
2.4	Classification of Upper Limb Prostheses	11
2.5	Bielefeld Bracelet	12
2.6	Thalmic Labs - Myoband	13
2.7	CTRL-Labs - CTRL-Kit	13
2.8	Research Wristband: Otto Bock 13E200	14
2.9	Research Wristband: FSR based Force Myography	14
2.10	Research Wristband: EMG based from OT Bioelettronica	15
3.1	Thesis Workflow	17
4.1	Skeletal Muscle	22
4.2	Muscle Fiber: Single Twitch	22
4.3	Muscle Fiber: Rate Coding, Recruitment	23
4.4	Sarcomere	24
4.5	Wave Summation	24
4.6	Electromechanical Action Delay	25
4.7	Forearm Anatomy	26
4.8	Forearm Cross-Section	27
5.1	Electromyographic Phenomena	31
5.2	Electrode Shape to Fiber Distance	31
5.3	EMG: Amplitude, Power Spectral Density	33
5.4	EMG Sensor Setups	34
5.5	EMG: Difference Monopolar - Bipolar	35
5.6	Isovolumetric Muscle Behavior	38
5.7	FMG: Power Spectral Density	39
5.8	Comparison EMG versus FMG from [2]	41
5.9	MMG: Sensor Signal	43

5.10	MMG: Wave Summation	44
5.11	MMG: Amplitude and Frequency	45
5.12	MMG: Power Spectral Density	45
6.1	Force-Myographic Sensor Compilation	52
6.2	FMG: Weiss & Wörn Sensor Principle	52
6.3	Conductor Resistance	53
6.4	FMG: Weiss & Wörn Sensor Principle 2	53
6.5	FMG: Sensor Schematics	54
6.6	FMG: Designed Electrodes	55
6.7	FMG: Sensor Materials	56
6.8	Electromyographic Sensor Compilation	57
6.9	EMG: Noise	58
6.10	EMG: Circuit	59
6.11	EMG: Monopolar, Bipolar Amplifier	59
6.12	Electrical Filter	61
6.13	EMG: Inter-Electrode Distance Pick-Up Volume	62
6.14	EMG: Electrode Shapes/Types	62
6.15	Electromyographic electrode designs (bipolar)	63
6.16	Electromyographic electrode designs (monopolar)	64
6.17	Mechanomyographic Sensor Compilation	66
6.18	Principle of an Accelerometer	66
6.19	Functional Block Diagram Accelerometer	67
7.1	Standardized Myographic Setup	72
7.2	FMG-Setup	73
7.3	FMG-Results: Force Dependency	74
7.4	FMG-Setup Myography	75
7.5	FMG-Results: RMS Value	76
7.6	FMG-Results: 2nd Derivative PSD, RMS, mean Frequency	76
7.7	EMG-Setup	78
7.8	EMG-Results: RMS, median Frequency	79
7.9	EMG-Results: filtered Amplitude	79
7.10	EMG-Results: PSD	80
7.11	MMG-Setup	81
7.12	MMG-Results: PSD, RMS, mean Frequency	82
8.1	Sensor Module Components	87
8.2	Designed Sensor Modules	88
9.1	Standard SPI Protocol	92

9.2	Customized SPI Protocol	93
9.3	Sensor Matrix Forearm Cross-Section	94
9.4	Designed Sensor Matrix	95
9.5	Designed Sensor Matrix Mounting	95
10.1	Control Scheme - Electromechanical Delay	98
10.2	Compliant EMG Electrode	98
11.1	Functional Block Diagram AD8232	XVII

List of Tables

2.1	Transducers	4
3.1	Design Principles	19
5.1	Literature Review Myography	30
5.2	Tactile Sensors	40
10.1	Design Principles Status	100

1 Introduction

In our daily life, we face many situations where we interact with a variety of machines to manipulate our environment to reach our goal. The interactions between the user and the machine are diverse, like pushing the button of an electronic toothbrush compared to the concurrent and proportional control of a car. The electric toothbrush has an easy on-off switch, and the car has a proportional steering wheel, brake, and accelerator. Due to the high amount of various interactions, the research field of human-machine interfaces has a crucial role in our digital era to simplify our daily life. Current human-machine interfaces are limited in their control, and demand the end effectors to manipulate buttons, wheels, or similar mechanical transducer. Some interfaces use binary signals, which makes them inaccurate in many tasks, due to its non-proportional output. These limitations demonstrate that there is a need to understand the human's intention further. It can be proposed that with obtaining the user's intention before he manipulates the environment, a higher output can be achieved. The emerging market of human-machine interfaces and especially interfaces based on biological signals, was proved with Facebook's (Menlo Park, CA, USA) acquisition of CTR-Labs (New York, NY, USA) in September 2019 for a non-confirmed price of 500 million to 1 billion US\$ [1].

The Institute of Robotics and Mechatronics from the German Aerospace Center researches in this field to provide new interfaces to achieve a more dexterous control for robots. The research is closely linked to the adaptive bio-interface research group but conducted in the group of terrestrial robotic assistance. Based on an earlier research collaboration with Prof. Dr. Risto Kõivas team, a force myographic sensor matrix (wristband) was developed, which produced promising results [2, 3]. However, the wristband has some drawbacks, which should be solved. The modules of the wristbands were used in multimodal sensor approaches, but the sensor modalities were locally separated from each other, which made it difficult to compare their effectiveness. Thus, a sensor matrix should be designed, which provides a higher spatial resolution of multiple myographic modalities and solve the later discussed drawbacks of the current system.

This thesis strongly focuses on the underlying basics and provides neuromechanical insight into possible myographic modalities and their origins and phenomena. The design process is iterative from chapter to chapter and uses decisions and principles from earlier chapters to base the decisions on solid ground. The main focus is on myographic solutions and the used

sensors to obtain these.

The work is structured into ten chapters and shows the developing objectives of this work. The background provides insight into the field of human-machine interfaces, shortly introduces the origin of intentions and sets requirements for the design process of the work, based on the target group and used intention prediction method. The chapter explains why human-machine interfaces on the basis of myographic information are nowadays superior. The objective and design principles are stated in chapter 3, and the following work refers back to these. The bigger picture of the muscle physiology and architecture at the sample recording site of the human forearm is explained to derive myographic sensor principles. Literature research was conducted to introduce possible myographic solutions and to pick the most promising modalities for a low cost and high-density sensor matrix. The sensor solutions are introduced in chapter 6, and a small pre-evaluation was conducted in chapter 7 to proof the concept of the designed sensors. Chapter 8 merges the sensor modalities to a sensor module and treats the necessary electronic components for data acquisition. Finally, chapter 9 designs a sensor matrix on the basis of the myographic information of the sensor modules. Drawbacks of the current system are discussed and solutions proposed. Chapter 10 gives an overview of the covered topics, and decisions are interpreted.

2 Background

2.1 Human-Machine Interface

The interface between a human and a machine should expand human capabilities. The system behind a HMI contains all necessary components to exchange information, as shown in figure 2.1. The data flow is bidirectional to enable the user to control the machine and receive its feedback. Human factors research states that the human output consists of intentional and non-intentional signals, where non-intentional behavior is a type of human error [4]. Non-intentional components of the signal are treated as noise and should be suppressed, while intentional signals are required for distinct actions.

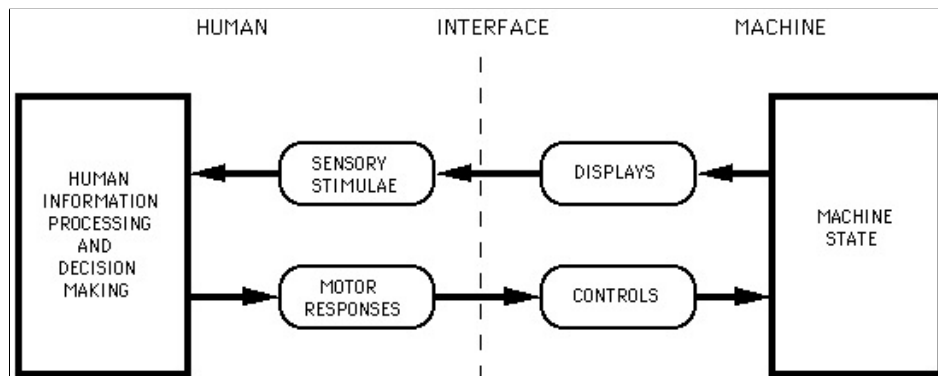


Figure 2.1: Components of a Human-Machine Interface by MacKenzie (1995) [5]

Intentional signals are classified into biological signals and non-biological signals or implicit and explicit intention [6, 7]. Non-biological signals are recorded with an external tool like a mouse, keyboard, or switch. Biological signals represent physiological time-series data, which mostly result in non-biological signals [8]. E.g., the intention to manipulate a switch can be recorded as a biological signal in between the brain and the end-effector movement or at the manipulated switch.

Biological signals are divided into the six general transducer types from table 2.1 [9]. These approaches represent the bigger picture to detect biological signals of the body and are applied to myographic signal acquisition approaches in chapter 5.

Table 2.1: General transduction principles from [9]

Transducer	Example
Bio-acoustic	Respiration rate
Bio-chemical	Calcium inflow / pH distribution
Bio-electric	Electromyography
Bio-mechanical	Oscillations (kinematic), force (kinetic)
Bio-optical	Videometry
Bio-thermal	Thermal radiation

Humans utilize human-machine interfaces several times a day, and a life without them seems impossible for the majority. They play a key role in factories and offices. In medical applications, human-machine interfaces are called assistive systems. Impaired patients can operate these systems to reduce their impairment and increase their autonomy. Tetraplegia patients can control wheelchairs or robotic arms by thought [10, 11, 12, 13]. Amputees can control their prosthesis by using motor patterns in their brain, which result in a myographic activity. However, without feedback, the control of a prosthesis does not lead to an embodiment. Thus, bidirectional feedback was restored by transcutaneous or invasive nerve stimulation [14, 15, 16]. Antfolk et al. (2013) summarized approaches to close the loop between action and perception to achieve the embodiment of bidirectional systems [17].

Controlling a human-machine interface can be achieved by already existing or, due to brain plasticity, new brain activation patterns. The advantage of present patterns is apparent, but to achieve a high dimensional dexterous control, it requires more input signals for the interface. To restore or mirror a physiological capability, it is helpful to record a higher density of multi-modal signals and fuse them to detect the intention of the user. Thomas Reardon, the co-founder of CTRL-Lab (New York, NY, USA), introduced his talk in 2019 about human-machine interfaces with the inability of the human to manipulate the environment at a greater extent [18]. Reardon further mentioned, that their system could potentially increase the human throughput by the factor 3-4 with the detected muscle signals [18].

In summary, the optimal human-machine interface uses multi-modal sensors to detect pure intentional biological signals, which are present patterns in the brain. The control should be intuitive and reproducible if the user needs to create new brain patterns. Furthermore, human-machine interfaces should provide sensory functions to lead to the embodiment of the system.

2.2 Motor Pathway

Supplemental information about the origin of intentions and how they are processed are helpful to deduce interfacing possibilities and argue about useful methods to obtain these. This section introduces the general motor pathway of the central nervous system. Figure 2.2 depicts the motor pathway and splits it into upper and lower motor neurons. Starting from brain activities in the motor cortex the signal propagates through the spinal cord and the motor nerves to the motor end-plate of the muscle.

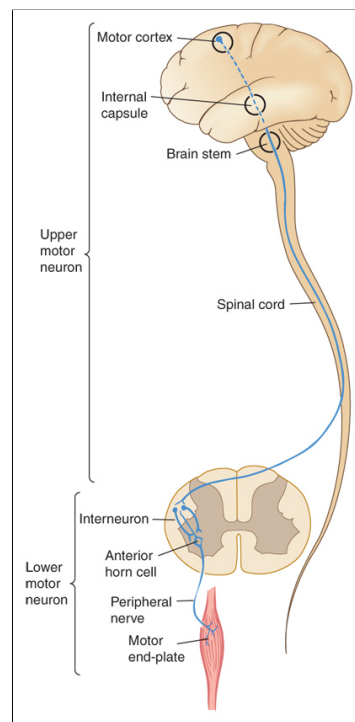


Figure 2.2: The simplified human motor pathway - From brain activities to evoked potentials at the motor end-plate by Waxmann (2016) [19]

Based on the sensory input, the human perceives his environment and fulfills voluntary actions to achieve his desired goal. The action/plan to achieve the goal is called intention. Unintentional actions are involuntary contractions like reflexes. Furthermore, unintentional actions appear due to sensory and motor noise, which is essential for motor learning but results in noisy signals [20, 21, 22]. At the neuronal level, the sensory input neurons in the cortex are activated due to the afferent signals of the biological transducers, e.g., retina, skin receptors, and others. In simplified terms, the primary stage of the associated cortex of the sensory signal transmits their activity to higher areas where information from several inputs is merged. Information in the brain is transmitted by electrochemical processes, i.e., a neurotransmitter or electrical potentials which "activate" the coupled neuron. Messages, in the form of activation,

travel from neuron to neuron. The neuron can excite or inhibit the postsynaptic potential. Hence, active neurons in higher brain areas are a result of well-facilitated neural pathways which passed the activation from lower brain areas. The way the activation in neurons work is an all-in-or-nothing reaction called "action potential", or colloquially "spike".

Neurons in the motor cortex are primarily used for motor activities by transmitting signals to the motoneurons, which innervate the muscles. A specific pattern of active motor neurons fulfills the linked intentional movement [23]. The active neurons in the pattern send their motor signals through the neural pathway in the spinal cord to the lower motor neurons.

The spinal cord is part of the central nervous system and covers and protects the neural pathway with the surrounding vertebral column. It contains motor neurons that transfer signals through the peripheral nervous system to the muscles. Motor neurons are clustered in muscle-specific motor pools in the motor anterior horn cell in the spinal cord [24, 25]. In addition to the activation from brain signals, the motor pool can also be activated unintentionally, e.g., from spinal reflexes, interneurons, or higher-order inputs. A motoneuron connects to several muscle fibers. Depending on the aimed dexterity and strength of the movement, motor neurons with a higher or lower number of muscle fibers are activated [26]. Muscle physiology is further explained in chapter 4.

The axons of the motor neuron leave the vertebral column at a junction close to the muscle. The action potential channels in a nerve towards the intended muscle, innervate its muscle fibers and cause them to contract. The compound of a motor neuron and its muscle fibers is called a motor unit. The contraction leads to a shortening of the muscle and pulls on the tendon, which is coupled in series. The tendon's origin on the bone has a distance to the joint; thus a muscle contraction results in torque around the joint.

The motor pathway offers a broad spectrum of possibilities to derive the intention of the user. The intention detection is more accessible at a distal occasion of the motor pathway, due to a higher spatial resolution and less cross-talk. Nevertheless, the temporal latency suffers from distal signals, especially at the neuromuscular junction, where the motor unit action potential (MUAP) is transduced into kinetic actions.

2.3 Target group and use case

The target group of this thesis are persons operating complex machines with a high degree of freedom. Possible applications are aerospace missions, rescue missions in harsh environments, or rehabilitation. It can be used in teleoperations and telepresence mode. However, human-machine interfaces (HMI) are suitable for everyone and can be applied with a variety of biological and non-biological signals. Current research regards, among other gaming, entertainment, and medicine. The fewer degrees of freedom, or the more generalized the task,

the less complex the interface needs to be. The dexterity of the movement or task directly correlates to the degrees of freedom the interface can simultaneously control.

A use case is the reduction of the impact of radiation on astronauts, caused by the number of extra-vehicular activity. Research was made in space missions using a game controller or complex sequential and proportional interfaces to control a robot arm to be able to manipulate the extra-vehicular environment [27, 28]. Furthermore, research was conducted in solving these tasks in advance and using these patterns to solve the task in space [29]. However, both systems are limited in their input and lack dexterity and complexity, which makes them fragile in case of errors and new situations. Using a HMI in harsh environments requires a high degree of freedom, which is similar to space missions, except for the aeronautic constraints. The application in rescue missions, e.g., in unstable houses, decreases the risk of accidents with humans. While the application in space needs a highly dexterous system to decrease the risk of unintentional errors, the application in rescue missions focuses on unexpected situations, which were never trained by the system. Applications of a HMI for entertainment and gaming early emerged with computers. Taken together, most of the current HMI are based on switches or other mechanical, non-biological signals.

Research in medicine and rehabilitation seems like an exception to this trend. This field aims to develop systems that demand less cognitive load and extend or restore human capabilities. There is one major constraint in acquiring signals from these fields: the users are mostly limited in their capabilities due to accidents or diseases. Thus recording bio-signals at the forearm is not always possible, or the muscle architecture in between the users is different. Nevertheless, the field of amputees is a major target group of this thesis and give insight about acceptance and necessary design principles for this work.

Assistive devices are classified in standard ISO 9999:2016. Ribeiro et al. (2019) distinguish between active and passive interfaces [30]. Passive devices for upper-limb prosthesis are yet better in everyday tasks, shown at the Cybathlon 2016 in the ARM Challenge. However, active prostheses are the future due to the possible control of a high degree of freedom. Biddiss & Chau discovered that 80% of users with upper-limb absence use a prosthesis [31]. Approximately 33% of these amputees use passive prosthesis [32] and 30% – 50% use myoelectric prosthesis [33, 34]. A survey from Engdahl et al. compared the interest of the community in four complex biosignal acquisition techniques [35]. Non-invasive myoelectric control was interesting for 83%. The invasive techniques of targeted muscle reinnervation, peripheral nerve interfaces, and cortical interfaces were less interesting for the community, due to the surgical risks. Non-invasive concerns were weight, cost, durability, and difficulty of use. Most of the studies use myoelectric approaches in their surveys. Nowadays, hybrid approaches with multi-modal sensors are seen as a key for better data capturing [36, 37, 38]. Other concerns about myoelectric prosthesis are the lack of dexterity, poor reliability and long reaction times [31, 39].

This target group splits up into two fields. The first field is using the sensor matrix as a tool to manipulate machines to avoid dangerous situations. Currently, most of the human-machine interfaces in the first field base on non-biologic signals. The second field consists of disabled persons who want to restore lost motor functions. The field of amputees provides valuable information about the necessary design principles to satisfy the user experience.

2.4 Intention prediction

Knowledge about intention prediction algorithms guarantees a better conceptualization of the sensors for HMIs. As introduced in section 2.2, myographic signals lead to the original intention of the user. Digital signal processing techniques, which mind neuromechanical principles, create features for Machine Learning or biomechanical models. A deep learning approach is fully independent of any digital signal processing and uses raw data.

The goal strategies of a HMI control task are proportional and simultaneous control [37, 36]. Proportional control ensures fine and precise movements, e.g., with a regression. Simultaneous control is the ability to perform two movements together, e.g., supination and flexion. There are two main approaches to compute the intention. The first approach follows the biological pathway and simulates it using biomechanic models. The second approach trains a machine learning algorithm for classification or regression. Classification models are less precise than regression models, due to the instability in between two classes. Regression models change their state in smaller steps and are more dexterous but lack accuracy with a bigger pool of gestures. Due to the rapid change in technology, the applied technique in control tasks shifted from model-based approaches to machine learning algorithms. Nevertheless, the model-based approach is still used in research to acquire more detailed data. Nowadays, Deep Learning techniques are pushing into the field, but they require a large dataset and generalization are critical due to different sensor data at each user.

Model-based

The model-based signal processing approach bases on neuromechanical knowledge about the underlying tissue and muscles. High-quality data is necessary for a model-based approach simulation. Due to the complexity of the musculoskeletal system, the model needs parameters like the joint angle to consider the force-length relationship. The higher the desired accuracy, the more complex the model. In a model-based approach, the obtained signal is assigned to a specific muscle. A high dexterity can be achieved with high-quality muscle recordings. Famous biomechanical models to determine the muscle force are the simple Hill-Model and Huxley-Model [40, 41]. Biological information of the distance from the tendon to the joint is preset, based on scientific data, to calculate the torque. Torques are mainly used to describe movements of bodies, e.g., in robotics [42]. The dynamic of the movement can be calculated

with sensing all occurring torques.

Closely related to the mechanical calculations, an imaging electromyographic approach from Urbanek (2016) uses cross talk to decompose the activation from deeper muscles [43]. Similar to this, De Luca et al. (2014) and the start-up CTRL-Lab are using a motor unit decomposition based on biomechanical properties of the motor unit action potentials (MUAP) to enhance the accuracy of their model [44, 45]. Decomposing electromyographic signals is done by the extraction of the neural code with motor unit spike trains and applying a machine learning blind source separation algorithm [46]. Based on the decomposed intramuscular coordination, a forward model can be used with the obtained high quality and specific muscle activation.

Machine learning

Machine Learning or artificial intelligence is a trending term for applying statistical methods, which predict an outcome based on a trained/learned model. Rather than one-dimensional amplitude-based control approaches, it uses features for pattern recognition or a complex net to predict the intention. Bonnin (2017) divides machine learning into reinforced, super- and unsupervised learning algorithms [47]. Supervised learning algorithms need label data to train their model, while unsupervised learning algorithms can use the raw data. Reinforced learning adapts its model based on non-labeled data. Unsupervised learning approaches need a large amount of data until they outperform supervised algorithms [48, 49]. However, research in the trending field also covers myographic activation; thus a flood of papers are published with a variety of new approaches and models.

The most common supervised models predict gestures based on classes or with a regression. Each model has its advantages and disadvantages in the application of upper limb prosthesis. Regressions satisfy the proportional control paradigm but are limited in their amount of classes. Classifiers are capable of distinguishing between many classes but need subclasses to increase dexterity. Each approach has a variety of basic statistical methods. Prominent classify algorithms are linear discriminant analysis, support vector machine, and k nearest neighbor [50]. Prominent regressions are Ridge Regressions based on random Fourier features or Gaussian process regression [51, 52].

Figure 2.3 shows an amplitude pattern of a power grasp gesture; based on these and other features, the current signal processing and software computes the predicted intention of the user with pattern recognition based on a Ridge Regression with random Fourier Features. It can be seen that the most prominent pattern is the power grasp, while the smaller and less colorful index finger pattern is less activated. The gray hand is used to train the patterns, and the colored hand is the prediction after training. The polar plot is divided into 8 slices, and the sensor data is plotted with a step width of 45° .

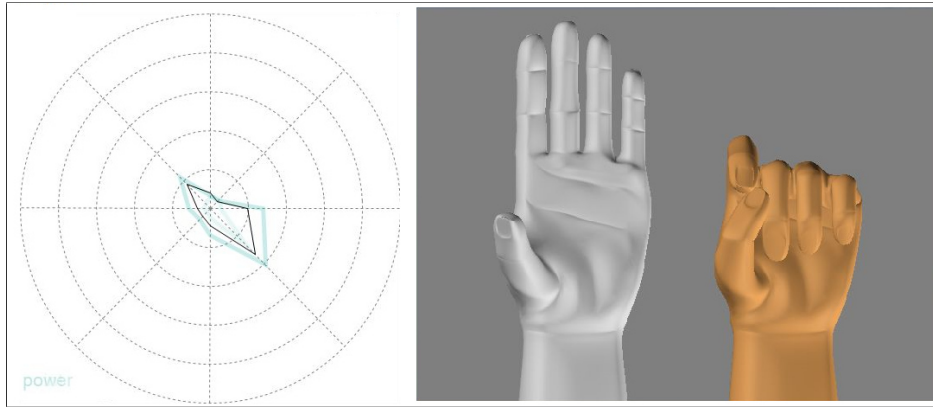


Figure 2.3: Snapshot from the intention prediction software with three trained patterns (rest, power, index) and the current pattern (black) in a polar plot with 8 electrode amplitudes. Used sensor matrix: Thalmic Lab - Myoband

In contrast to biomechanic model-based approaches, machine learning approaches do not require specific and high-quality information about the recording site. The more information the system acquires, the more patterns the machine learning approach possibly detects. Nevertheless, when applying machine learning, it is essential to check the system for overfitting and redundancies. High-density approaches are trending in the research of electromyographic control interfaces, because of their amount of information [53, 54]. Furthermore, a high-density approach is independent of the rotational alignment of the sensor due to the re-calibration at the beginning. Further information about machine learning applications in upper-limb prostheses are available in the review paper of Scheme et al. [55].

In summary, promising results were obtained with machine learning algorithms with features based on biomechanical knowledge. Deep neural networks are trending in research, but are not yet ready for application in human-machine interfaces. The decomposing algorithm based on blind separation is the most exciting approach, but the applicability depends on the training period to detect single motor units. A biomechanical model is challenging and not suited for a human-machine interface. However, the design of this work is focusing on optimal data for a pattern recognition based intention prediction, and decisions could have been different, considering other approaches.

2.5 State of the Art

This section introduces the current commercially available state-of-the-art and cutting-the-edge research of myographic sensor matrices, which are used as human-machine interfaces. The general classification will be shown, and current solutions, which compete against the future wristband will be quantified. Figure 2.4 classifies upper limb control devices concerning their

intent interpretation, activation profile, and preprocessing. Simultaneous and proportional control was already introduced in chapter 2.4. The multimodal preprocessing approach adds a third dimension to the general classification of an optimal interface of Fougner et al. (2012) [56]. Since the paper was published in 2012, the field developed new modalities and aimed for a higher dexterity.

In contradiction to the other parameters, the commercially available state of the art in intent interpretation changed with the company coaptengineering, which provides a classification algorithm based on myographic features. The activation profile of commercially available upper limb prostheses remained at the level of binary control. Multimodal preprocessing approaches are still limited to additional sensors like inertial measurement units and lack different myographic modalities. However, research went further by exploring the fields with new data processing algorithms and sensor solutions. Current myographic solutions will be further examined in chapter 5.

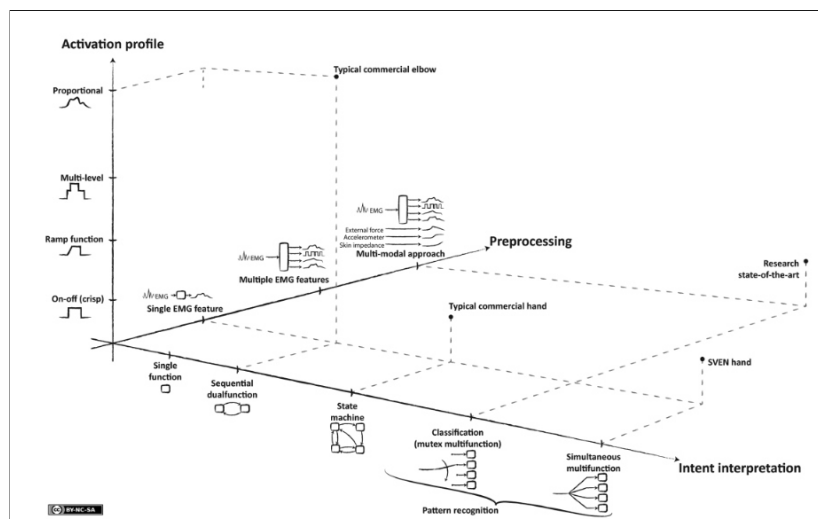


Figure 2.4: Classification of upper limb prostheses based on three parameters by [56]

Many research groups in the field are using existing myographic sensors and place them in a wristband to use it as a sensor matrix. Most of the sensor matrices use single myographic features, lack spatial resolution, and one gets the impression that they were built without the knowledge about the determining parameters and resulting information. They may aim for an easy solution to acquire data to apply machine-learning algorithms but ignoring the neuromechanics of the human. In the upcoming sections, the most promising custom-build sensor matrices are introduced, which influenced the design principles and used sensor modalities of this work.

Bielefeld Bracelet

The so-called Bielefeld bracelet, shown in figure 2.5, is a research project and not commercially available. It was developed by Prof. Dr. Risto Kõiva's team at the center of excellence - cognitive interaction technology (CITEC) in Bielefeld and published in a paper in 2015 [57]. The bracelet uses a force sensing approach to measure myographic signals, which is explained in chapter 5. Up to 12 sensor modules are placed at the circumference of the wristband. Each module contains 4 x 8 "M" shaped electrodes in a 5 mm grid. The temporal resolution is 88 frames per second while converting analog signals into 12 bit values. The research states promising results, with applications in smaller studies [2, 3]. Results showed that the bracelet is capable of providing further information when used with EMG, and could potentially outperform EMG [58].

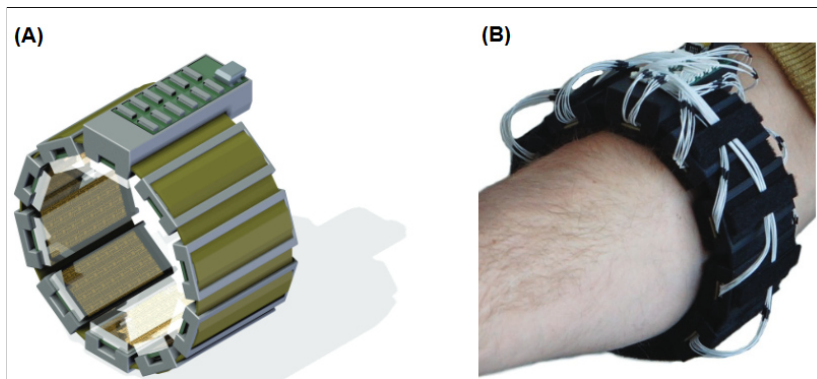


Figure 2.5: (A) Sketch of the Bielefeld Bracelet (B) Applied on the forearm from Kõiva et al. [57]

Myoband from Thalmic Labs

The Myoband from Thalmic Labs (Canada, Ontario) was launched in 2013 and was the first fully developed commercially available wristband for human-machine interactions based on EMG and an IMU (see figure 2.6). It is widely used in research, even if the company stopped the distribution in 2018 [59, 60, 61, 62]. The price was 199\$ [63]. The Myoband uses eight sensor modules with three EMG electrodes. Each module obtains one differential EMG signal [64]. Furthermore, one board contains a 9 DOF IMU [65]. The wristband transfers the signal via Bluetooth with a sampling rate of 200 Hz and a resolution of 8 bit [66]. The intended business case was to provide a wristband that controls music and other entertainment devices by gesture control. Their patents show that they worked on a multimodal approach, e.g., with a mechanomyographic sensor [67]. The Myoband became famous because of its easy-to-use application, its wireless data acquisition, its included battery, and a well-documented API.



Figure 2.6: Thalmic Lab - Myoband bracelet with 8 sensor modules [68]

CTRL-Kit from CTRL-Lab

The CTRL-Kit of the New York start-up company CTRL Lab adapted the approach of Thalmic Labs and continued the development of an EMG-based wristband for the human intention detection. The patents from Thalmic Labs were bought in June 2019. CTRL-Lab was acquired from Facebook Inc. (Menlo Park, CA, USA) for a sum in between \$500 million and \$1 billion US\$ in September 2019 [1]. Details about the wristband are available in conference talks, articles, and on their website [69]. As shown in figure 2.7, the idea of CTRL-Lab is to use high-density EMG signals, with 16 modules, to get a more considerable amount of features for their machine learning algorithm. According to an article from Douglas Fields (2018), CTRL-Lab aims to decompose the EMG-Signal [45]. The EMG sensors seem to use a single differential amplification and are compliant with contact pressure. It is not evident whether they use single or double differential recordings (see chapter 5.1). According to their patents, the setup contains one or more inertial measurement units [70]. Regarding the hardware, advantages of the CTRL-Kit compared to the Myoband, are the higher spatial resolution and compliant electrodes, which are more comfortable to wear. CTRL-Lab aims for the consumer/entertainment market.



Figure 2.7: CTRL-Kit with up to 16 sensor modules by CTRL-Labs[71]

Further Research Wristbands / Related Work

Ravindra et al. (2014) compare three non-invasive human-machine interfaces for the disabled [72]. They use a force-myographic, an electromyographic, and an ultrasonic approach, all shaped to be applied on the human forearm. The electromyographic approach uses the Otto-Bock 13E200 electrodes (Duderstadt, Germany), as shown in figure 2.8, in a wristband setup. This setup was originally built with a lower spatial resolution from Castellini et al. in 2009 [73].

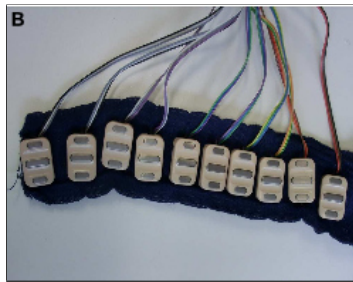


Figure 2.8: Otto Bock 13E200 sEMG setup by Ravindra (2014) [72]

Connan et al. (2016) adapted this approach and added force sensing resistors to the setup to record signals with a multimodal setup [2]. Cho et al. (2016) developed a plain FSR setup, shown in figure 2.9, to prove the feasibility of the force myographic approach to control upper extremity prostheses [74].



Figure 2.9: Force Myographic Wristband by Cho et al. (2016) [74]

The company OT Bioelettronica SRL (Torino, Italy) builds EMG setups upon a request. The German Aerospace Center ordered the sensor shown in figure 2.10. This sensor is capable of measuring monopolar and bipolar signals and has a remote reference electrode. Furthermore, it has an in-built AC (500 Hz) and DC impedance check. The resolution is 24 bit with a high-performance biopotential amplifier ADS1298 (Texas Instruments Incorporated., Dallas, Texas, USA). Furthermore, the chip has a lead-off detection and a programmable gain amplifier.

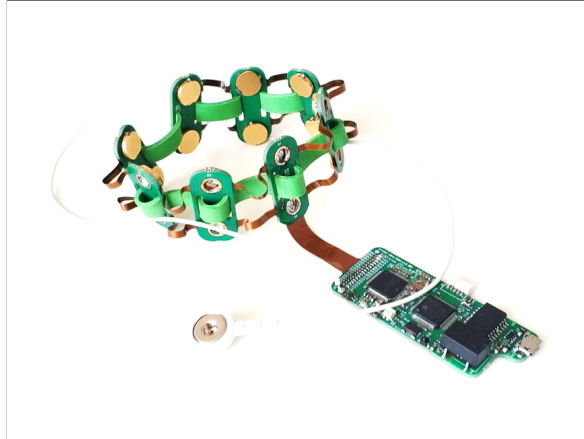


Figure 2.10: Bioelletronica Electromyographic sensor with 8 modules

Acquiring data of everyday tasks, the limb is moving in the peripersonal space, and actions are required at different postures. Due to gravity, the muscles need to exert more or less force at different limb positions to accomplish the intentional gesture. The so-called limb-position effect influences the predictions negatively. Fougner et al. (2011) resolved the limb position effect with accelerometers on the arm [37]. They were able to decrease the average classification error from 18 % to 5.0 % [37]. Krasoualis et al. (2017) added an IMU to the setup to add information to their electromyographic signals and increased the accuracy of an upper limb control task as well [75].

In conclusion, since the rejection of Thalmic Labs Myoband, no competitor is on the market of myographic wristbands. However, extensive research was conducted into myographic control for upper limb prosthetic control. Some problems are already solved, and researchers are working on a proportional and simultaneous intention prediction. Occasionally there is just one paper from mid-2019 trying to implement a full span of myographic sensors together in a sensor matrix filling the gap since Thalmic Labs rejection and Facebook's acquisition of CTRL-Lab [76]. However, none of these wristbands provide a high spatial resolution concerning the human's forearm complexity.

2.6 Conclusion

The background and constraints of the design of a human-machine interface show that human-machine interfaces on the basis of biologic signals are superior in terms of a low temporal latency. Aiming for a perfect interface, the goal of an embodiment can be achieved with sensory feedback. Stepping down the motor pathway demonstrates that the signal of myographic sensors is directly linked to the intention of the brain. The periphery acts like a signal amplifier and decomplex the signal due to reduced cross-talk from different signals. Depending on the

target group, the human-machine interface has limitations in its application and objective. Taking the target groups and problems from current sensors into account, this thesis aims for a high spatial resolution to either fulfill the high robustness for amputees and the high dexterity for teleoperations in harsh environments. The possible intention prediction algorithms impact the design decision. While model-based approaches desperately need high-quality signals and further information about biological parameters, machine learning algorithms use the input features and create a model based on its settings. This thesis aims to be used with the introduced myocontrol software in figure 2.3. Quadruple as much input parameters could benefit a pattern recognition algorithm and thus improve the accuracy and robustness. Nevertheless, the created features for machine learning should be based on neuromechanical phenomena. Consequently, this thesis has the aspiration to design a human-machine interface and further offer the signal composition of the provided signals. Despite the consensus in research that the objectives in the field should not just focus on new and better intention prediction algorithms, a full span of myographic signals in one sensor matrix was not designed to the current date and is still an open field in research. The increased density of local information could potentially benefit the prediction with a broader spectrum of non-redundant muscle parameters. The system to be developed should take these general notes into account.

3 Objective

The general idea, why the design of a low-cost sensor matrix for use in human-machine interactions on the basis of myographic control is promising, was given in the first chapter. The approaches from other research teams influenced the workflow, first to understand the processes in the muscle and then design the sensor matrix step by step. The workflow is presented in figure 3.1. The design process of myographic sensors highly benefits from the knowledge about the muscle basics. In total, this thesis aims to prove the concept of the used sensors and provides a concept for building a sensor matrix.

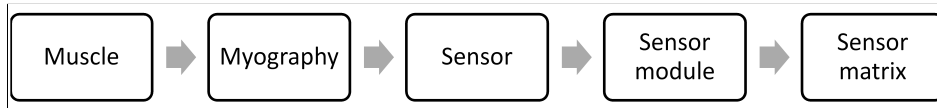


Figure 3.1: Work flow of the design process for the myographic sensor matrix

Concluding the knowledge of the first chapter, the development of a muscle-machine interface is most promising in terms of a low temporal latency and less complexity. The human has more than 600 skeletal muscles from which we can potentially record the activation [77]. The use of specific muscles, which are less relevant for most of the daily activities, would give the user the possibility to use them to control machines. To achieve this, the user needs to learn new patterns that are not intuitive but possible due to brain plasticity [78, 79]. The logical solution is to use end-effector muscles, which limits multitasking, but enables a dexterous control, e.g., mirroring the intended movement to a robotic arm. Thus, the sensor matrix should be applicable to the human limbs.

The hand is an essential end-effector of the human, and most of our environmental manipulations are fulfilled with it. We use the hand for accurate and subtle movements as well as for strong and large movements. To be able to achieve the desired dexterity, the hand and wrist consist of 27 bones and 45 muscles with at least 23 degrees of freedom at the joints [80]. Therefore, the research about upper limb myocontrol is more prominent in research, and this work follows this idea. However, the sensor matrix should also fit other limb regions and limb diameters without decreasing the spatial resolution.

In human-machine interactions, it is essential to provide real-time feedback to the user re-

garding his input. Time delays lead to rejections and keep the user unsure if the machine understands the user's intention (see 2.3). A delay of more than 300 *ms* was noted as crucial [81]. Farrell et al. (2007) stated the currently acceptable controller delay in between 100 – 175 *ms* and a delay smaller than 100 *ms* as their goal [82]. Linking to electroencephalographic measurements and their event-related potentials can show the satisfaction of the user [83]. The general norms for ergonomics in human-computer interfaces are listed in ISO 9241. The user experience is stated in ISO 9241-11 and has three main guiding criteria: effectiveness, efficiency, and satisfaction. Thus, a design process needs to consider functional as well as nonfunctional constraints in the development. The main scope includes medical purposes as well as the application as a control instrument in future aerospace missions. In both cases, the robustness is crucial for the success [84].

The thesis introduces myographic principles and establishes possible features for a digital signal processing algorithm, which is not included in the thesis. The sensor matrix output will consist of raw signals, which can be processed into the time domain, spike, and amplitude parameters. This work merges all promising measurement techniques to provide more and better features for the intention detection concerning the design principles of the following section. The sensors are optimized for a machine learning approach, and the design would change if aiming for a deep learning algorithm.

The ultimate goal for human-machine interfaces is to achieve the embodiment of the system. This requires a more complex system, which can not be covered in this thesis. The thesis solely aims to provide raw data for human intention prediction software. Nevertheless, the system could be used in a more advanced system with an actuator and a separate feedback device.

3.1 Design principles

The design principles are guiding through the development cycle of the sensor matrix. Decisions in this work are always related to these design principles. At some point, decisions are further explained regarding the proposed principles.

Table 3.1: Design principles of the sensor matrix sorted by relevance and collected from [85, 58, 81, 84, 37, 38]

Nr.	Design principle	Explanation
1	medical technology laws	ISO 13485
2	non-invasive	non harming sensors
3	robustness	high accuracy in different environments
4	temporal resolution	record the specific frequency domain
5	spatial resolution	distinguish small muscle activations
6	delay/latency	shorter than 200 <i>ms</i>
7	low cost	cheaper than current solutions
8	modular	exchangeable modules
9	compact	minimal size and weight
10	free positioning	no fixed application
11	safety	non harming
12	intuitive	ease of use
13	mobile	free to move in space
14	wearability	use as an amputee with one hand
15	durability	durable in everyday use
16	feedback	embodiment / closed loop
17	comfort	materials
18	calibration	in-built calibration
19	in-built power	no power cable
20	wireless	data transfer without cable
21	resource friendly	sustainable
22	good looking	style

4 Muscle architecture

4.1 Muscle physiology

This chapter introduces the general muscle, tendon, and tissue architecture, which is related to myographic principles. Closing the loop from chapter 2.2, the action potential propagates from the brain through the spinal cord towards the motor neurons, which innervate the muscle. The human body provides three types of muscles: skeletal, cardiac, and smooth [86]. Skeletal muscles can be contracted voluntarily and important to detect the user's intention. The cardiac and smooth type is controlled by the autonomic nervous system. Skeletal muscles are located all over the body, and their main purpose is the manipulation of the environment [87]. To fulfill all types of manipulations, skeletal muscles are divided into parallel, circular, convergent, and pennate muscles [86]. Each of the four types is made for special applications in the human body. Parallel and pennate muscles are the most common types at the limbs, where the sensor matrix is applied.

Muscle:

Figure 4.1 depicts the main architecture of skeletal muscles with the example of a parallel-fusiform muscle. The bottom picture of figure 4.1 shows the muscle fiber, which is innervated by the central nervous system, more accurate the motor neuron, at its neuromuscular junction/innervation zone. A motor neuron is connected to several muscle fibers of the same type and creates a motor unit [26]. The motor unit action potential (MUAP) propagates with a mean velocity of about 4-5 m/s from the neuromuscular junction in both directions towards the end of the muscle fiber [88, 89]. The velocity changes with induced activation and muscle fatigue [90]. Measuring the MUAP is a way to obtain myographic information and called electromyography.

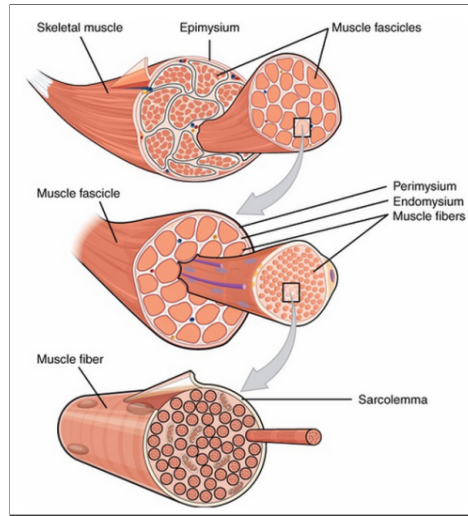


Figure 4.1: Skeletal muscle architecture (fusiform) by [91]

Muscle Fiber:

Muscle fibers can be classified into three groups [92, 26]. The type 1 fiber (slow twitch) is slow but endurable. Type 2 fibers are fast twitching and further divided into two subcategories, based on their endurance. Type 2a (fast-twitch fatigue resistant) is more enduring than Type 2b/2x (fast-twitch fatigable). Muscles have a full set of all fiber types, but the exact composition differs between humans and muscles based on their function, training, and other constraints [93]. Aerobic and anaerobic training shifts the fiber spectrum towards lower, respectively higher twitch frequencies [94, 95]. Figure 4.2 shows the time domain of sample muscle twitches, which are mainly distributed with the introduced fiber types. The twitching time differences are apparent and part of the mechanomyographic information.

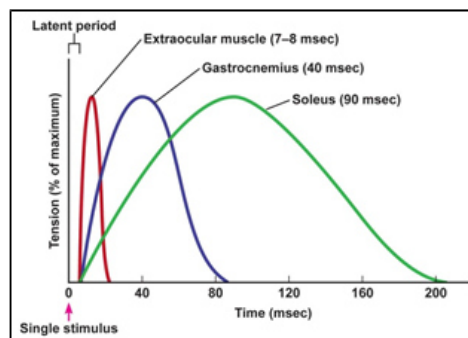


Figure 4.2: Muscle Fiber Activation Time: Extraocular mainly fast twitch [96], Gastrocnemius about 50% slow twitch fibers [97], Soleus about 64-100% slow twitch fibers [98] [99]

The activation/recruitment of muscle fibers is described in the Henneman Size Principle, shown in figure 4.3 (B) [100]. Slow-twitch fibers are recruited in any case, while fast-twitch

fatigue fibers are just used in addition to the others, which is mainly the case for short ballistic movements [101]. Muscles are orderly recruited to be able to achieve fine dexterous, as well as strong movements [102]. Exhausted muscle fibers get replaced by bigger and stronger fibers, which results in less dexterous movements with muscle fatigue. To achieve the maximal voluntary contraction, the central nervous system recruits its full set of muscle fibers. Recording an electromyographic signal from a muscle and using the frequency domain gives insight into the activation rate, which leads to knowledge about the intensity of the movement (see figure 4.3 (A)).

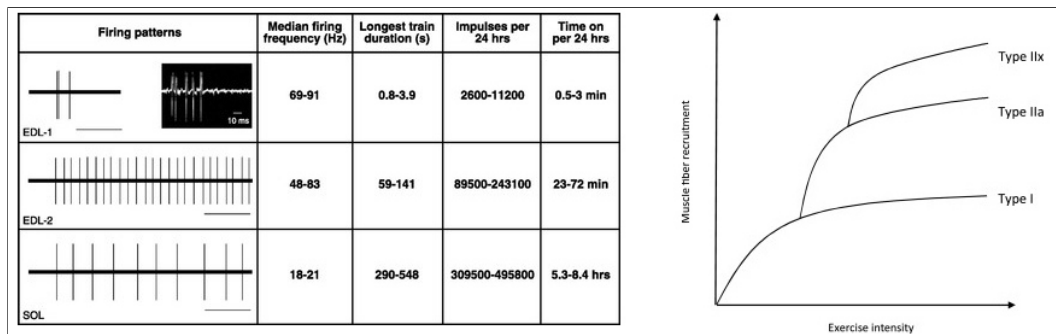


Figure 4.3: Left: Fiber usage and median frequency from a rats extensor digitorum longus and soleus muscle. EDL1 (type 2B), EDL2 (type 2A), SOL (type 1) [103, 104]; Right: Hennemann's size principle from [101]

The contractile element of the muscle (sarcomere) is shown in figure 4.4. The sarcomere distributes in parallel and series in a muscle fiber. The evoked action potential from the neuromuscular junction changes the polarity of the muscle cell, which results in an inflow of calcium (Ca^{2+}). Ca^{2+} is the trigger for the Cross-Bridge Cycle. The Cross-Bridge Cycle is the mechanical twitch of the contractile element. More detailed, the myosin head couples with ATP and snaps further along the actin towards the z-line. Each MUAP results in a twitch, which shortens the contractile element. The accumulation of all twitches, fast and slow, leads to the pulling force on the tendon [105, 106, 107, 108]. The lateral oscillations of the twitches are measured with a technique called mechanomyography.

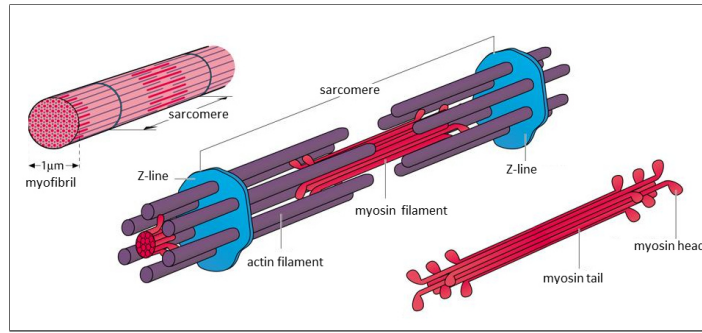


Figure 4.4: Sarcomere translated from [109]

Figure 4.5 shows the dependency between the tension and summation of twitches over time. A complete/fused tetanus has less amplitude oscillations and reaches its resonance frequency [110]. When measuring muscle oscillations, biological tremors should be taken into account [111].

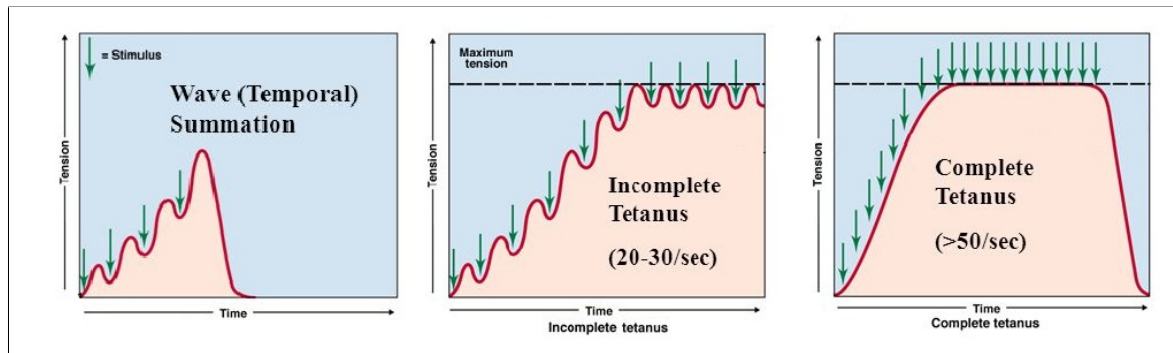


Figure 4.5: Wave Summations modified from [112]

Muscle-Tendon Compound:

The muscle is connected to the tendons, which stores elastic energy with enlarging (tension). When the muscle contracts, the tendon pulls on its origins, which has a distance to the joint to exert a torque. The connection between the tendons and the muscle fibers are differing between pennate and parallel muscle types. The parallel muscle has parallel fibers pulling on the tendon, and the pennate muscle has a pennation angle that allows a higher number of fibers in the muscle and a smaller change in length [113].

Due to the accumulation of twitches, the muscle shortens, which results in a bulging muscle, due to its isovolumetric behavior. The muscle bulge is measured with a myographic technique called force myography. In pennate muscles, the pennation angle is also part of the enlarging width of the muscle [114, 115]. Hodges et al. (2003) conducted a test setup with ultrasound and EMG measurements and discovered that the gradient of the muscle thickness decreases at 30% MVC [113]. Hodges et al. (2003) also discovered that the dependency on muscle

architectural parameters differs in between different muscles and does not always occur. Nevertheless, parallel and pennate limb muscles should show a related behavior between activation and bulge. The joint angle plays a crucial role in determining the activity, the muscle - length relationship describes this behavior [114].

Electromechanical Delay:

The electromechanical action delay describes the latency of the musculoskeletal system before exerting force after the motor unit potential propagated through the muscle fiber. The delay is a major drawback in capturing intentions based on mechanic phenomenons (see figure 4.6). The reasons are chemical, e.g., the Ca^{2+} inflow, and mechanical, e.g., the tendon elasticity, constraints. This impedes the application of myographic techniques based on mechanical information in real-time applications. Cavanagh & Komi (1979) stated the delay of the mechanic response as in between 30 to 100 ms [116].

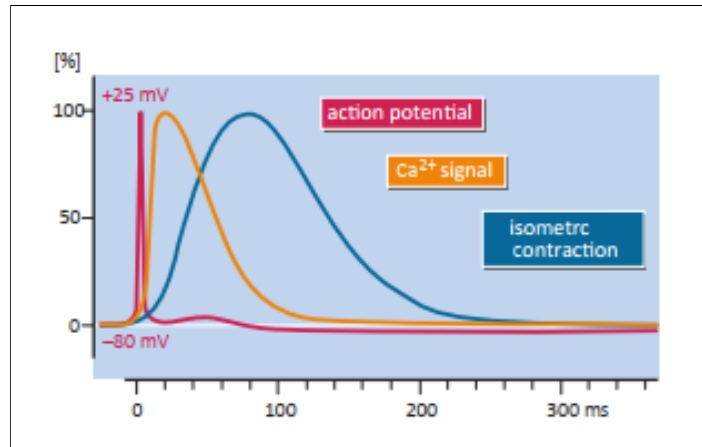


Figure 4.6: Electromechanical action delay and the latency of the muscle processes from [117]

Conclusion:

In summary, the work focuses on parallel and pennate skeletal muscles. The muscle fibers are connected to a motor neuron and build a motor unit, which consists of one motor neuron and many muscle fibers. Muscle fibers are divided into three types depending on their twitch behavior and endurance. The twitches are accumulated and pull on the tendon. While twitching, the muscle bulges and decreases in length. The neuromotor control processes in the muscle are summarized as intramuscular coordination and consist of recruitment, rate coding, and sequencing. The control processes between muscles are called intermuscular coordination and aim to improve movement coordination by using synergies and improved agonist-antagonist synchronization.

4.2 Forearm anatomy

Knowing the anatomy of the role model location of the human forearm augments the knowledge about applications of the sensor and possibilities and difficulties regarding the obtained signals. The muscle dimensions differ interpersonally, but the principal architecture remains, as long as no pathologic state occurs. For example, the musculus palmaris longus is absent in 12.9% of humans [118]. The muscles in the forearm are mostly divided into extensors and flexors, even if they also have rotational and abduction/adduction characteristics. Flexors are the agonist for closing the fingers or bending the palm towards anterior. Extensors can open the hand or bend the wrist posterior. Specific finger muscles in the hand are small and weak. Consequently, finger movements are possible due to synergies of muscles or a particular muscle innervation from forearm muscles [119]. Larger muscles are placed in the proximal forearm and connected via tendons to the joints of the hand or wrist (see figure 4.7a).

The dexterous finger flexors are mostly located in the depth of the arm, while the stronger wrist muscles are superficial (see figure 4.7b). The extensor muscles are better distributed for recordings, which could lead to an enhanced prediction of opening, compared to closing movements of the hand (see figure 4.7a and 4.7c). Moreover, it is obvious that the application of a wristband does not always align in muscle direction, which makes it more difficult to use a differential recording technique in a generalized setup. Nevertheless, for some locations, it seems possible, and current research is based on this simplification. Research needs to be conducted to show the influence of a wrongly aligned differential setup.

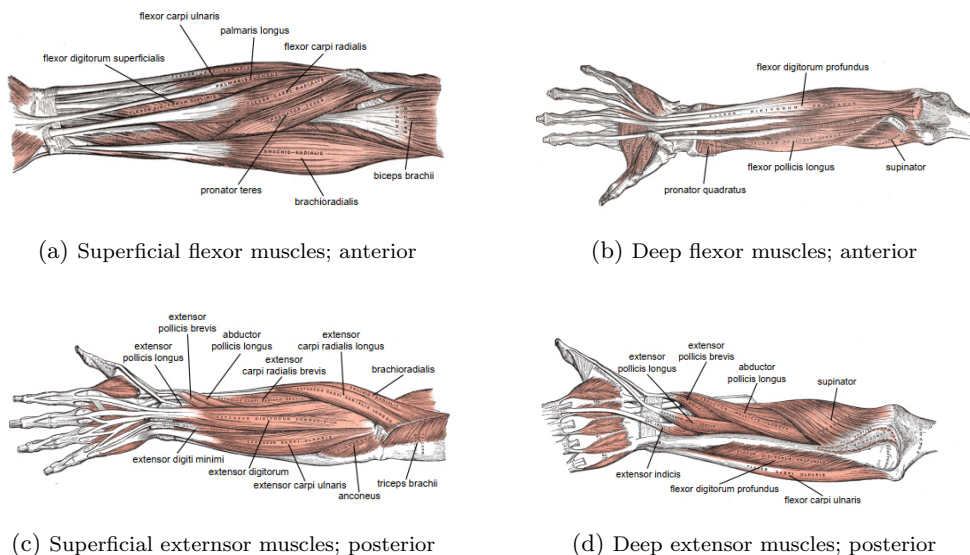


Figure 4.7: Left forearm anatomy from [120] annotated with modern names from [121]

Taking the cross-section image of figure 4.8 into account, it shows the difficulties of a surface recording. Deep muscles are not directly accessible with a surface recording. Nevertheless,

if the spatial resolution of the sensor is high enough, ten superficial muscles should be distinguishable in the shown cross-section. No major muscle signals can be obtained above the ulna, which makes it an interesting spot for calibrations and reference electrodes. Using the open-source human cadaver data from the Visible Human Project of IMAIOS, different cross-sections can be examined to theoretically evaluate promising sections [122, 123].

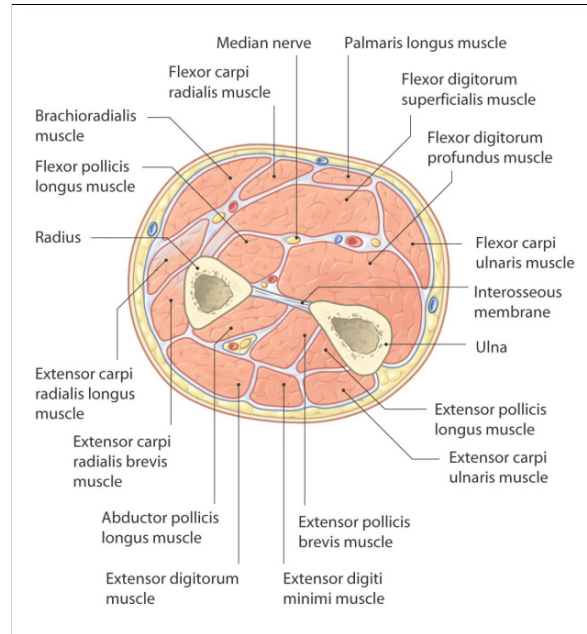


Figure 4.8: Cross-Section of the middle human forearm, transversal plane [124]

5 Myography

To clarify the term "Myography", its etymology is from the ancient Greek words *mys*, which means muscle and *graphos*, means write. Consequently, myography aims to display muscle functions. The Merriam Webster dictionary defines a "Myogram" as:

"A graphic representation of the phenomena (as velocity and intensity) of muscular contractions" [125]

Myography is used for all types of muscles, including large skeletal muscles and small smooth muscles in the blood vessels. Thus the field of myography covers voluntary and involuntary muscle functions. A short literature review resulted in myographic applications for neuromuscular rehabilitation, blood vessels, and muscular functions. The latter will be further examined. Obtaining muscle parameters is based on the six biosignal transducer types in chapter 2.1. Since muscles are inside our bodies, there are invasive and non-invasive recording methods, which brings up the necessity to clarify the law for medical technology in this field.

The current medical law states that an invasive measurement is a measurement which harms the body in a direct or indirect way to obtain a physiologic parameter [126]. Medical technology constraints are standardized in ISO 13485:2016 [127]. Using electricity or high-frequency rays or waves can potentially destroy cells. Permitted tomographic techniques should still be treated with care. The user receives more potentially damaging electricity, rays, or waves in long term applications than in short term applications like medical screenings.

Nevertheless, the research community in the field of myocontrol explores new solutions to improve the dexterity and acceptance of their systems [37, 36, 38]. Medical imaging techniques like ultrasound systems are nowadays used as myographic sensors [38]. Despite new recording types for myography, the research tends to apply multi-modal approaches to enhance their prediction [128, 2, 58, 51]. Especially dynamic movements without laboratory conditions are difficult to obtain and potentially require sensor fusion approaches. In everyday applications, the muscle structure and activity obtained at the surface are changing due to the limb position (rotation, gravity), fatigue, and others [37, 129]. Isolated myographic methods are only capable of recording a fraction of the complexity of the task.

Table 5.1 shows the difference between the research of the three main myographic methods. Research in Mechanomyography (MMG) and Force Myography (FMG) is still wide open, and many research questions are waiting to be solved. Nevertheless, it needs to be mentioned that MMG and FMG have a variety of names, which refers to very similar principles. It shows that the research community is not able to define a common name. Reviewing and explaining the different names and techniques extends the thesis.

Table 5.1: Short literature review about EMG, MMG, FMG in the title, ignoring subcategories (Scopus, 02.10.2019)

method	articles	first article
"Electromyography"	5960	1938
"Mechanomyography"	164	1972
"Force Myography"	37	2015

5.1 Electromyography

History:

The basis of electromyography (EMG) was first discovered by Jan Swammerdam, a dutch anatomist in 1664 [130]. In 1771, Galvani electrically stimulated an animal muscle, which resulted in a contraction; he described this phenomenon in his book in 1791 [131]. Adrian (1929) invented a method to record an isolated motor unit action potential by connecting needle electrodes to an amplifier circuit and a loudspeaker [132]. Following Adrian's work, the field of EMG was intensively researched. The invention of new amplifiers, which are capable of amplifying small currents, highly benefits the EMG research until now. The field of rehabilitation and prosthetic control further improved through surgery techniques like targeted muscle reinnervation, which acts as a biological amplifier for the remnant neural signals/intentions [36].

Phenomenon:

Figure 5.1 depicts the principle of EMG. The motor neuron innervates the muscle fiber at the innervation zone/neuromuscular junction, and the chemical depolarization propagates in both directions through the fiber towards the terminal zone. EMG measures the polarization and depolarization of the muscle cell due to propagating motor unit action potentials (MUAP) (see chapter 4). The electrodes act as a dipole with the polarized muscle cells. The signal at the surface consists of superimposed MUAPs. The known raw action potential ranges between -95 mV and 50 mV, while obtained motor unit action potentials differ in shape and amplitude [133]. Invasive EMG showed that the mean motor unit action potential

(MUAP) amplitude is approximately $701 \mu V$ and it decreases with neurological disorders [134].

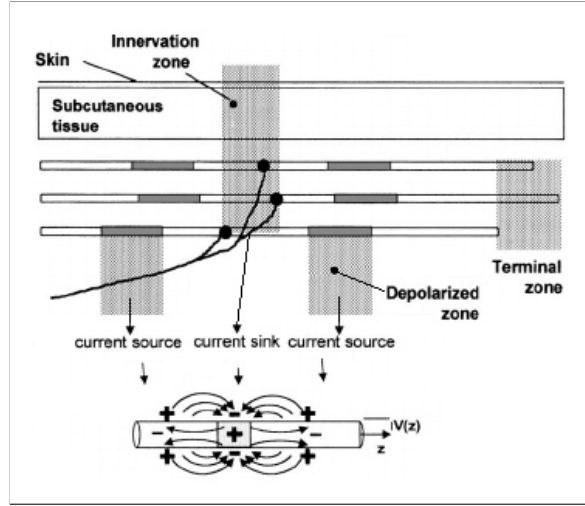


Figure 5.1: Electromyographic phenomena, modified from [135]

Skin Impedance:

Using non-invasive EMG, the effects of the human skin need to be considered. The human skin has capacitive and resistive characteristics, which low-pass filters and damps the signal, as seen in figure 5.2 [136]. The capacitive characteristic of the skin introduces DC and other types of noise, which its captured like an antenna from the environment. Thus, the obtained surface EMG signal will be very low, approximately about $10^{-3} - 10^{-4}$ in magnitude and need to be amplified with rejecting common-mode noise. Merletti (2009) shows the impact of fat tissue and EMG recording depth [137].

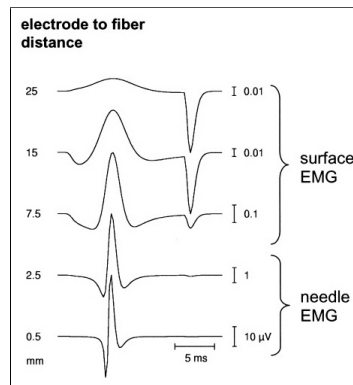


Figure 5.2: Electrode shapes in dependency of the electrode to fiber distance from [138, 139]

Signal composition:

Referring back to the conclusion of chapter 4, the intramuscular coordination consists of recruitment, rate coding, and sequencing. The electromyographic signal can provide this information with the motor unit spike train of the signal. These spikes can especially be seen in smaller and isolated muscles, e.g., finger muscles on the finger. The signal of larger muscles consists of superimposed MUAPs. Neighboring muscle signals at the recording site produce noise, which is called cross-talk. In contradiction of filtering the noise, many researcher use cross-talk to decompose the signal and deduce back to single action potentials and their location (see chapter 2.4) [43, 44, 140].

Taking the two possible approaches of invasive and non-invasive EMG, the invasive approach results in a higher signal to noise ratio but contradicts the design principles in chapter 3.1. Thus, the focus will be on surface electromyography.

The EMG signal further consists of different types of noise due to: muscular characteristics, skin impedance, perspiration, muscular tone, fatigue, Body Mass Index, movement type, sensor hardware characteristics, and sensor positioning [141, 142, 143, 144]. Amrutha et al. (2017) summarized the noise sources in their review and described techniques to reduce them [141]. Many of these errors can be faced with preparations prior to the acquisition, and others need to be filtered afterward. Filter frequencies between 10 to 500 Hz, and even higher for invasive fine wire EMG, are mentioned in the literature [142, 145]. Some systems use a power line notch filter to decrease the remnant 50/60 Hz power line interference [146, 142].

The digital signal processing procedure to filter noise and obtain the desired information is described in many papers and instructions like Reaz et al. (2006) or Konrad (2011) and ranges from amplitude, frequency, and spike analysis to wavelet, higher-order statistic, and machine learning approaches [142, 147]. The amplitude signal and the frequency domain of a sample EMG time series are shown in figure 5.3. Figure 5.3 (A) shows the rectified EMG signal, which relates to the superimposed MUAPs, and thus, to the recruited motor units and its connected muscle fibers. Figure (B) shows the frequency domain of the signal, which relates to the rate coding of the motor unit action potentials.

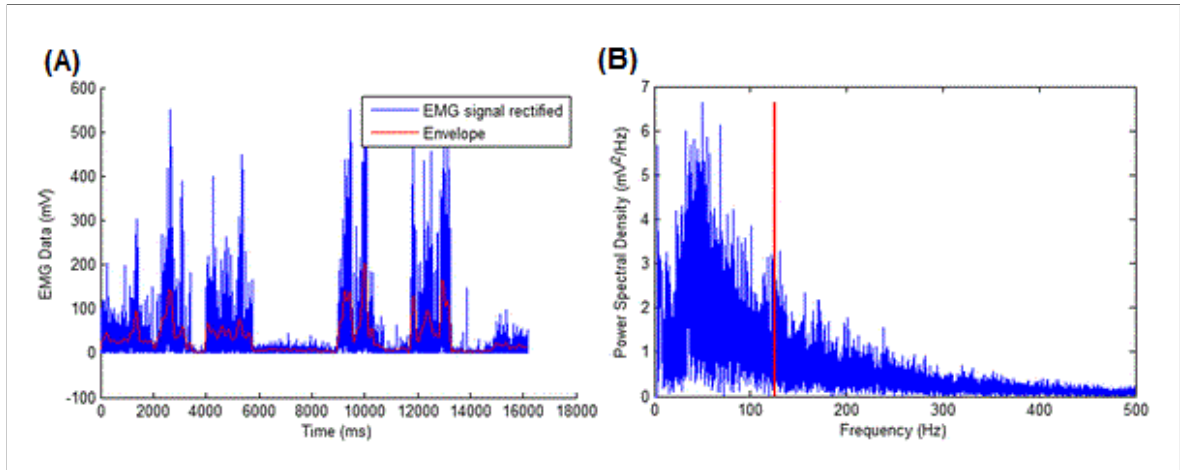


Figure 5.3: Sample EMG-Signal from [148]: (A) rectified and the envelope, (B) Power Spectral Density

Principles:

This section introduces the general setups, other important parameters for an EMG recording like electrode shape, size, and inter-electrode distance are covered in chapter 6.2. EMG setups differ in their general method. Active and passive amplifying circuits are available, which vary in their principle and closely related in the used electrode material. Passive electrodes often use a high conductive material like Ag/Cl and transmit the analog signal via cable to an external amplifier. Active electrodes are amplifying the signal at the origin, i.e., close to the surface electrode. This setup prevents noise and enables a more robust signal, in which cable movements manipulate the signal to a smaller degree. Furthermore, in an active amplification the electrode material can have a higher impedance, which enables the usage of dry electrodes out of stainless steel or synthetics.

Differential acquisition techniques, using two or more electrodes, reject the common-mode noise of the signal, which means that if both electrodes measure the same signal, it will be rejected, e.g., power line interference. Figure 5.4 depicts the major EMG setups, a newer approach of a tripolar setup with a double differential setup can be found in De Luca (2012) [149].

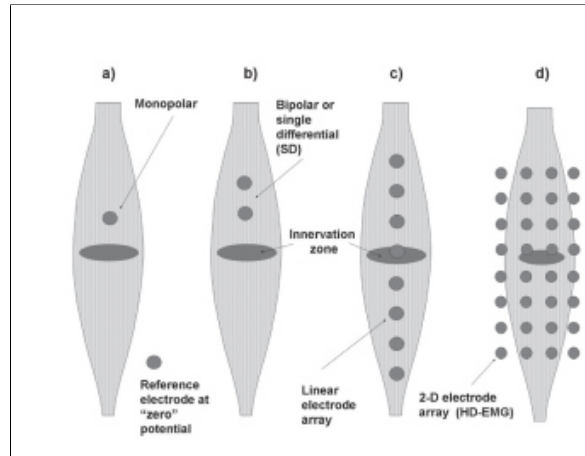


Figure 5.4: EMG recording setups from [150]

A monopolar setup (referential) records the raw signal of the muscle with a remote reference electrode at a bony structure, where no muscle activation can be measured, e.g., the elbow. In a wristband approach, a reference signal could be obtained on the surface of the ulna bone (see chapter 4). External noise, like power line interference, is also part of the reference signal and will be suppressed by a differential amplifier with its degree of common-mode rejection, which should be around 100 db [151]. A rejection of 100 db results in a common-mode amplification of 100.000 times smaller than before, i.e., 1 V common-mode has a fraction of $10 \mu\text{V}$ in the differential output signal. The effect of common-mode rejection is reduced with a different noise magnitude due to a greater distance between the electrodes.

Bipolar recordings (single differential) measure the muscle activity with two active electrodes on the muscle in muscle fiber alignment. The differential amplification results in reduced noise and cross talk. Reducing the cross-talk leads to a more local signal, without the information from deeper and neighboring muscle fibers. Figure 5.5 illustrates the differential approach of a bipolar setup and the raw monopolar signal, with a simulation of one signal source. The linear array setup in figure 5.4 (c) is often used to analyze the conduction velocity of the muscle fiber and the localization of the innervation zone.

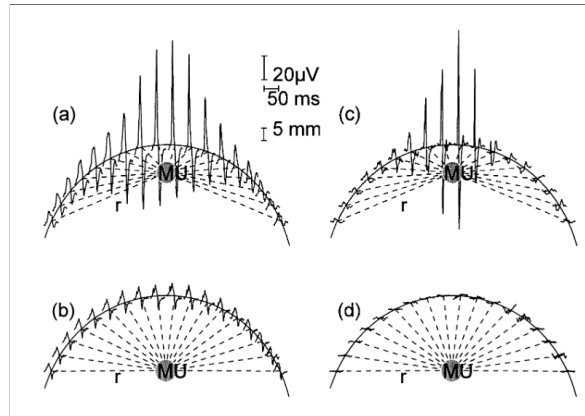


Figure 5.5: Simulated signal of a monopolar recording (a,b) and from a single differential recording (c,d) from [152]

Application

Monopolar recordings are used in high-density array setups with sophisticated digital signal processing using spatial filters, higher-order statistics, or machine learning algorithms [137, 153, 154, 54]. Using these processing techniques, a high-density setup is capable of comparing neighboring electrodes by merging the signal with spatial filters. Spatial filters make the setup suitable for complex muscle architectures, i.e., the human forearm. In addition, monopolar setups are suited to use the newest electromyographic processing technique of signal decomposition to extrapolate the single motor units (see chapter 2.4). Nevertheless, the most common setup for scientific modeling and medical checks is the bipolar setup. The acquisition of a bipolar setup requires knowledge about the anatomy of the recording site to align the electrodes in the muscle fiber direction.

Low-Cost Solutions

The ninapro database was set up to provide EMG data for the biorobotics community [155]. Pizzolato et al. (2017) acquired data for the ninapro database with six different sensor setups from the most prominent distributors and research sensors [146]. The use case was a sensor placement similar to a wristband to acquire data for upper limb prosthetic control tasks. The already introduced myoband from Thalmic-Lab, which is cheaper than the high-performance solutions from Otto Bock, Delsys, and Cometa Wave was able to compete with the more expensive setups in terms of accuracy in a classification task with 41 hand movements.

Advantages:

The biggest advantage of electromyography compared to other myographic approaches is the high temporal resolution due to the recording of the motor unit action potentials from the central nervous system without measuring mechanical signals. Thus, the prediction of muscle forces is possible in real-time and applying it to control a human-machine interface,

e.g., a robotic hand is mainly limited to the actuators' speed. Furthermore, electromyography complies with the design principles, with not actively sending energy into the human body. The digital signal processing possibilities with using electromyography as a neural interface by decomposing the signal into single motor unit activation makes it highly promising for future research (see chapter 2.4).

Difficulties / Open positions:

On the contrary to these advantages, electromyography has some difficulties and open research positions. Farina et al. (2004) divided the factors that influence surface electromyography in two groups, "non-physiological" and "physiological" factors [144]. The small signal amplitude introduces all kinds of errors due to the high impact of normally neglectable smaller noise sources. After amplifying the signal, it is more robust against cable movements and other external influences. The application of EMG should suit the circumstances of the muscle, and especially differential setups require knowledge about the underlying muscle architecture and alignment. Another factor is muscle fatigue, e.g., if the subject is holding a bar for a long period of time, the electromyographic signal amplitude decreases due to orderly recruitment (see chapter 4). Consequently, the isolated application of electromyography in an upper limb prosthetic control tasks is difficult for everyday tasks like holding a cup of tea [156].

Electrode-Skin Impedance

A drawback of EMG is the electrode-skin impedance change due to the electrode material, perspiration, or other distortions. Some years ago, it was necessary to measure the skin impedance before measurements, nowadays it is not mandatory, due to the higher input impedance of the amplifiers [157]. Nevertheless, the voltage drop changes due to impedance changes, and the signal will change as well. The skin impedance without skin preparations of $10 - 100\text{ k}\Omega$ at DC is a small fraction compared to the impedance of dry electrodes of around $1\text{ M}\Omega$ at DC. The input impedance of an amplifier is nowadays $100 - 10000\text{ G}\Omega$ (INA333 (Texas Instruments Incorporated., Dallas, Texas, USA), AD8224 (Analog Devices, Norwood, MA, USA)). Using EMG electrodes the drift in long term applications should be monitored, unless it can be assured, that the difference between the electrode, skin and the amplifier impedance is neglectable and guarantees consistency [158].

Conclusion:

In conclusion, electromyography has a major advantage in its high temporal resolution, but the small amplitude is very sensitive to electromagnetic interference and electrochemical reactions at the electrode interface. Nevertheless, the application of electromyography in a real-time control system seems mandatory at this time. High-density grids and decomposition algorithms enhance the prediction and inherit high potential for future applications [159].

5.2 Force Myography

History:

The measurement technique of force myography (FMG) was first introduced in research from Lucaccini (1966) with a review about the French electric Hand, which used myo-pneumatics as their transduction principle [160]. Research for the french electric hand started during the second world war in Berlin from Dr. Edmund Wilm [160]. Half a century later, researchers in the team of Prof. Dr. Craelius showed that myosignals could be obtained by embedding force-sensitive resistors (FSR), which reduced the size significantly [161, 162, 163]. This technology was developed and is now spread into different measurement principles and general ideas. Thus, FMG does not have a standardized name in the literature and is also mentioned as surface muscle pressure, residual kinetic imaging, myo-kinetic, or tactile myography. The various names are used in different applications and setups. Most of the names specifically relate to the area of rehabilitation as residual kinetic imaging, others specify with the application of a high-density sensor arrangement like tactile myography.

Phenomenon:

Force myography measures the pressure distribution at the recording site. The obtained pressure appears by the shortening muscle bulge during contraction. The phenomenon results from the shortening contractile elements of the muscle fiber and the isovolumetric constraint of the muscle, which causes a moving muscle and increasing bulge (see chapter 4). The change in width of a pennate and fusiform muscle is shown in figure 5.6. Hodges et al. (2003) investigated the changes in the muscle architecture by ultrasound recordings and stated, that the biceps brachii changed its muscle thickness significantly at 50% of the maximum voluntary contraction (MVC) [113]. Nevertheless, Hodges et al. remarked that some muscles behave differently, e.g., obliquus externus abdominis and medial gastrocnemius [113, 114].

Taking the muscle physiology from chapter 4 into account, it can be concluded, that the muscle thickness is an indirect parameter of the evoked motor unit action potential and is directly related to the isometric muscle activity in particular muscles. The muscle pressure distribution depends on the joint angle, e.g., if the joint is already flexed, the muscle needs to decrease its length to be able to exert a torque at the joint. More details about force dependencies are stated in the literature covering "muscle-length", "tension-length" and "joint angle-force" relationships [164, 165]. Thus, the phenomenon is more complex to analyze during dynamic movements, as Rasouli et al. (2015) stated in his research [166]. Radmand et al. (2016) demonstrated that the classification error decreased with an included position variation in the training protocol [167].

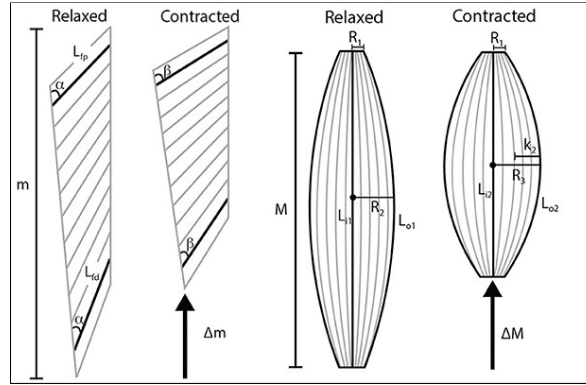


Figure 5.6: Muscle architecture of unipennate and fusiform skeletal muscles relaxed and isometric contracted; modified from [115]

Signal composition:

The signal of the FMG sensor can not be directly linked to the intramuscular coordination. However, the signal consists of the mechanical coupling of the recruitment and rate coding. In detail, the muscle activity, joint angle, and external noise, i.e., the inertia of the sensor is obtained. Due to its active principle, the signal is insensitive against low-level electric noise. The FMG amplitude is robust and represents the applied pressure on the sensor.

Xiao & Menon (2019) researched about the resulting frequency ranges of the force myographic signal and concluded that a sampling frequency of 70.84 Hz is sufficient to obtain dynamic actions at the forearm or wrist [168]. Figure 5.7 depicts that the highest magnitudes are found in the frequencies below 1 Hz. The literature concerning the cut off filter frequencies is very heterogeneous and dependent on the measurement principle or classification methods. However, the cut-off filter frequencies vary between 0 and 50 Hz, some researcher applies a high-pass filter around 0.5 Hz, and others use a low-pass filter at 1 Hz [167, 2, 72, 3]. Reasons for filtering were long-term signal drift due to memory effects of the sensor material, humidity changes, skin elasticity effects, and high-frequency noise [3, 57, 2]. It should be emphasized that these studies were using different sensor principles, and a generalized signal bandwidth seems not feasible.

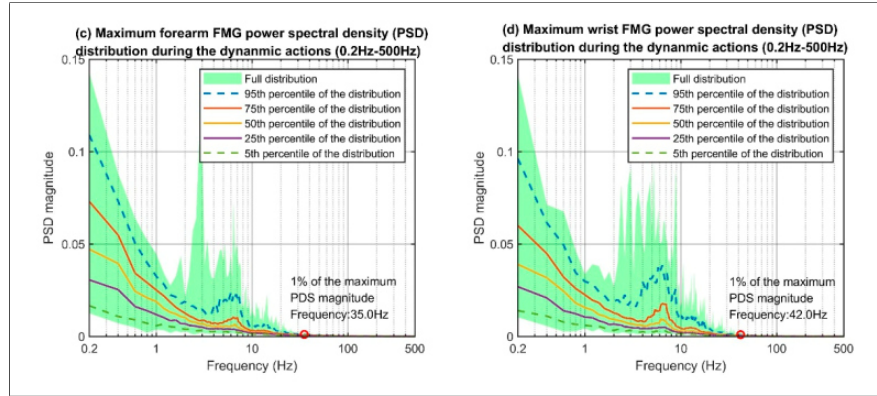


Figure 5.7: Maximum FMG power spectral density (PSD) distributions of the forearm and wrist [168]

Principles:

Stassi et al. (2014) reviewed the area of tactile sensing principles and created table 5.2 [169]. The presented measurement principles have advantages and disadvantages for their application in intention detection interfaces on the basis of myographic information. Due to the design principles of a high spatial resolution, strain gauges and piezoresistors are suited techniques for the application in high-density human-machine interfaces. The most used principle in the literature is the force-sensing resistor (FSR) [167, 168, 170, 171, 85]. The electrical principle behind these sensors is a changing resistance with a deforming sensor material. Using this principle, the sensor needs to be applied close to the skin and could cause mechanic stress, which results in potential damage at the electrode and noise in the signal. The mechanic stress is also the main reason against strain gauges. Weiss & Wörn (2005) developed a piezoresistive principle which uses a conductive sensor material and two electrodes. This system does not have wires and includes many of the advantages from table 5.2 [172]. Schürmann et al. (2011) from the team of Risto Kõiva used the principle of Weiss & Wörn to develop a tactile sensor module for human manipulation research [173]. Due to the inhomogeneous surface of the muscle bulge, a high-density sensor grid results in a more detailed pressure map compared to a FSR grid. The spatial resolution of most of the high-density piezoresistive sensors ranges in between 4 mm^2 and 6.12 mm^2 [174, 175]. A recent paper by Kõiva et al. (2019) used a modified barometer as a $2 \times 2 \text{ mm}$ tactile sensor with in-built digitization [176]. This approach should be researched further in terms of an application on a narrow sensor module but was out of scope for this thesis.

Table 5.2: Comparison of tactile sensor principles from [169]

Parameter	Sensor Type			
	Piezoresistors	Strain Gauges	Percolation Mechanism	Quantum Tunnelling Mechanism
Sensitivity	High sensitivity	High sensitivity	Low sensitivity	High sensitivity
Repeatability	High repeatability	High repeatability	Hysteresis Problem	Hysteresis Problem
Spatial resolution	High	Quite high	Low (except OFET)	Low
Working area	Suitable for small area (<i>i.e.</i> , fingertip)	Suitable for small area (<i>i.e.</i> , fingertip)	Small and large area	Small and large area
Working range	Low	Medium	Low, but tunable with composition	Very high and tunable
Fabrication techniques	Costly materials and techniques	Costly materials and techniques	Simple fabrication techniques	Simple fabrication techniques
MEMS/electronic integration	Ease integration	Ease integration	Complex integration (except OFET)	Complex integration
Mechanical properties	Fragile (better with protective elastomer)	Fragile (better with protective elastomer)	Stretchable and robust	Stretchable and robust

Application

Research was conducted comparing the accuracy between FMG and EMG with machine learning methods. The scientists concluded, that FMG had similar results or outperformed sEMG in controlling proportional and simultaneous motor tasks [51, 58, 2, 167, 74]. Ravindra et al. (2014) state that the obtained myographic information from FMG differs from the information of EMG and could benefit a sensor fusion approach, which was also stated by other researchers [72, 36, 2, 51, 167]. Furthermore, a pilot study with one subject of Nowak et al. (2017) showed, that FMG itself could outperform a sensor fusion approach [58].

Advantages:

The force myographic modality has advantages against the current gold standard of electromyography. First of all, a FMG sensor has less background noise and thus a more stable signal [2, 177]. This advantage is due to the underlying phenomena and measurement principle of the approach. Compared to EMG, a FMG sensor can also measure the muscle activity at the tendons, which enables the possibility to record the activity of deeper hand muscles at the wrist, where the tendon stiffness directly link to the movement. Cross talk from deeper muscles is absent at the wrist, which makes it a good location for FMG recordings.

Another advantage is that the FMG signal decreases less than EMG signals with muscle fatigue [2]. In an isometric task with a constant force, the muscle bulge stays constant in its width, while the dexterous motor units get replaced by stronger units to exert the same pulling force on the tendon. Thus, fewer motor unit action potentials can be obtained by the

EMG sensor, which results in a smaller amplitude. Figure 5.8 shows the difference between a FMG sensor, based on an FSR (FSR 400 Short, Interlink Electronics Inc., Camarillo, Ca, USA), and an EMG sensor (Otto Bock, MyoBock 13E200). The effect of muscle fatigue and noise can be clearly seen, especially in higher amplitudes, i.e., larger recruitment.

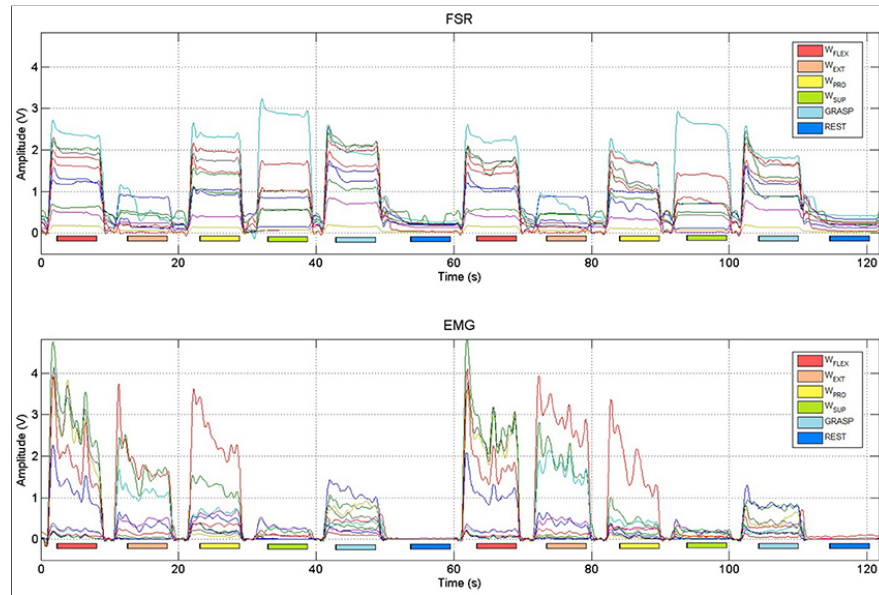


Figure 5.8: Comparison of FMG and EMG in an isometric gesture task. The FSR-Signal stays nearly constant, the EMG signal decreases with time [2]

Furthermore, the FMG sensor is not sensitive to skin impedance changes due to perspiration [3], but it should be taken into account, that the sensor material characteristic could vary due to humidity changes. The capability to wear a FMG sensor on top of clothing makes its application easier.

The total setup of a FMG sensor consists of a resistor and the sensor unit itself. Therefore, a FMG setup needs less and cheaper components compared to EMG. The detailed components depend on the measurement principle of the FMG and EMG Sensor and will be introduced in chapter 6.1.

Difficulties / Open positions:

The ability to decrease the size of the sensors is a major deal in this research. Yousef et al. (2011) & Stassi et al. (2014) described specific requirements for the design of tactile sensors for human robots and stated a desired size of 1 mm for a fingertip sensor [169, 178]. The minimal size of the sensor should be capable of measuring the smallest part of the musculoskeletal system, which can be captured from the surface. Taking the width of the muscle into account, the most narrow tissue, which can be measured from the surface, is the tendon. Thus, the

optimal size is smaller than 5 mm, which is, self-measured, the diameter of a tendon connected to the finger. The cross talk from deeper muscles can be faced with a high-density approach and a machine learning algorithm that is capable of detecting the components of the signal and state it as a different source, similar to approaches to decompose EMG Signals [44, 159, 140]. The current solution of a FMG wristband, the Bielefeld Bracelet (chapter 2.5), has problems to capture pressure on the lateral side of the sensor. The sensor modules of the Bielefeld bracelet are 2 cm wide and not curved; thus, the round forearm is not always in contact with the sensor. Taking this constraint into account, we aim for a narrow sensor module, to avoid edge effects. In conclusion, the open research task is to decrease the size of the sensor module remarkably.

Castellini et al. (2018) summarized further critical aspects regarding FMG in his research and stated: the movement of the sensor, the contact with the skin, noise through contact forces, accelerations and orientations, deformations of the body, tendons [3]. Another major drawback of FMG is its dependence on the joint angle. Knowing the joint angle would significantly increase the knowledge about the current activation. The electromechanical delay makes it difficult to use FMG in a real-time system. The usage of FMG in an EMG triggered feed-forward approach could enhance the prediction after their delay, due to the robust and consistent signal.

Conclusion:

In summary, FMG provides robust mechanical myographic information, which is less sensitive to external noise but has systematic errors due to muscle and sensor characteristics. The open positions need to be investigated to ensure a high myographic signal quality. Applying biomechanical knowledge, the vital pressure signal bandwidth of the sensor is low, and higher frequencies are not expected due to the inability of the musculoskeletal system to change the muscle width at a higher frequency. High-priority research positions concerning the Weiss & Wörn principle are a smaller sensor size and to reject the memory effect of the foam.

5.3 Mechanomyography

History:

The basics of mechanomyography (MMG) were first discovered from Francesco Maria Grimaldi and published post mortem in 1665 [179]. Placing his thumbs over the ear and clenching his fists, he noticed a rumbling sound. William Hyde Wollaston (1810) further researched these sounds and compared them with a carriage, which was pulled on a cobblestone street [180]. Using this comparison, Wollaston deduced that the mean frequency of the sound is around 24 Hz. Gordon and Holbourn (1948) were one of the first researchers using a microphone to

obtain muscle signals [181]. They concluded that surface MMG is the mechanical counterpart of the electrical activity of motor units using a simultaneous EMG recording [181]. Nowadays, the field of mechanomyography covers the terms sound myography, phonomyography, acoustic myography, and vibromyography [182, 183, 184, 185]. Some researches including force myography into mechanomyography due to the mechanical principle of measuring contact pressure in FMG. In general, MMG is the 2nd derivative of the FMG signal. Taken the variety into account, the following sections are strongly related to the transduction technique, and the shown signals slightly differ from each other, as shown in figure 5.9.

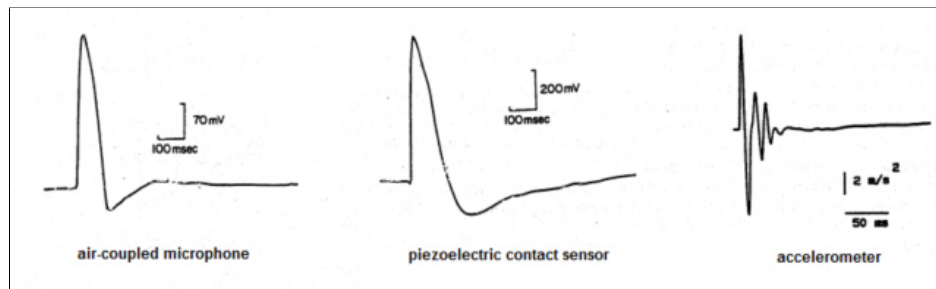


Figure 5.9: Mechanomyographic signal of a single supramaximal twitch from an air-coupled microphone, an piezoelectric contact sensor and an accelerometer from [182, 186, 187]

Phenomenon:

The underlying biological process was unknown and heavily discussed for a long time. Oster and Jaffe (1980) were one of the first authors who conclude that mechanomyographic muscle sound is generated by contracting muscles [188]. More precisely, they result from lateral oscillations of contracting muscle fibers, i.e., myofibril accelerations [189]. Due to this direct relation, mechanomyography is capable of observing the accumulation of twitches, which result in a wave summation and a muscle tension (see chapter 4) [190]. Figure 5.10 shows a study from 1987 with an isolated frog muscle, in which the direct correlation from the applied force and measured sound is shown (compare with figure 4.5). However, it does not fully reflect the superimposed signal on the human skin above a muscle belly [182]. Beck (2005) states that the amplitude is related to the number of active motor units [191]. According to Cescon et al. (2008), the gross lateral movement of the central muscle region is the primary factor in the signal [192]. The increase in fiber diameter is the second underlying factor. Thus, for a high signal to noise ratio, an application on the belly of the targeted muscle should be aimed.

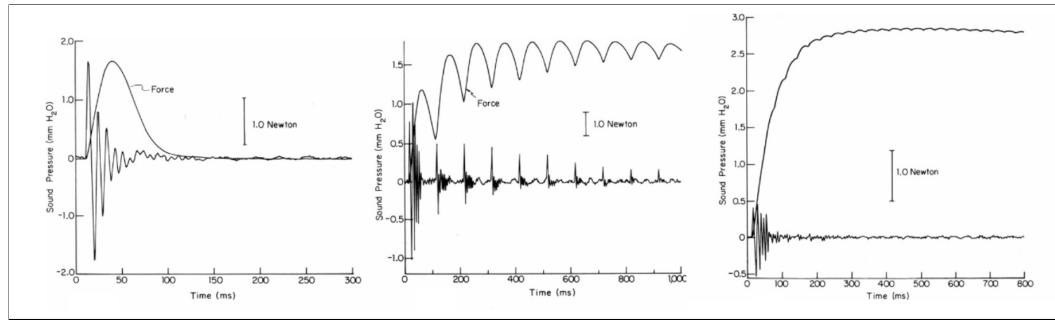


Figure 5.10: Sound myographic wave summations of an isolated frog muscle; From left to right: single twitch, unfused tetanus, tetanus [193]

Signal composition:

As already introduced in the previous section, the MMG amplitude shows the recruitment of motor units and their connected twitching muscle fibers. The literature concerning the frequency domain is heterogeneous and contradictory. Some authors claim that the spectrum is independent of the muscle activity, and some contradict these theses [194, 195]. In the research of Fara et al. (2013), the frequency domain enhances the accuracy of an upper limb control task [196]. Furthermore, they conclude that the frequency domain comprises information about muscle stiffness. In more recent studies, like Anders et al. (2019), the mean power frequency is used as a feature for muscle fatigue determination [197].

Figure 5.11 (A) shows the Root Mean Square (RMS) amplitude and mean power frequency of the myographic signal in dependence of the maximal torque. The RMS amplitude of the mechanomyographic signal is related to the number of active motor units (recruitment) [191, 194, 190]. Wang et al. (2019) characterize a linear behavior in between 20-80% torque [194]. Bichler (2000) disclosed, that fast twitching muscle fibers have a higher fraction in the amplitude (see figure 5.11 (B)) [198]. However, as depicted in figure 5.11 (A) above 80% torque, the force rises due to increased motor unit firing rate.

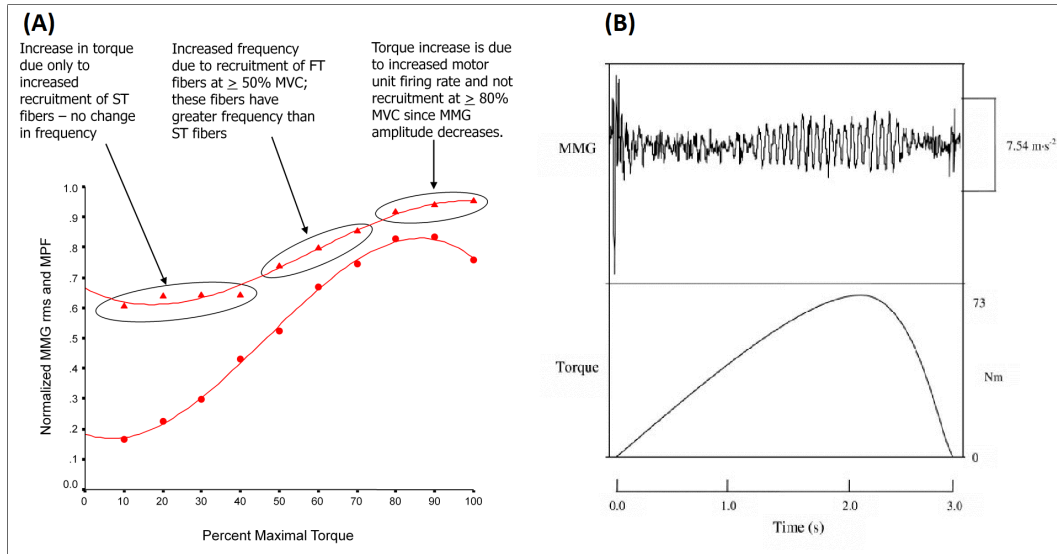


Figure 5.11: (A) - Circle: Amplitude, Triangle: frequency, (acoustic myography) [199]; (B) - MMG accelerometer with torque [191]

Figure 5.12 shows the power spectral density of a mechanomyographic signal within a muscle fatigue task. The spectral density is stated as in between 2-120 Hz, with the majority of information between 5-50 Hz [200, 201, 191, 111]. The signal needs to be applied with a higher high-pass filter cut-off frequency, to attenuate movement artifacts, when dynamic movements were measured with an accelerometer.

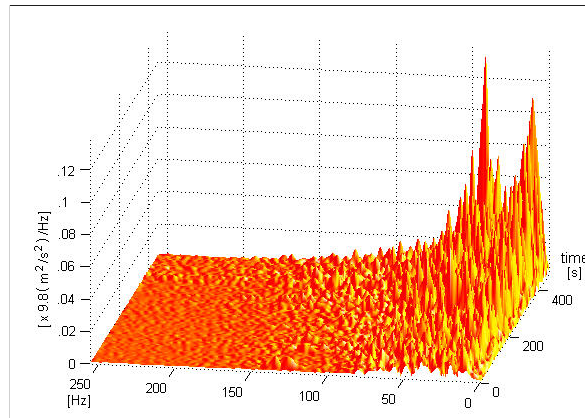


Figure 5.12: Power spectral density of a biceps brachii muscle fatigue task, measured with an accelerometer from [111]

Researchers notice that the muscle temperature, stiffness, mass, intramuscular pressure, viscosity of the intracellular tissue, muscle fatigue, extracellular fluids, and the resonance frequency can determine the signal output and the signal [202, 182, 203]. In addition, the authors mentioned the negative impact of the physiological tremor on the signal, which is

between 6 to 12 Hz [110, 204, 205]. The amplitude of the MMG signal rises with an increase of the temperature [203]. Studies were made regarding the pressure, which resulted in an amplitude increase with higher pressures [186, 206, 207].

The mechanomyographic signal to noise ratio strongly depends on the measurement principle, while the mechanical principle stays the same [208, 209, 210, 211]. Using unidirectional microphones as a transducer, the signal consists of sound waves that were created by skin oscillations. They have a higher signal to noise ratio than accelerometers, which directly measure the surface oscillations [212]. Accelerometers are more sensitive and closer to the origin, but their noise inherits gravitational and movement accelerations. Using the results from Posatskiy & Chau (2012), a high-pass filter should be applied to cut the lower frequencies of an accelerometer-based measurement (≈ 10 Hz). However, attenuating low frequencies also results in suppressing typical MMG bands of interest [212].

Principles:

Mechanomyography has a large variety of principles, as already shown in previous figures. The main groups are acoustic- and vibromyography. Transducers for these techniques are condenser microphones, piezoelectric contact sensors, accelerometers, and laser distance sensors [191, 213]. The only commercial available sensor is a piezoresistive unidirectional measuring acoustic sensor with gel from MyoDynamik ApS [214]. Krueger et al. (2014) reviewed the field of mechanomyographic sensors and summarized a higher interest in accelerometer-based sensors [215]. The research of mechanomyography is still under investigation. Newer papers adapt to electromyographic approaches like differential MMG, fusion with a microphone and accelerometer, or high-density MMG grids [216, 217, 192, 85]. Additionally, the proceedings in the digital signal processing field enhanced the signal and the contained information [194]. Krueger et al. (2014) compared a microphone with an accelerometer and stated that the RMS amplitude of a microphone was more valuable, while the accelerometer provided a more valuable spectral density [215].

Application

Silva et al. (2004) note that their setup with three microphone sensors inside silicone may exceed electromyographic functionality in a prosthesis control task [218]. Xie et al. (2009) state that MMG can provide some notable advantages over sEMG [219]. Krueger et al. (2014) concluded in their review, that MMG enriches EMG [215].

Fara et al. (2013) built a 10\$ microphone MMG sensor for use in "brain-machine" interfaces [196]. Their microphone outperformed sEMG recordings in higher intensity contractions while lacking performance in lower intensities [196].

Advantages:

The mechanomyographic signal measures the myographic information, which appears between the EMG and FMG signal. Compared to the gold standard of EMG, MMG obtains a mechanical signal which is independent of skin contact and perspiration and can be applied above clothing [220]. The accelerometer-based mechanomyographic sensors are lighter, smaller, implemented in ICs, more sensitive, and cost-effective compared to other myographic approaches.

Difficulties / Open positions:

MMG sensors can be tiny but still lack in its spatial resolution because of the underlying phenomenon, which also measures propagating oscillations of neighboring muscles [196]. To resolve spatial resolution, and it might be necessary to apply a high-density grid to distinguish between muscle activities. Having a rigid mechanical mounting a high-density grid measure redundant information.

Due to its mechanical characteristic, it suffers from the electromechanical delay (see chapter 4). Cabral et al. (2013) determined a delay of 23 ms after the electric signal in a study with healthy volunteers [221, 222]. The delay after an externally evoked stimulus ranges around 2-7 ms, as a reason, Cè et al. (2015) suggest that the detachment of the cross bridges and the elasticity of the tendon are main contributors, which are not present in an isolated externally evoked setup (see chapter 4)[221, 182]. It should be taken into account that the delay heavily depends on the muscle fiber composition (see figure 4.2)

The biggest drawback of acoustic myography is the size of the sensor. While accelerometers can be tiny in size, condenser microphones should, according to Watakabe et al. (2001), have a length of 15 mm and a diameter of 10 mm to cover the frequency range of the mechanic waves [210]. In contradiction to these scales, Guo et al. (2017) build an upper limb control setup with a smaller low-cost microphone, which is still larger and heavier than an accelerometer [223]. However, microphones have a higher signal to noise ratio, and limb position changes are not part of the signal [186].

An open position remains the feasibility of a mechanomyographic sensor on a force myographic system based on a polymer. The force myographic signal should measure oscillations as well, but it depends on the damping factors of the sensor material and sensitivity of the sensor itself. Research should be conducted in comparing mechanomyographic signals and the 2nd derivative of force myographic signals. Moreover, the sensor matrix is tightly fixed on the arm using FMG. Thus, a contact pressure occurs, which determine the mechanomyographic amplitude. The application of an embedded temperature sensor to reduce the impact of the systematic error in the MMG signal needs to be investigated.

Conclusion:

In conclusion, mechanomyography seems capable of adding further information to a setup containing electro- and force myographic sensors. Taking the human biomechanics into account, the frequency domain should consist of the used fiber spectrum. The basic idea behind this hypothesis is that slow-twitch fibers exert their twitch less often compared to fast-twitch fibers (see 4 and figure 4.2). However, the relation is not easily accessible. Due to the variety of sensor principles with different signal compositions, it is important to consider if the sensor fits the objectives. Aiming for a high spatial resolution of each sensor module, a low-cost integrated circuit accelerometer could be used. Drawbacks could be down-scaled with machine learning, an additional inertial measurement unit (IMU) for motion detection, and a temperature sensor. Nevertheless, the applicability of an accelerometer together with a force-myographic sensor material needs to be proven at first. Then research should be conducted to compare mechanomyographic and force myographic signals to avoid redundancy.

5.4 Tomography

A tomographic device images its underlying structure. Using a time series of images, these techniques can determine the movement and changes of the inner tissue. The principle behind tomographic biosignals varies from oxygenation levels, hydrogen spins, and other tissue-dependent characteristics like absorption and scattering. This short section introduces approaches which could be applied in a wearable myographic setting.

Despite testing the neuromuscular activity with impedance measurements, researchers built a tomographic setup, which sends an electric current through the arm and creates an impedance cross-section [224, 225, 226, 227, 228]. The moving tissue, and especially the blood afflux, changes the measured impedance. The resistivity of blood is about half of the muscle resistivity [229]. Relying on hemodynamic changes results in a delayed signal. However, research with an applied electric impedance tomographic sensor for use in human-machine interactions showed promising results [227, 228]. The feasibility of a multi-modal setup of electric impedance tomography and electromyography need to be proven.

Near-Infrared Spectroscopy uses light (spectral range: 600-1000 nm) to create an image of the underlying hemodynamic activity in a non-invasive way [230]. Thus, the intention of the user can be detected due to a neurovascular coupling of the hemodynamic activity. The light is absorbed or scattered at the biologic tissue. Thus, the setup can retrieve the information about oxidative metabolism functions, i.e., muscle oxygenation and blood volume of the targeted muscle [231]. Current solutions are able to provide a low cost, portable, and wearable system to acquire the muscle activity. Near-Infrared Spectroscopy is mostly used as an addition to an EMG sensor [232, 233]. The hemodynamic response decreases the applicability in real-time

systems. In addition, the size of Near-Infrared Spectroscopy limits its usage in high-density approaches.

Sono- and Ultrasonomyography uses high-frequency sound waves (>20 kHz) to penetrate the tissue [234, 235]. The analytic theory bases on wave propagation and tissue-dependent reflections (Doppler effect) [236]. Depending on the frequency, the sound waves penetrate in deeper areas or get reflected earlier at the tissue. As a result, the ultrasound method can display an image of the underlying tissue, which can be further processed with image processing methods. The application of ultrasonomyography in an upper-limb control task was promising, but the smallest device is as big as a smartphone, which is not matching our requirements [38, 235]. Guo et al. (2011) summarized that their sonomyographic setup is more consistent than an electromyographic setup in the performance of a discrete tracking task [237]. If the modality of Ultrasonomyography would shrink its setup the advantages of a high consistency, high spatial resolution, and low temporal latency would be enormous.

In summary, tomographic approaches provide a high spatial resolution but lack characteristics like size and weight or temporal latency. The changes in technology need to be observed to use promising techniques when they are miniaturized.

5.5 Further techniques

To further enhance myographic systems, especially facing its difficulties, e.g., the introduced limb position effect from chapter 2.5, additional techniques are shortly introduced. Krasoulis et al. (2017) used a MEMS inertial measurement unit (IMU) to enhance the accuracy in an upper limb control task [75]. An IMU consists of an accelerometer, gyroscope, and magnetometer. The IMU added information about the position, rotation, and acceleration of the forearm segment to the machine learning algorithm [75]. Basically, the IMU provides the necessary information about the gravitation, which needs to be compensated by the muscles in addition to the muscle activity for the movement itself. Nowadays IMUs with an automatic sensor fusion are available on the market, which reduces the complexity of the computational effort for the developer and microcontroller.

The second promising sensor is a barometer. A barometer measures the environmental pressure and is sensitive to the altitude of the sensor. In addition to the IMU, it provides important information about the forearm height, which will face limb position related errors. Moncada et al. (2014) used a barometer for a movement classification task and stated enhanced accuracy [238].

Further techniques can face the temperature dependency of the myographic approaches and sensors for the changing electrode-skin impedance.

5.6 Discussion

Summarizing the myographic possibilities and taking the constraints into account, the most promising techniques are electromyography, force myography, and mechanomyography. EMG has a major advantage in its lower latency while having a disadvantage with the small amplitude, which is very sensitive to external noise. A real-time control system would highly profit from embedded electromyographic sensors. The research of high-density electromyography and the decomposition of motor units need to be observed. Force Myography has shown its potential and robustness in many studies, but there are still many open positions where research needs to be conducted. Embedded in a human-machine interface, the setup benefits from a reliable and consistent force myographic signal, which is less prone to noise. Mechanomyography adds mechanic information about the twitching muscle fibers to the signal, which differs from the obtained information from EMG signals. Accelerometer-based sensors contain motion artifacts but provide a signal with a small footprint on the sensor module. Promising tomographic techniques are electric impedance tomography and ultasonomyography, but the techniques are not mature or contradict the principles of size and weight. Additional myographic sensors are used to detect the motion to improve the information of the main myographic methods. Taken together EMG, FMG and MMG can be miniaturized and offer a wide spectrum of different myographic information.

6 Sensors

Chapter 6 introduces the sensor principles, based on the most promising techniques from chapter 5. It covers the conceived transducing principle and necessary components for the circuit. The chapter starts with the force myographic sensor, which creates constraints for the other sensors. At the end of each section, open research questions are stated, which need to be evaluated to ensure the signal quality.

6.1 Force Myography

Background:

Shortly summarizing the outcome from the force myographic section in chapter 5.2, force myography (FMG) is currently trending in the field and has posed promising results (see 5.2). FMG is capable of recording mechanical myographic information with a high consistency, which makes it a valuable asset for a human-machine interface based on electromyography. Nevertheless, further development is necessary to be able to use it in the desired context and to understand the determining constraints.

As already mentioned in chapter 5.2, FMG has different methods and principles. Some of the principles and methods are shown in the research wristbands in figure 6.1. The most promising principle is introduced in 5.2 and was developed from Weiss & Wörn (2005) [172]. The principle is applied in a setup from Kõiva et al. (2005) (see figure 6.1 (A)) [57]. The measurement technique is cheap, robust, and has a high signal to noise ratio. The desired force myographic sensor should shrink the current setup and obtain a higher spatial resolution. The main parameters which can be changed to modulate the signal are the electrode geometry and the sensor material.

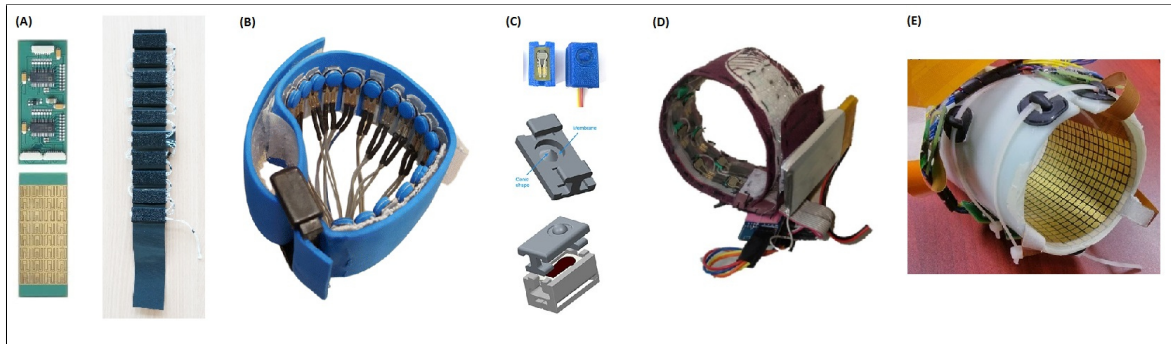


Figure 6.1: (A) Bielefeld Bracelet from [57], (B) Research Wristband from [239], (C) FSR sensor from [2], (D) Research Wristband from [170], (E) Research Wristband from [167]

Working principle:

Based on the principle from Weiss & Wörn (2005), Kõiva et al. (2015) invented a high density force myographic sensor wristband [57] as shown in figure 6.1 (A). The sensor principle is based on a sensor material, e.g., conductive foam or other conductive elastomers. Two electrodes are placed on a printed circuit board with a small gap in between each other (see figure 6.2). Depending on the applied force on the sensor material, the contact area between the electrode and sensor material enlarges. The increase in contact area further depends on the roughness and hardness of the sensor material. An enlarged contact area between the electrodes and the sensor material results in lower contact resistance. The change in contact resistance can be obtained with a voltage divider circuit. The circuit needs a high precision resistor and a high precision voltage supply to not acquire noise, i.e., ripple voltage in the signal. Kõiva et al. (2015) were able to show a nearly linear behavior of their sensor and the applied force with a resolution of 12 bit [57] (see figure 7.3 (A)).

Weiss & Wörn (2005) model the measured resistance by decomposing it into contact related resistance and material-dependent resistance, marked as R_s and R_v in figure 6.2 [172].

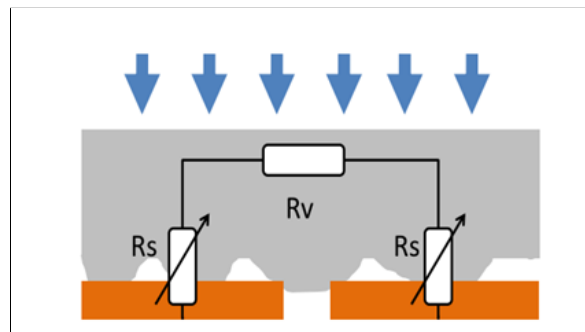


Figure 6.2: R_s contact resistance between material and electrode, R_v material resistance [172]

Figure 6.3 shows the basic equation for the resistance of an electrical conductor. The conductor's specific resistance ρ describes its conductance. The larger the area, the lower the resistance, the longer the distance, the higher the resistance. Based on this principle the conductor's resistance can be quantified.

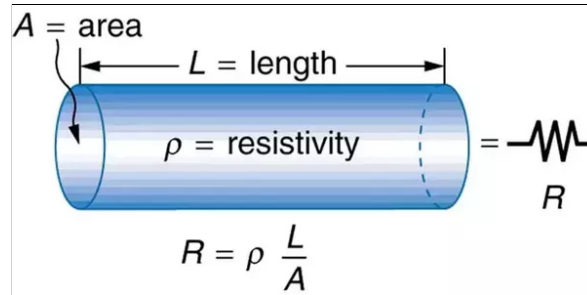


Figure 6.3: Basic equation for the resistance of an electrical conductor from [240]

As shown in figure 6.4, the unstressed sensor material is minimally connected to the electrodes; thus, it has a small summed up area of parallel resistances in total. Consequently, the resistance is high in an unstressed condition. By applying pressure on the sensor, the rough surface is pressed on the electrodes. Depending on the hardness of the material, the contact area enlarges, which in turn results in a decrease of the measured resistance. Taking the sum of the two surfaces and one material-dependent resistance, the surface resistance has a higher impact [172]. The sensor should use a material with a homogeneous roughness and hardness, to be able to compare future sensor results.

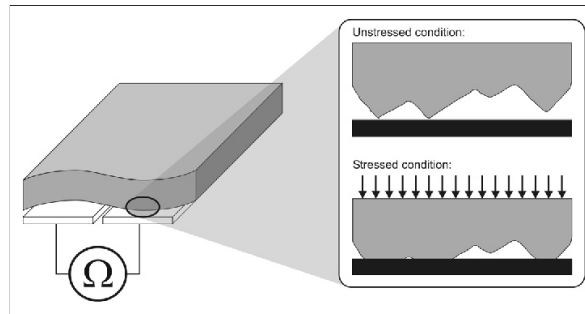


Figure 6.4: Stressed and unstressed sensor and the changed contact area [172]

Circuit:

A basic schematic of the sensor is shown in figure 6.5, with a linear dropout regulator and a voltage divider. The voltage divider consists of the active sensor resistance and the passive resistance of R_1 . The dimensioning of R_1 depends on the resistance of the sensor and was at first set as $10\text{ k}\Omega$, a higher resistance makes the sensor more sensitive but decreases the resolution [57]. However, the desired sensor adapts the sensor material characteristics to

increase the resolution. The power supply (VCC) passes capacitors and a linear dropout regulator to filter ripple and noise from the power line and provide a convenient voltage. The desired V_{constant} is used for the sensor circuit. The divided voltage is acquired with an analog to digital converter. It is recommended to place R_1 as close as possible to the input pin to decrease the influence of noise.

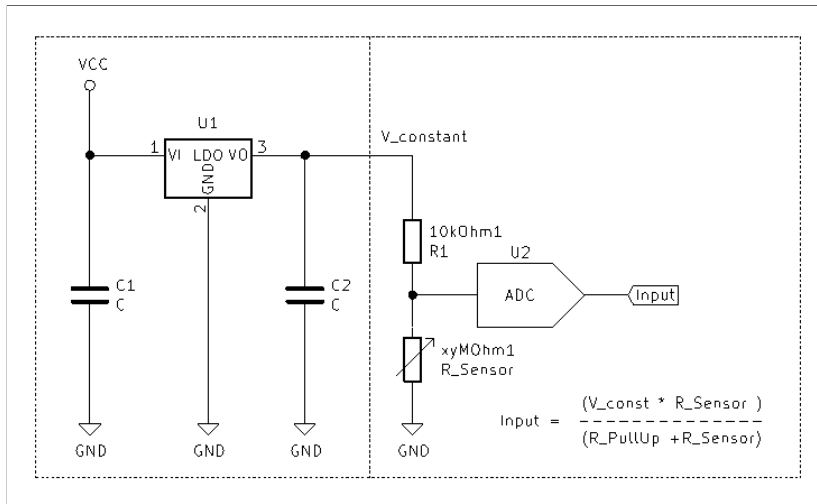


Figure 6.5: The basic circuit for the desired FMG sensor based on a filter circuit on the left and a voltage divider on the right

Electrodes:

The preferred electrode from Kõiva et al. (2015) is "M" shaped and based on the research of Schürmman et al. (2011) [173]. The "M" shape was evaluated in the paper from Schürmman et al. (2011) and is optimized to their sensor material (foam). The evaluation was not very consistent, due to changing properties in between the shapes, e.g., electrode sizes, gap length, gap distance (see table 1 in [173]). Consequently, this thesis goes for a different approach and use a circular-shaped electrode. Thus, it can be assured that the obtained phenomenon has the same influence from all directions and is easier to model. To ease the integration into a module, a tree-shaped electrode will be investigated, to avoid blind vias in the sensor module PCB, which is essential to reduce design effort and production cost (figure 6.6). In future projects, the tree electrode should be investigated with a smaller opening, to ensure high sensitivity for pressures from the open side. These two shapes have been rapid-prototyped with different sizes. For each type and size of the electrode, the active surface is designed to be of equal area and gap distance (0.1 mm). Thus, we can compare the sensors against each other.

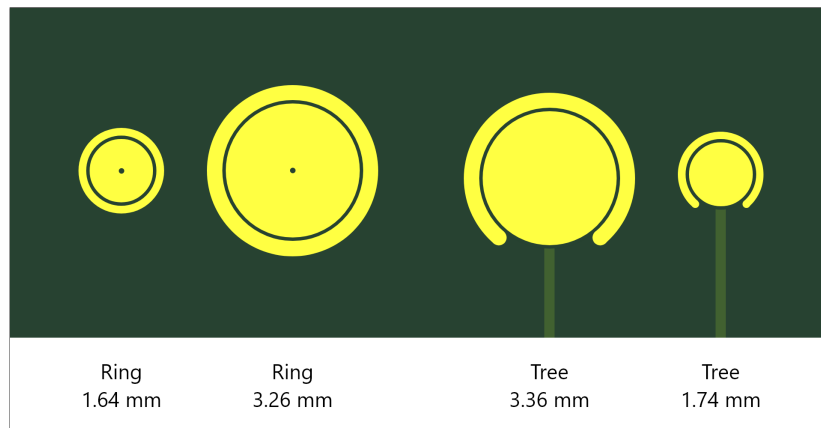


Figure 6.6: Designed force myographic electrodes

Research was already conducted to determine the sensitivity of the sensor, i.e., the ability to measure subtle changes at the first contact. Schürmann et al. (2011) linked the gap-distance, gap circumference, and the passive resistor in the voltage divider to the sensor's sensitivity [173].

Sensor material:

The current solution for the sensor material from Schürmann et al. (2011) uses a conductive foam that is originally used for ESD applications (see figure 6.7). The foam is of a closed-pore structure which means, that gas from the production of the foam is still enclosed in micro-cavities formed by the polymer. The residual surface of the foam is rough due to the micro-cavities. The roughness of the foam is crucial for the sensor principle, as described above. Squeezing the foam increases the contact area with the electrodes, leading to a lower resistance. The foam is highly prone to creep under pressure, which results in a long term signal drift [241].

Research in the German Aerospace Center resulted in a more homogenous and less creeping sensor foil, which can be combined with an intermediate transducer material to measure the applied pressure. The combination of a rough sensor foil and hard intermediate has both characteristics and will be called sensor material. Figure 6.7 shows the different materials, which vary in their resistance or purpose. A special sensor foil was developed to improve electromyographic measurements through the material. For this purpose, the material comprises silver particles, which decreases the capacitive filtering effect and provide a more stable electrode-skin (half-cell) potential [242]. Polymer electrodes are already used in the field, but are not suited for low noise systems due to its high resistivity and prone to generate artifacts [242].

The thickness of the sensor foil is about 30 μm , and the thickness of the intermediate material depends on the desired hardness. The soft intermediate material with a hardness of Shore

A 20 is 2 mm thick. The harder intermediate material is 0.88 mm thick and has a hardness of Shore A 50. The roughness of the active sensor foil has not been measured so far but is estimated to be much smaller than the material thickness.



Figure 6.7: Different types of foams, sensor materials and intermediates. Sample setup of an intermediate - sensor material coupling

Open Positions:

The evaluation of the sensor should at first focus on the general proof of concept with the new sensor material. If the sensor provides force-related information, the electrode sizes and shapes should be tested and compared. The evaluation should compare the new material against the current foam to show improvement. To provide a good calibration for human-machine interfaces, the pre-applied pressure range, when worn, needs to be determined to optimize the sensitivity of the sensor. A maximal pressure should be researched to increase the sensor's sensitivity in the full spectrum of expected pressures. In a future evaluation, the "M" shaped electrode shape should be compared against the new electrode shapes in terms of sensitivity, measurement range, and consistency.

Summary:

In summary, the Weiss & Wörn sensor is well suited for pressure measurements, but adds the constraint of a sensor material for the whole sensor, to avoid edge effects. Its principle is easy and needs a small number of components while enabling a high spatial pressure distribution. The roughness, hardness, thickness, and specific resistance of the sensor material and the electrode size are mainly influencing the sensor output. The developed sensor material will be pre-evaluated in chapter 7.

Nevertheless, research should be conducted with the hardness and roughness of the sensor material, which theoretically links to the sensitivity as well.

6.2 Electromyography

Background:

Referring back to chapter 5.1, electromyography is widely used in the field and seen as the gold standard. Many sensor solutions with different shapes and circuits were developed. Currently, monopolar recordings are trending in research and economy due to the advanced digital signal processing capabilities and techniques, e.g., Delsys Tiber in figure 6.8 (A), chapter 2.4). Nevertheless, bipolar recordings still have their *raison d'être*. A recent paper from Tankisi et al. (2019) introduces new standards of instrumentation of EMG, which can be used as a resource to understand further processes which are not mentioned in this section [157]. The terms of active, reference and ground electrodes are contradictorily used in the field. This thesis uses the term active electrode for both electrodes on the muscle and reference electrode as a mostly remote electrode, which can also be placed in the middle of two active electrodes.

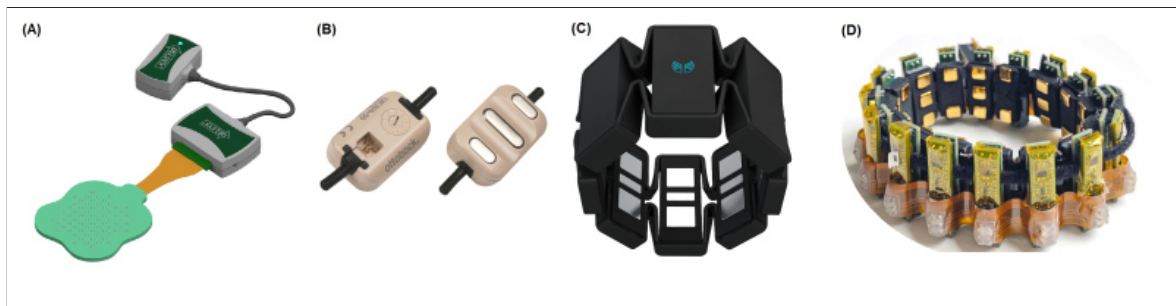


Figure 6.8: (A) Delsys Tiber from [243]; (B) Otto Bock 13E200 from [244]; (C) Thalmic Lab, Myoband from [68]; (D) CTRL-Lab, CTRL-Kit from [245]

Working principle:

Taking essential design principles for electromyographic sensors into account, the sensor should have a high spatial and temporal resolution and a high signal to noise ratio. The main challenge of the design is to decrease the inherited noise. The common-mode rejection rate of the sensor is crucial for obtaining a high signal to noise ratio. Using bipolar setups, the whole system is capable of rejecting noise without a remote reference electrode (also called ground), but reference electrodes are still used in commercially available sensor matrices to suppress the noise level further. For example, the wristbands in figure 6.8 (C, D) have a reference electrode between the active electrodes. This approach results in a tripolar setup but is less beneficial than a reference electrode at a remote bony location (see 5.1). Monopolar setups use a remote reference electrode at a bony structure to solely obtain external noise. The perfect setup depends on the objectives and processing methods (see 2.4). Current sensor solutions, which influenced this work, are shown in figure 6.8. All shown solutions use an

active circuit and amplify the signal close to the origin to avoid cables and connections prior to the amplification.

The difference between bipolar and monopolar setups is the attenuation of cross talk from other motor unit action potentials. Bipolar setups reduce the signal information in trade for a clearer signal with less cross-talk. Monopolar setups are mostly used in a high-density grid to observe single motor unit action potentials. Depending on the following intention prediction algorithm, the setup could provide a signal which consists of the highest possible information density. The current system uses features as input parameters, which result from the raw signal.

Merletti et al. (2011) cover more sophisticated circuits like driven right leg, virtual grounds, and virtual references to further decrease the common-mode from external influences [150]. In this approach, the increased size of the circuit is not arguable for a more detailed signal. Consequently, the signal needs to be digitally filtered at the power line frequency, which is also depicted in figure 6.9. The notch filter needs to be applied even if there is a vital electromyographic signal in this frequency domain. Some researchers mention the usefulness of an electrode-skin impedance circuit. This option was shortly taken into account, but discarded due to size and power constraints. Some small integrated circuit (IC) components like the ADS1298 (Texas Instruments Incorporated., Dallas, Texas, USA) have these features in their chips. However, newer amplifiers increased their input impedance, which makes a change in impedance less pregnant. Nevertheless, a more sophisticated research could lead to a small and efficient measurement circuit which could re-calibrate an automatic gain amplifier to match the input impedance.

The magnitude of the raw input signal composition is depicted in figure 6.9. It clearly shows the reason for ambitious noise canceling circuits in the field of electromyographic recordings. In addition, it shows that ignoring analog filters leads to a smaller resolution and potentially saturated values in the analog to digital converter (ADC).

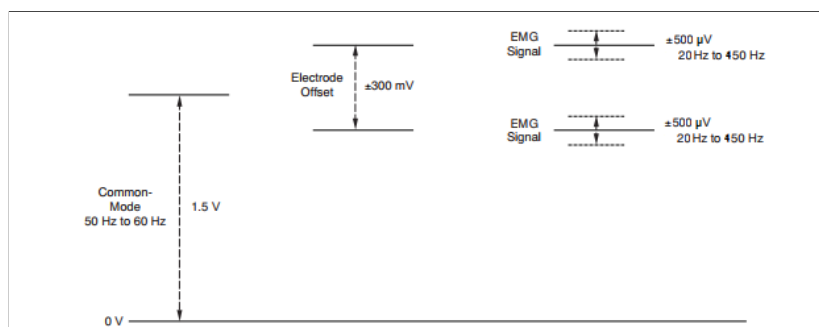


Figure 6.9: Electromyographic signal characteristics. Modified to an EMG typical amplitude and bandwidth from [246]

Circuit:

The circuit of an electromyographic sensor depends on the measurement principle (monopolar, bipolar, tripolar) and if a remote reference electrode is used. The general principle is depicted in figure 6.10. More advanced circuits are discussed in detail in two papers from Prof. Dr. Merlettis group [137, 150].

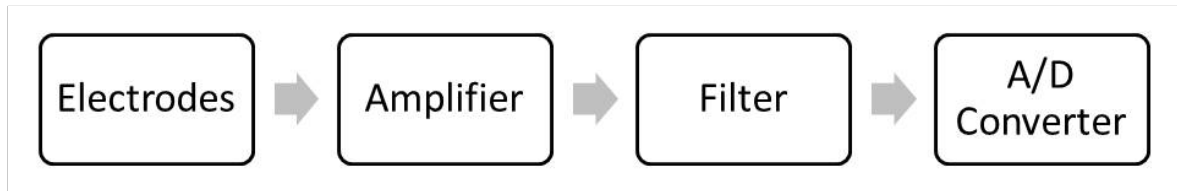


Figure 6.10: General block diagram of an EMG amplifier circuit modified from [247]; A/D Converter = ADC

The principle understanding of differential amplifiers is shown in image 6.11, which shows that a differential signal consists of two monopolar signals. The advantage of a bipolar setup is the higher common-mode rejection, e.g., for muscle cross-talk. The literature and patent research showed a variety of schematics for an EMG/ECG amplification. The pre-evaluation study will use an already built kit, e.g., the Grove - EMG Detector (seeed, Shenzhen, China) or the SparkFun Single Lead Heart Rate Monitor - AD8232 (SparkFun Electronics, Niwot, CO, USA). In general, integrated circuit components are always preferred due to its minimal footprint. Furthermore, it is obligatory to match the length of the traces before amplification to match the resistance. Some setups introduce a level-shift before entering the ADC, due to a limitation in the ADC ability to convert negative potentials.

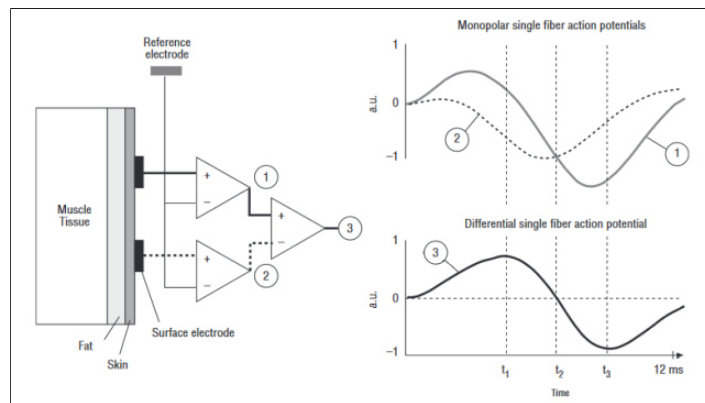


Figure 6.11: Differential EMG modified from [247]

Components:

To match the design principles in chapter 3.1, a small footprint of the components is preferred, which also ensures a higher spatial resolution, because of a possibly higher number of sensors on one module. EMG sensors need a higher number of components compared to an FMG or MMG sensor. The desired components and their requirements, for monopolar and bipolar recordings, are introduced in this paragraph. A biopotential amplifier like the ADS1298 (Texas Instruments Incorporated., Dallas, Texas, USA) could be beneficial but is still large (8 x 8 mm). Using only one electromyographic recording, an AD8232 (Analog Devices, Norwood, MA, USA) integrated circuit could be used with a 4.1 x 4.1 mm footprint size.

Amplifier:

For the acquisition of EMG signals, operational amplifiers and a compound of operational amplifiers named instrumentation amplifier can be used. Critical parameters, which need to be considered for the amplifier, are the input impedance, input-referred noise, and the common-mode rejection ratio. The input impedance is set up in series with the impedance of the electrode and skin; thus, we aim for a high input impedance to get a higher fraction of the signal. The minimum is stated as 100 times higher than the electrode-skin impedance [137]. The common-mode rejection is the parameter that describes the attenuation of the common-mode of the amplifier. A common-mode rejection ratio of 100 dB should be aimed, e.g., to be able to reduce the influence of the power line interference, which is in the range of V, versus μV for the muscle signal (see figure 6.9) [248]. Furthermore, it is important to set the gain appropriately to avoid saturation of the ADC or end up with a poor resolution.

Filtering:

High-pass filtering prevents the DC signal source from propagating further, and it is achieved with a capacitor in series with the signal (see 6.12). DC signal fractions act as an offset in the signal and could lead to a saturated ADC, filtering it increases the resolution (see figure 6.9). High-pass filters are no longer necessary in the amplification chain if the ADC resolution and range is large enough. Nevertheless, a digital filter is mandatory afterward. On the other side, low-pass filters filter high-frequency signal components; this is used in achieving a small ripple, but useless in our application. Nevertheless, the circuit needs a low-pass filter to avoid antialiasing due to the sampling frequency of the analog to digital converter. A low-pass and high-pass filter can be achieved using a Resistor-Capacitor element (see figure 6.12).

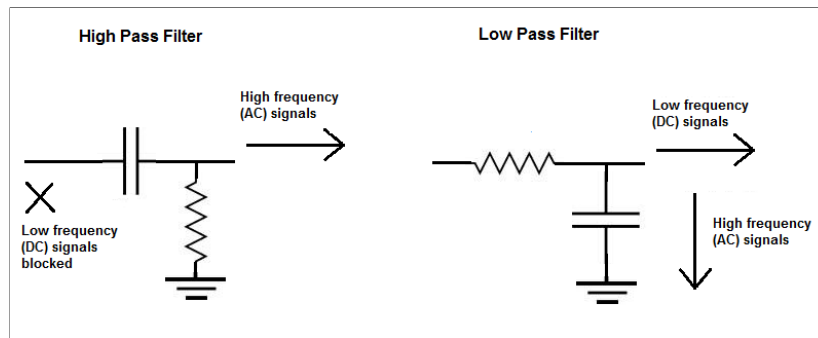


Figure 6.12: High-pass and Low-pass filter circuits from [249]

Electrodes:

Electrode shapes and inter-electrode distances were widely discussed over the last decades [250, 137]. For monopolar recordings, Merletti et al. (2010) deduced distances in an older review and a recent paper using underlying biomechanical principles [150, 251]. The electrode size averages the signal in space, thus a diameter of $d < 3 - 5 \text{ mm}$ is suggested but can also be reduced to 1 mm [251, 135]. To avoid aliasing, the sampling frequency in space must be small enough to satisfy the Nyquist criterion ($e < 5 - 10 \text{ mm}$) [150, 251]. Merletti et al. (2010) and Afsharipour et al. (2019) also propose that the signal frequency shifts with different setups and is not comparable to other approaches.

Bipolar recordings still have larger electrode sizes (max. 10 mm), which are capable of detecting deeper muscle signals. The inter-electrode distance (e) is a crucial parameter for bipolar recordings. Smaller distances suppress the muscle cross-talk heavily, while larger distances offer more motor unit action potentials in the signal, as seen in figure 6.13. Double-differential (tripolar) recordings suppress noise in both longitudinal directions and isolate the signal. De Luca et al. (2012) researched the inter-electrode distance from bipolar setups and examined a distance of 10 mm from center to center as optimal for reduced cross-talk [149]. Smaller inter-electrode distances are critical due to lower potentials and thus higher baseline distortion [149].

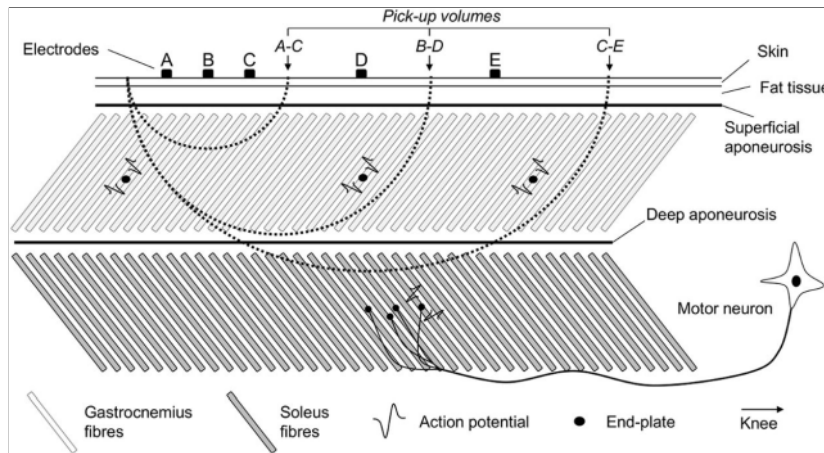


Figure 6.13: Dependency between the inter-electrode distance and pick-up volume from [252]

Using round or rectangular electrode shapes does not make a difference for the setup; however, it is important to use the same electrode size for bipolar setups to match the input impedance and to obtain the same amount of peripheral information/noise [149, 253]. Compared to standard shapes, Farina et al. (2001) brought back an older idea of round electrodes with a reference circle (see. figure 6.14) [250]. The results were promising, but the technique was not further developed. The positive idea of these electrodes is the shielding against cross talk from all directions, which suites them for the high density of muscles in the human forearm (see chapter 4). According to Merlettis principles about the inter-electrode distance (e) of smaller than 5-10 mm, a setup containing a concentric ring electrode should be evaluated. In the prototype in figure 6.16, the match of the electrode area is ignored. In future setups, the area should match.

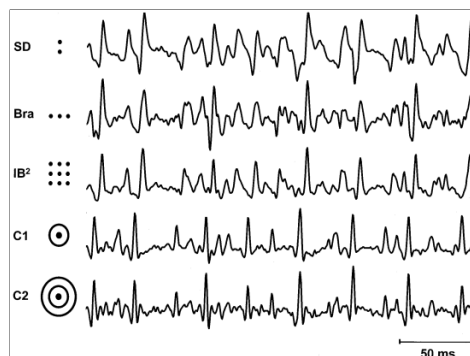


Figure 6.14: Motor unit spike trains of five different electrode principles [250]

The electrode size directly correlates with the amount of collected motor unit action potentials [253]. Thus, one set will have smaller and one set larger electrode sizes. Larger electrode sizes will have a higher density of information, while smaller will provide more obvious and

easier features for a feature-based detection algorithm. In addition to research-based bipolar setups, some state-of-the-art commercial setups were designed. A setup with a larger reference electrode, which is adapted from Otto Bock's 13E200, but limited in width, is shown in figure 6.15 (4). The adaption of the Myoband in figure 6.15 (3) uses a smaller reference electrode. A universal setup that can be used with a remote reference electrode was developed in figure 6.15 (1). Figure 6.15 (2) follows the research of De Luca et al. (2012) with an inter-electrode distance of 10 mm [149]. It can be used with a remote reference electrode or in a double differential setup (tripolar). The electrode size could not be adapted to the literature preference of 10 mm diameter and was maximized to 5 mm, due to the limited PCB width, which aims to obtain a high spatial resolution.

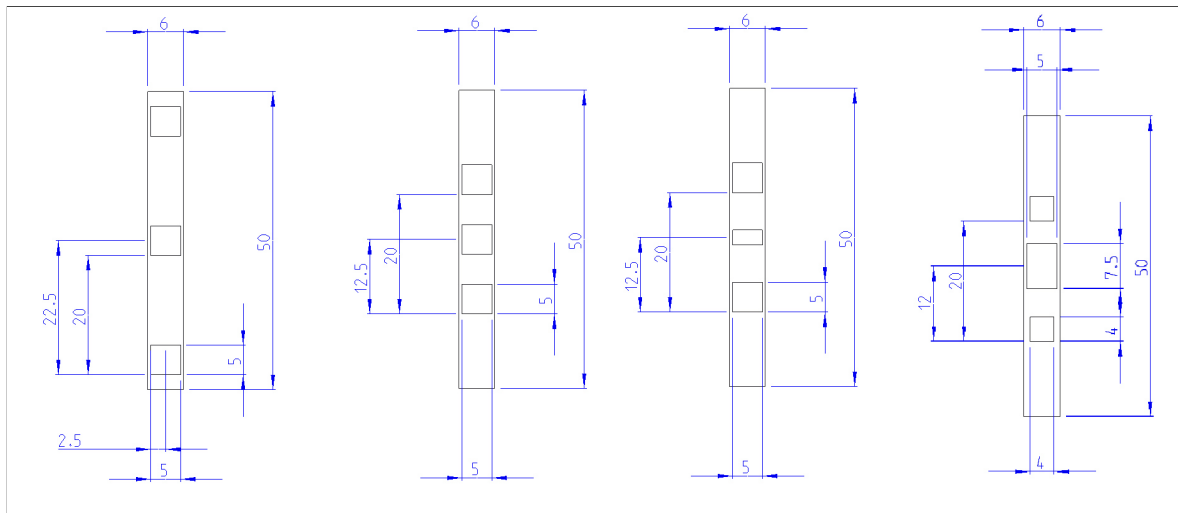


Figure 6.15: Units: mm; (1) Bipolar (Double Differential) setup with a high inter-electrode distance; (2) Bipolar (Double Differential) setup with a smaller inter-electrode distance; (3) Bipolar (Double Differential) setup with smaller reference; (4) Bipolar (Double Differential) setup with a larger reference

The monopolar approaches follow the research of Merletti et al. (2010) and Afsharipour et al. (2019) [251, 150]. The first sketch in figure 6.16 uses a small inter-electrode distance of 4 mm and a small electrode size. This setup will potentially be able to track single motor unit action potentials. The second sketch has larger electrodes to obtain more and deeper motor unit action potentials with an inter-electrode distance of 8 mm. Both monopolar setups require a remote reference electrode.

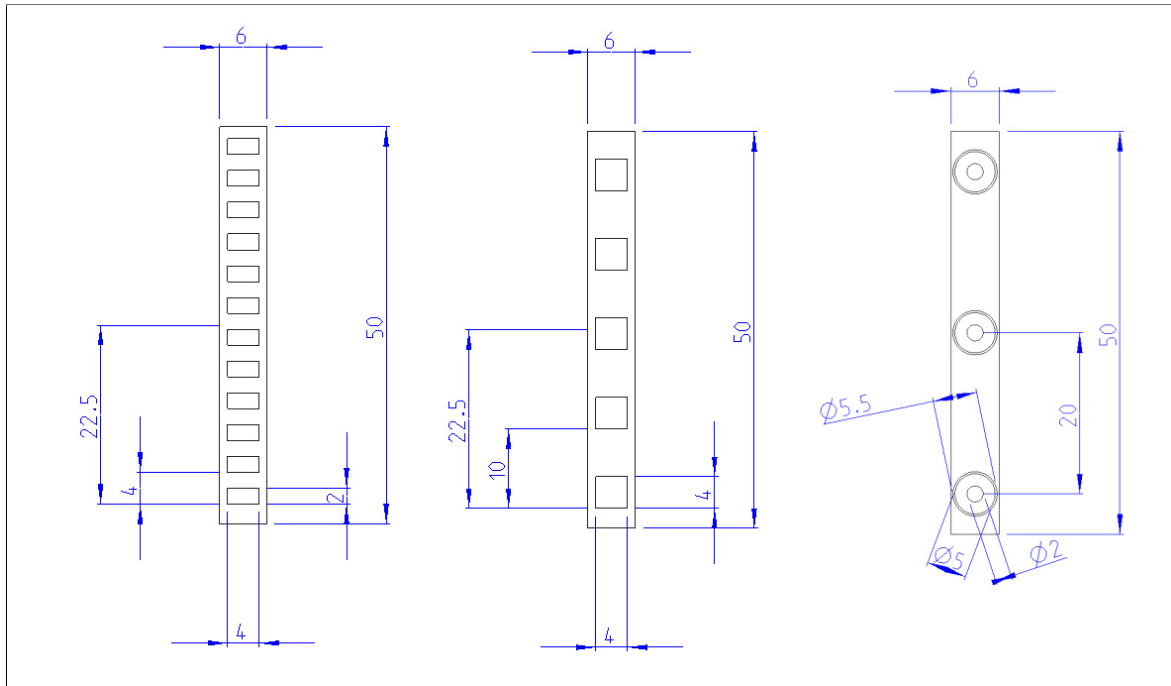


Figure 6.16: Units: mm; (1) Monopolar setup with a small electrode size and a small inter-electrode distance; (2) Monopolar setup with a larger electrode size and inter-electrode distance; (3) Monopolar setup with a small reference ring

Sensor material:

Using a force myographic sensor, the outer sensor material should be consistent and not vary in height. The introduced force myographic sensor in chapter 6.1 uses a sensor material that is applied on the sensing electrodes. Thus, the electromyographic sensor should also use the sensor material. The sensor material can also act as a protective membrane against dust and perspiration and adds robustness to the sensor. The thesis assumes that applying silver particles into the sensor material, enhances the recording of EMG signals, which needs to be proven in an evaluation. The general idea is to decrease the half-cell potential. Silver-chlorid (Ag-Cl) is used in commercially available electrodes and has a small half-cell potential; thus, silver molecules could also be beneficial in the designed setup [254]. The sensor material should be directly applied to the electrode surface, enabling a close and low impedance connection compared to a loose connection.

Open positions:

Research about the electromyographic sensor resulted in a range of open positions. The most important position is to prove the concept of recording through a sensor material. The impedance of the setup should be measured to set the gain of the amplifier and fulfill the ratio of a 100 times higher amplifier impedance. The signal to noise ratio should be calculated to

determine the least significant bit of the ADC to define the necessary resolution. The future evaluation should test the designed setups regarding their accuracy in an upper limb control task. Furthermore, the effectiveness of a remote reference electrode for bipolar recordings should be investigated. It is urgent to not compare the setups directly, due to different parameters and recording techniques, just an intention detection accuracy test is capable of providing a full comparison.

Summary:

In summary, the design covered monopolar, bipolar, and tripolar recordings, also called referential, single differential, and double differential. The sensor consists of one or more electrodes, an amplifier, a filtering circuit, and an analog to digital converter. The electrodes differ in size and inter-electrode distance, depending on the goal. The amplifier should have a high input impedance, low input-referred noise, and a high common-mode rejection ratio. The gain of the amplifier is crucial; if set wrong, the digital signal is cut off or has a small resolution. The filtering circuit consists of a low-pass filter and optionally a High-Pass filter to reject DC-Noise. The last component in the circuit is the analog to digital converter, which translates the analog signal into a digital value. In total monopolar circuits have fewer components, but due to its application in high-density grids, the higher number of sensors also ends up in a high number of components. In addition, monopolar signals need a remote reference electrode, while bipolar recordings can reject noise at the recording site.

6.3 Mechanomyography

Background:

Referring back to the mechanomyographic chapter 5.3, there is a variety of different techniques to obtain the oscillations of the muscle fiber. Acoustic myography has advantages regarding the signal to noise ratio but is larger. The only commercially available acoustic myographic sensor, shown in figure 6.17, is from the company MyoDynamik ApS [214]. It samples at 4 kHz, has a size of 20-mm, and is coated with acoustic gel to improve the signal quality. Other mechanomyographic sensors like the ViBand use smartwatch accelerometers or piezoelectric sensors (see figure 6.17) [255, 256].

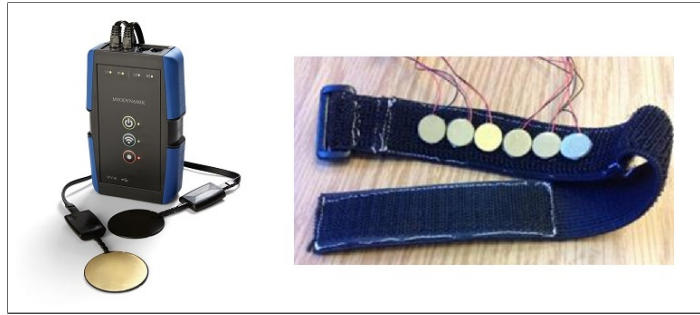


Figure 6.17: (A) Myodynamik acoustic myographic sensor from [257], (B) Research piezoelectric sensor from [256]

Due to size constraints in the setup, large components like the acoustic or piezoelectric sensor can not be used. Thus, the focus is on accelerometer-based recordings. Promising research was made with accelerometers, and some researchers concluded that their sensors could enhance the signal density of an EMG system [215, 219]. For this purpose, a micro electrical mechanical system (MEMS) will be used. The disadvantages in terms of noise should be faced with sophisticated digital signal processing techniques and an IMU on the master module of the sensor matrix. Further information about digital signal processing and features regarding MMG recordings can be found in Krueger et al. (2014) [215].

Working principle:

Lateral muscle oscillations can be measured with a free-swinging body's inertia, which slower adapts to external accelerations. A MEMS accelerometer, as depicted in figure 6.18, consists of fixed plates and a spring-mounted body with a known mass. The capacitance between the fixed plates and the moving body is obtained. Depending on the distance between the two plates, the capacitance will change. Moving the whole sensor system, the body will accelerate, and the spring-mounted mass wants to stay in its position, based on newton's first law (inertia). Thus, the fixed parts are moving, while the spring-mounted mass will stay in its position until it adapts.

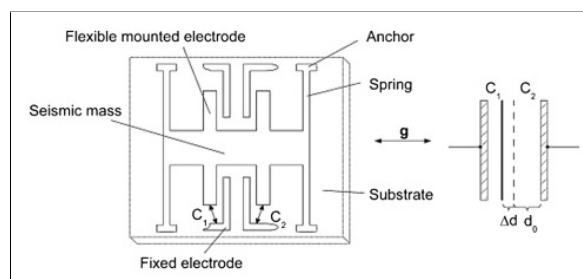


Figure 6.18: Measurement principle of an accelerometer from [258]

After the muscle fiber twitch, small muscle oscillations propagate to the skin (see chapter 4).

The sensor adapts the oscillations, which leads to a change in the capacitance of the described sensor (see figure 6.18). The obtained signal consists of the sum of all propagating oscillations. Advanced systems use a differential sensor setup, in which both sensors oscillate independently of each other. Free oscillations can be guaranteed if the sensors are mechanically uncoupled. These setups can attenuate the common-mode of the sensor with a differential amplification. However, the already stated design principles in chapter 3.1 are leading to a printed circuit board, where the oscillations are transferred through the sensor material and the circuit board. Hence a differential mechanomyographic setup is not possible. Nevertheless, a massive advantage of these sensors is the size and offer of integrated circuits (IC) on the market. Due to the application in many fields of everyday life, manufacturers can offer small footprints and a digital output signal for a low price. Thus, an accelerometer is using a small fraction of the limited space on the circuit board.

Circuit:

The circuit consists of a 3 degree of freedom (DOF) accelerometer with a digital output and a sensitivity of $\pm 2 g$ [111, 259]. Figure 6.19 depicts the functional block diagram of a sample accelerometer (ADXL345, Analog Devices, Norwood, MA, USA). It consists of an I²C interface, which transfers the digital value.

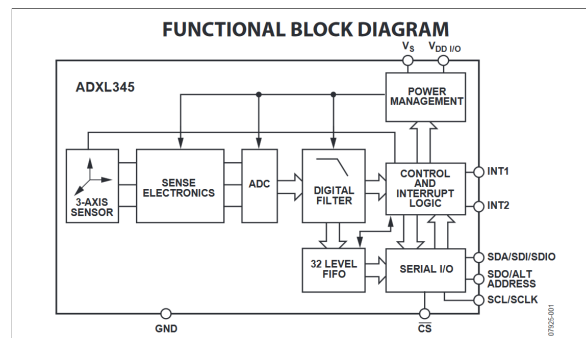


Figure 6.19: Sample functional block diagram of the ADXL345 accelerometer from [260]

Components:

As already introduced in the circuit, the only component for measuring mechanomyographic signals is an integrated accelerometer circuit. To obtain valid sensor data, the supply voltage to the IC should be consistent to avoid a noisy signal. The data lines of the integrated circuit can use a resistor to reduce the current flowing into the input pin. Having such an all-inclusive designed sensor, the residual constraints are a small footprint and a high resolution. The used IC from NXP Semiconductors (Eindhoven, Netherlands) FXOS8700 is small (3 x 3 mm) and offers a resolution of 14 bit [261].

Open positions:

Some open questions can be devised regarding our specific setup. Are low-cost accelerometers capable of measuring myographic signals and how much does the sensor material of the force myographic sensor attenuate the lateral muscle oscillations.

Summary:

Accelerometers have already shown to be a good additional modality for a sensor fusion [215, 219]. The designed sensor consists of a low-cost accelerometer, which potentially offers a mechanomyographic signal with a small footprint and a high resolution of 14 bit without blocking an ADC channel.

6.4 Further sensors

Sensors that enhance myographic measurements were already introduced in chapter 5. Two sensors provide promising signals and add further information about the orientation of the arm. Both sensors are used for motion detection and provide signals related to the current limb position. A temperature sensor can be used to compensate for systematic errors in the signal and to observe the temperature changes for the mechanomyographic principle.

Inertial Measurement Unit:

An IMU is widely used in areas for motion detection. It uses an accelerometer and gyroscope to predict the current position; in some circumstances, a magnetometer is additionally used. Using a magnetometer, which is vulnerable to electromagnetic noise, can lead to false predictions. There is a variety of IMU's on the market. Buying a raw IMU, the development process needs to deal with a sensor fusion approach to fusing the three components: gyroscope, accelerometer, and magnetometer. Bosch (Gerlingen, Germany) sells a variety of IMU's in their sensortec department, with a broad use case. Avoiding a self-made Kalman-filter sensor fusion, Bosch offers the BNO055, which has a sensor fusion software on board. The sensor has a small footprint of 5.2 x 3.8 mm. As output values, the BNO055 offers Quaternion, Euler angles, Rotation vector, Linear acceleration, Gravity, and Heading. Regarding the decreased workload of an in-built Kalman-filer and the size, a higher price is justifiable.

Barometer:

While using an IMU is a standard nowadays, fewer people use a barometer to enhance their motion detection algorithm. Authors who used an additional barometer for a movement classification task were able to enhance their predictions [238]. MEMS barometers are very sensitive nowadays and able to provide a high-resolution altitude change. The Bosch BMP085 provides a resolution of up to 10 cm. Other high-end sensors guarantee 1 cm resolution

(HP206C, Hope Microelectronics co., Ltd, Shenzhen, China) with a larger footprint [262]. These resolutions, in addition to the IMU output, should provide a valid sensor fusion for motion and limb position detection. The evaluation should predict the intention of the user in a test battery with both sensors, isolated and using no sensor, to proof the concept.

Temperature sensor:

Temperature sensors can be beneficial when applying a mechanomyographic sensor. They are available in small sizes and are sometimes integrated into an existing chip that measures other sensor data. The temperature sensor can also correct systematic errors/drifts in sensors. It should be beneficial for the system to use the temperature sensor in long term applications.

6.5 Discussion

The sensor fusion between FMG and EMG seems feasible and promising. The force myographic sensor is cheap, small, and needs few components. Nevertheless, the sensor material sets a constraint, which needs to be solved. However, the sensor material can also be used to create a separation between the sensors and electronics and the user's sweat. The electromyographic sensor was carefully designed and is optimized for a feature-based machine learning approach. The mechanomyographic sensor adds the lateral muscle oscillations to the signal with a small integrated circuit component. It needs to be evaluated if the base sensor material of the sensor matrix is transferring muscle cell potentials and high-frequency oscillations or if it suppresses the muscle potentials and low-pass filters the desired oscillations. To address the difficulties in the myographic signal recording, an inertial measurement unit, and a barometer are used to decrease the influence of the limb position effect. The sample rate of the sensors should use the widely applied four-time oversampling paradigm.

7 Sensor Pre-Evaluation

This chapter pre-evaluates the designed sensors and proves the general concept without statistical evidence. The designed force myographic sensor is measured in a standardized machine setup to obtain its sensitivity. Afterward, all sensor modalities are tested for the desired myographic information of one subject in a standardized test setup. The resulting parameters are presented and compared to the introduced signals from chapter 5. Due to its prominence, the musculus biceps brachii is recorded; thus, we can safely determine a muscle activation. The sampling size of one subject is insufficient to conclude the real effectiveness, but it shows if the general idea of a high-density multi-modal sensor setup with small sensors is feasible. A full evaluation with reference systems needs to be conducted with the final machine learning approach and compared in the resulting accuracy in an upper limb control task. Thus, this chapter does not aim for a full evaluation against the main quality criteria (reliability, validity, and objectivity) and is also not evaluating all setups. The goal is to show a small sample dataset, which proves the general concept and provides suggestions for adjustments.

7.1 Standardized myographic protocol

The goal of a standardized myographic protocol is a comparable dataset. The sensor was placed on the muscle belly of the biceps, as researchers state it as the most prominent signal location (see chapter 5.3). For EMG measurements, it can not be assured that the sensor is not located on an innervation zone. The recording site was marked to re-apply it in a second condition. The test protocol covered an isometric biceps activation. The elbow was placed on a table, and weight discs were stored in a bag. The subject lifts the bag and withstands the torque around the elbow with exerting a force in the biceps. A soft object was placed at the desired elbow joint angle, and the subject was instructed to gently touch the object while sitting upright (see figure 7.1). The elbow angle was about 45° flexion. The measurement lasted for ≈ 5 seconds until the subject got a self-paced break. The obtained load levels are 5, 10, and 15 kg. The load was randomized to avoid muscle fatigue and other load-related errors in the signal. For each load, 6 repetitions were obtained. The investigator noted the start and stop time of each trial.



Figure 7.1: Standardized myographic test protocol

7.2 Force Myography

The pre-evaluation of the introduced FMG sensor from chapter 6.1 is divided into two steps. The first step pre-evaluates the pressure dependency of the sensor. The second step is a force myographic measurement. The pre-evaluation study uses the smallest electrode to proof the concept. The sensor material differs between the two sets, due to sensitivity.

Test setup 1:

The first test setup shows the voltage-pressure characteristics of the new designed electrodes and sensor material, which is then used to optimize the sensor material and electrode shape to the desired sensitivity and measurement range.

Material:

The test-setup of the force myographic sensor consists of five circular sensors with an outer circle diameter of 1.64 mm (see figure 6.6). Two of the electrodes are connected to a small voltage divider circuit and a DAQ (Meilhaus 1208 FS, Meilhaus Electronic GmbH, Alling, Germany). The passive resistor has a value of 10 k Ω . The setup is shown in figure 7.2 (B). The resolution of the DAQ is 12 bit, and the measurement range was set to ± 10 V; thus, the smallest step-width is 4.88 mV. The pressure is applied with a Zwick-Roell ZMART.PRO BZ1-MM14450.ZW01 (ZwickRoell GmbH & Co. KG, Ulm, Germany) measurement setup, with an indenter diameter of 10 mm. Consequently, a load of 5 N results in 0.064 MPa. The indenter's contact area is minorly ellipsoid to compress the material starting from the middle to avoid edge effects. The used sensor material consists of the normal sensor foil in combination with the hard intermediate (see figure 6.7). The tested sensor material has a hardness of Shore A 50. The data acquisition software is written in LabVIEW (National Instruments, Austin (TX), USA) and acquires the data with a sample rate of 10 Hz.

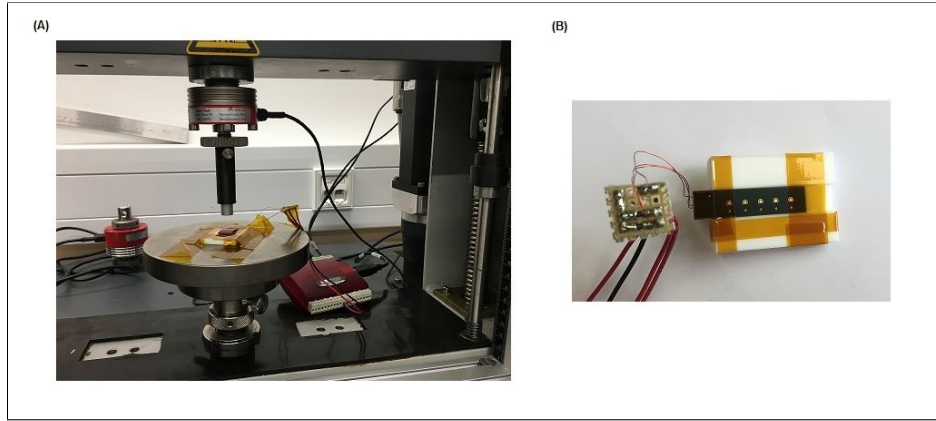


Figure 7.2: FMG-Setup: (A) Zwick-Roell setup with 10 mm indenter and the fixed sensor on the measurement table; (B) Sensor circuit with a custom made voltage divider circuit. The sensor is fixed in a hard plastic housing

Method:

Figure 7.2 (A) depicts the setup of the Zwick-Roell. The sensor is fixed with tape on the rigid Zwick-Roell measurement table to keep the sample in place. The traverse can freely move on the Z-axis to apply pressure on the sensor. A force-controlled protocol is used in the setup to control the load on the FMG sensor. The chosen test protocol is derived from DIN 53579-1, with a repetitive triangle-shaped load profile from 0 to 5 Newton. The pressure is applied to the sensor material with a maximum speed of 0.25 mm/s. This procedure is repeated 10 times to acquire a moderate number of samples, which can be used as a valuable guidance for improvements on the sensor.

Data processing:

The data processing was conducted in MATLAB 2018b (The MathWorks Inc., Natick, Massachusetts, USA). The data was split into each load cycle using the recorded force data. The cycles were divided into rising and falling edge. The rising edges are further used. The ten trials were interpolated to fit in length. The pressure was calculated using the area of the indenter and the desired force. The pressure is plotted as the abscissa and the analog to digital converter value as the ordinate to create the voltage-pressure characteristic.

Results:

Figure 7.3 (A) shows the tactile sensor performance of the "M" shaped electrode and a sensor material based on a soft foam [57]. The sensitivity starts at 0 N, and the analog to digital converter saturates at approx. 2 N or 0.02 MPa (based on the mentioned indenter area of 1 cm²). The acquired sensor-pressure characteristic of the designed sensor is shown in figure 7.3 (B). The sensitivity starts at 0.02 MPa, and a bending of the flank can be interpreted between 0.05 and 0.06 MPa. The resolution of the analog to digital converter was not fully used.

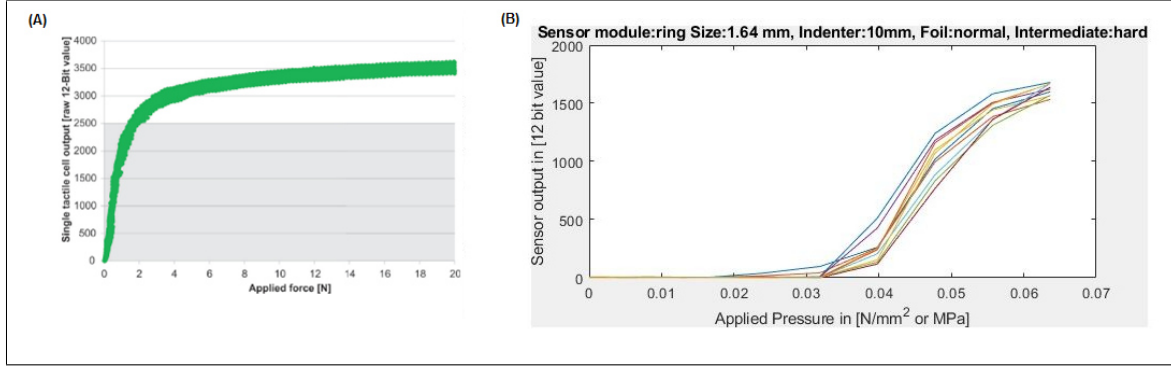


Figure 7.3: (A) Characteristic curve of Kõiva et al. (2015) [57]; (B) Rising edge of 10 repetitions from 0-5 N with a 10 mm diameter indenter using a 1.64 mm electrode and a sensor material combination of a normal sensor foil and hard intermediate

Discussion:

The results show that the sensitivity differs from the designed sensor from Kõiva et al. (2015) [57]. Adjustments to the setup are necessary to fit into the desired measurement range, being sensitive from the pre-applied pressure at the arm. The passive resistor in the voltage divider, the conductive properties of the electrodes contact area could be adapted to ensure a higher voltage under load, which increases the resolution of the sensor. The design idea from chapter 6.1 proposes to change the sensor material characteristics and keep the other constraints constant to achieve a high signal resolution (passive resistor) and spatial resolution (electrode size). In general, the sensor shows a clear pressure dependency and is suited to be used in a human-machine interface as a force myographic sensor. However, the sensitivity and other parameters need to be adjusted to optimize it for the application on the human forearm. The complete set of elastomer depended characteristics need to be examined to state the influence of creeping under load and hysteresis. In a future trial, the sample rate and maximum pressure need to be increased to sample a higher temporal resolution and a larger pressure characteristic of the sensor. The full evaluation study should also take the designed larger electrodes and different sensor materials into account to fully understand and model the behavior of the used sensor.

Test setup 2:

The second test setup records data from the designed sensor to show its myographic information. Furthermore, the signal will be processed to compare the frequency domain against the MMG frequency domain. Due to the missing sensitivity of the new sensor material, the setup changes to the rough and soft foam from figure 6.7. Thus, the pressure can not be stated; however, it is still possible to show the myographic phenomena.

Material:

The setup is shown in figure 7.4 and consists of the 1.64 mm ring electrodes from figure 6.6. The rough and soft foam from figure 6.7 was fixed with isolating tape on the electrodes. The electrodes are connected by hookup wire to the voltage divider circuit, which has a $10\text{ k}\Omega$ resistor in series. The signal is processed to a Meilhaus 1208FS DAQ (Meilhaus Electronic GmbH, Alling, Germany). The data acquisition software DAQAmi from Meilhaus Electronic GmbH was used to record the signals. The sample rate was set to 1 kHz.

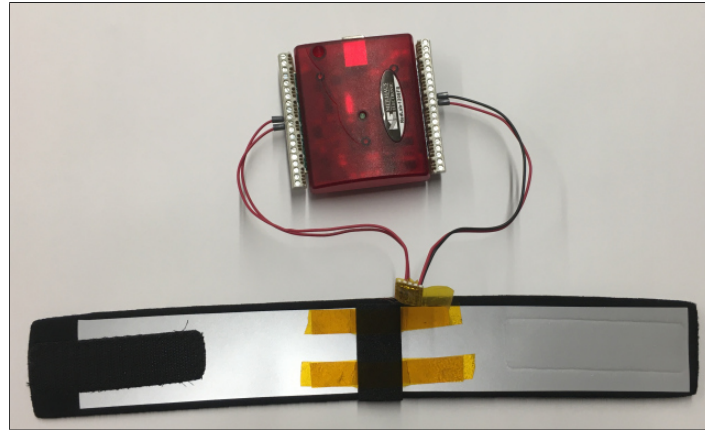


Figure 7.4: FMG-Setup 2: The electrodes are placed on the wristband, and the sensor material is fixed with tape on the electrodes

Method:

The test protocol is described in the standardized protocol section 7.1.

Data processing:

The data processing is conducted with MATLAB 2018b (The MathWorks Inc., Natick, Massachusetts, USA). The baseline shift of the signal was corrected, and the whole signal was downsampled to 200 Hz. To calculate the RMS values, the signal was low-pass filtered with a cut-off frequency of 99 Hz. To compare the MMG and FMG signals, the data was two times differentiated before a band-pass filter with cut-off frequencies of 5 and 99 Hz was applied. The mean frequency was calculated using the MATLAB inbuilt FFT-function with squaring the double-sided power spectrum to get the power spectral density.

Results:

The Root Mean Square value in figure 7.5 rises with an increased load. The standard deviation is small and does not span in the mean values of the other loads.

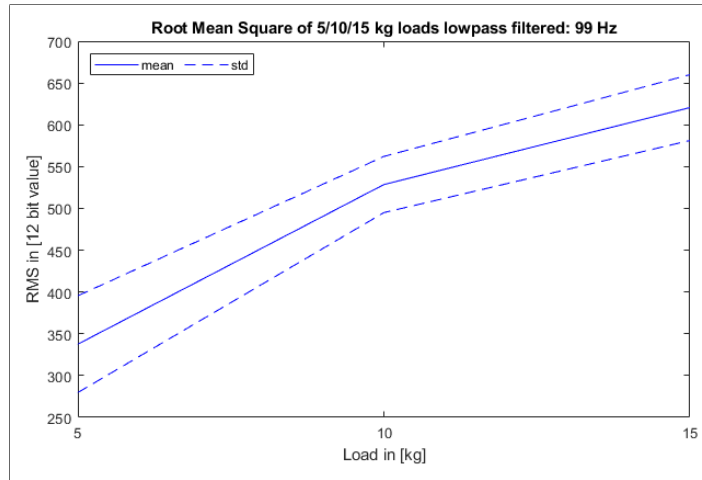


Figure 7.5: FMG - low-pass filtered at 99 Hz; 5/10/15 kg load; 6 repetitions; 1 subject

Figure 7.6 shows the bandpass filtered FMG signal with the same setup the MMG pre-evaluation will use in section 7.4. The mean power spectral density between the 3 loads is similar to each other. The mean frequency shows a decreasing spectrum with increasing load. The mean Root-Mean-Square value of the load shows the same behavior.

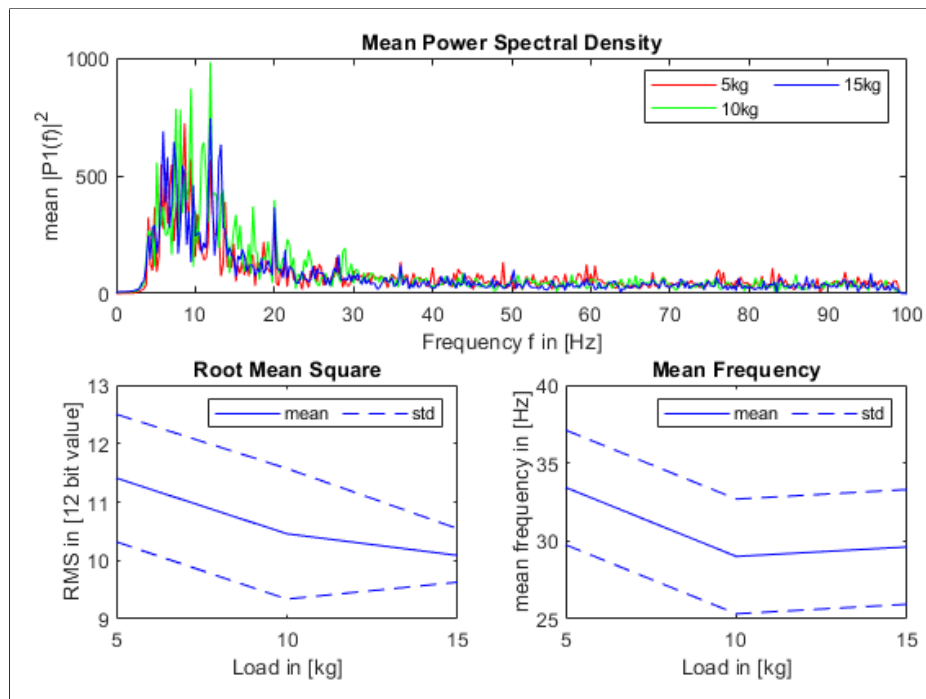


Figure 7.6: FMG 2nd derivative - band-pass filtered at 5-99 Hz; 5/10/15 kg load; 6 repetitions; 1 subject

Discussion:

The RMS value shows a clear and valuable dependency on the increased load; thus, the sensor adds myographic information to the sensor matrix if embedded. The second objective was a comparison between the signal of MMG and the second derivation of FMG. Comparing to the literature in chapter 5.3 it can be concluded, that the second derivation of our FMG sensor is not suited to obtain the MMG phenomena. Thus, redundancy between the two modalities is not expected. For a FMG sensor, it should be taken into account that the application in a stretchable band will act as a spectral filter in dependency of the elastic behavior of the band. Furthermore, an increased signal could occur on the opposite sensor (180°) of the band, which is on the same line of action. A creeping effect of the foam is not expected in the obtained short time activation.

7.3 Electromyography

Test setup:

The pre-evaluation of the electromyographic sensor uses the tripolar/double differential setup to proof the concept of measuring an electromyographic signal with small electrodes and a sensor material (sensor foil, no intermediate).

Material:

The used materials for the pre-evaluation are the prototyped tripolar printed circuit board with 10 mm inter-electrode distance (see chapter 6.2 (B)) in figure 6.15, the normal sensor foil and a modified SparkFun Single Lead Heart Rate Monitor - AD8232 with a gain modifying potentiometer (Bourns 3296, Bourns Inc., Riverside, CA, USA) instead of resistor 8 (R8) in the schematic (see [263]). The signal is transmitted in a non-shielded cable (1 mm diameter, 40 cm long) and connected to the proposed SparkFun board with a jack plug. The reference measurement used adhesive electrodes (ECG Solid Gel Electrodes, Bio Protech Inc., Wonju si, Korea) and passed the signal through a non-shielded cable (1.9 mm diameter, 100 cm long) to the jack plug. The SparkFun board amplified and pre-processed the obtained potential from the electrodes and transferred the analog signal by standard jumper cables to a Meilhaus 1208-FS DAQ (Meilhaus Electronic GmbH, Alling, Germany). The DAQ has a resolution of 12 bit and was set to a sample rate of 1 kHz. To ensure a constant electrode-skin impedance, the sensor material needs to be tightly coupled to the electrode. The setup used isolation tape to fix the sensor material on the electrodes. The sensor material should be isolated from each other to avoid noise. The used materials are shown in figure 7.7.

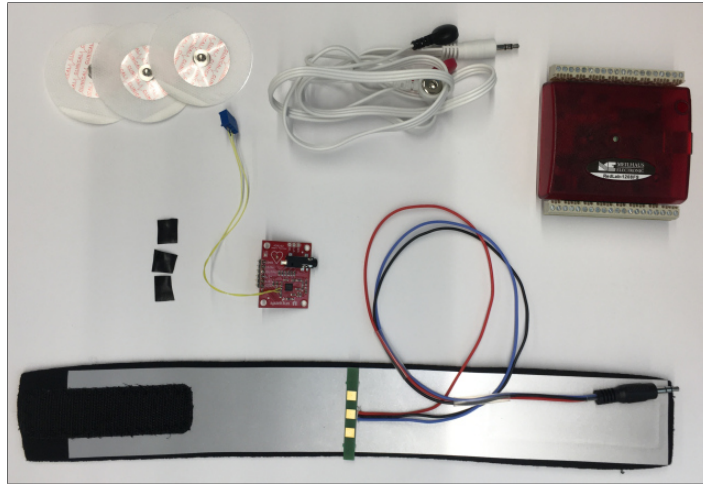


Figure 7.7: EMG-Setup: The reference measurement used the adhesive electrodes and the white cable. The sensor foils were fixed on the three electrodes with isolated tape

Method:

The test protocol is described in the standardized protocol section 7.1. The reference measurement was conducted first, the plain tripolar circuit board as the second and the tripolar circuit board with sensor foil as the last setup. For the reference measurement, the adhesive electrodes were cut to a smaller size and placed in muscle fiber alignment with an inter-electrode distance of 2 cm. A smaller inter-electrode distance was not possible due to the size limitations of the electrodes. The remote reference electrode was placed on the ulna bone close to the elbow joint.

Data processing:

The data processing was conducted with MATLAB 2018b (The MathWorks Inc., Natick, Massachusetts, USA). The raw data was split into each trial and reduced to the smallest occurring duration. The reduction cuts the beginning and end of the signal. Interpolation is not necessary due to the stationary signal of an isometric task. The raw data was filtered with a 3rd order band-pass filter at 20-450 Hz and a Notchfilter at 50 Hz with a q factor of 40 to suppress power line interference. The q factor was based on test-measurements. The Root Mean Square value was generated with the rectified and filtered raw signal. The power spectral analysis was conducted with the inbuilt FFT-function and squaring the double-sided amplitude spectrum before normalizing.

Results:

Figure 7.8 shows the normalized Root Mean Square (RMS) value and the median frequency in relationship of the load. The RMS is similar in the reference and plain PCB condition, while the normal sensor foil has a different slope. In general, all three conditions are showing a rise in RMS with an increased load. The standard deviation of the sensor foil measurement

is wider than the deviation of the two other conditions. The mean median frequency of all six trials shows a nearly constant behavior with an exception between 5 and 10 kg in the plain PCB condition. The median frequency is shifted in between all conditions. However, the standard deviation is stable in all conditions.

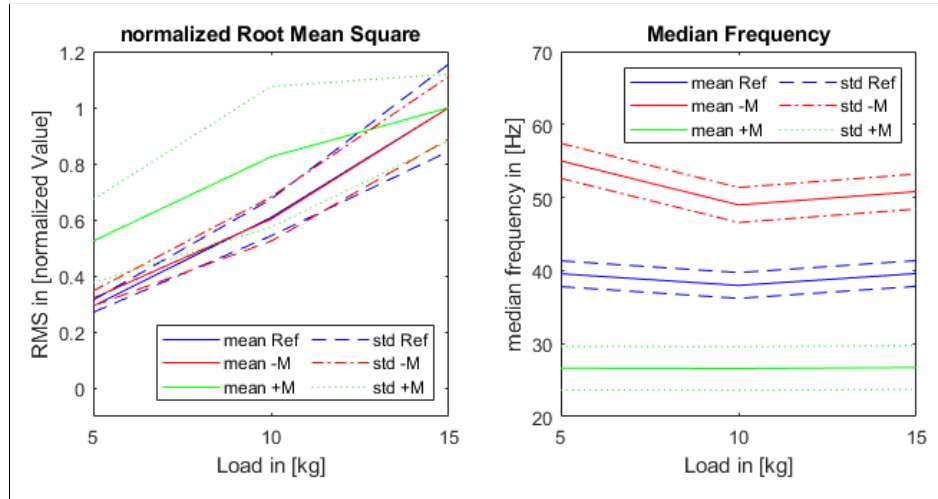


Figure 7.8: EMG RMS and Median Frequency: band-pass filtered at 20-450 Hz; 5/10/15 kg load; 6 repetitions; 1 subject

Figure 7.9 shows the filtered EMG-Signal with the two noted start and end times of the task. It can be seen, that the reference measurement has the clearest signal, while the other two conditions have less prominent activations.

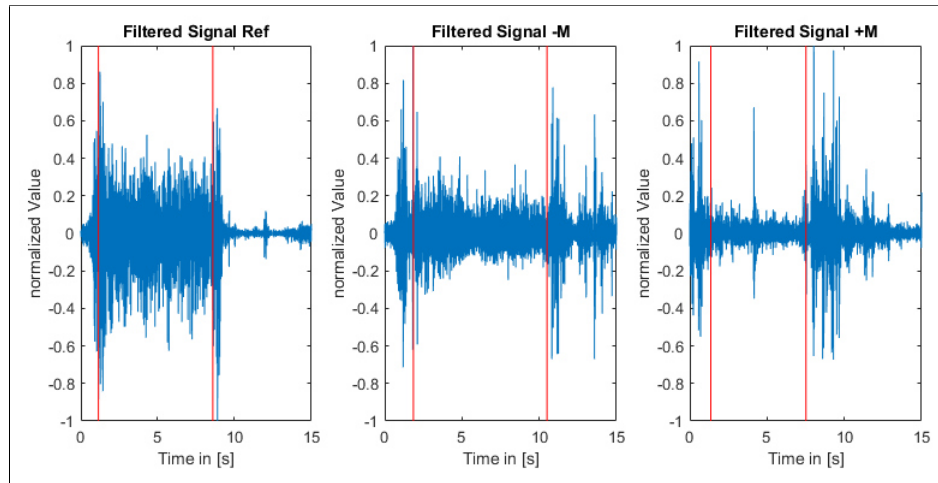


Figure 7.9: EMG Filtered Signal: band-pass filtered 20-450 Hz; 10 kg; Ref = adhesive electrodes, -M = raw PCB, +M = PCB with sensor foil

The mean Power Spectral Density of the three conditions is shown in figure 7.10. The frequency band was shortened, due to absent signal components after 200 Hz in all conditions.

The spectral density of the PCB without the sensor foil shows the largest frequency domain with powers in frequencies of up to 130 Hz. The PCB with the sensor foil shows a frequency domain of up to 70 Hz. The power magnitude differences between the loads are visually distinguishable.

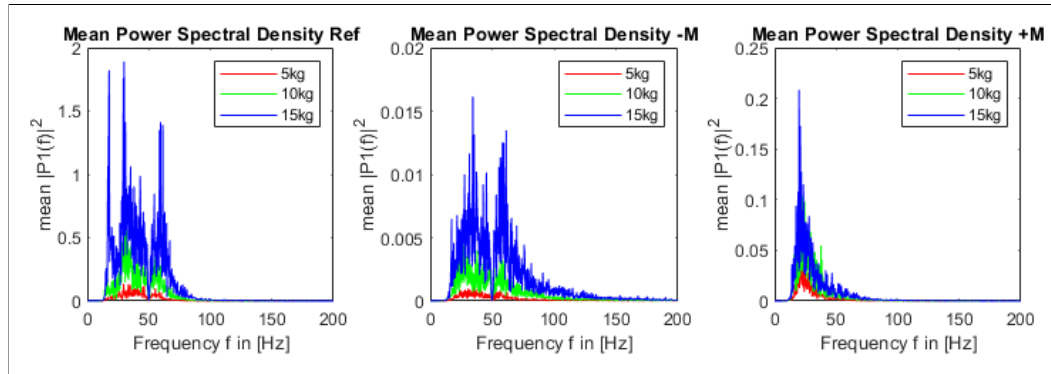


Figure 7.10: EMG mean Power Spectral Density: Ref= adhesive electrodes, -M= without sensor foil, +M= with sensor foil

Discussion:

At first, it is important to note that the reference setup does not allow a full comparison. The focus is on proving the general concept. The RMS comparison shows a promising result with which the muscle activity can be distinguished. The median frequency does not add any further myographic information to the setup, and the effect of the median frequency on load is also widely discussed in the literature [264]. The sensor foil shows a different slope. The difference could be decreased with a better fixation of the sensor foil. The filtered amplitudes and the visual signal to noise ratio add evidence to the general finding, that the designed PCB need to be further developed. A closer electrode to skin connection with prominent electrodes on the PCB could benefit the quality of the signal. The larger spectral density of the plain PCB, compared to the reference measurement, shows the capability of the approach; however, applied with the sensor foil, the density suffers from a low-pass filter effect. In all setups, the spectral density is similar, but low-pass filtered, compared to the literature in chapter 5.1. Thus, it can be concluded that a small sensor size can obtain electromyographic information. The sensor foil and fixation should be further developed. Weiß & Wörn (2005) showed that gluing the sensor on the electrode results in a nearly constant resistance [172]. It is urgent that the electrode is tightly coupled to the skin; a flexible electrode like CTRL-Lab developed would highly benefit the signal's quality. An idea of how it could be solved mechanically is shown in figure 10.2. In total, the future evaluation of electrode sizes and shapes is possible and can be conducted after fixing the introduced aspects.

7.4 Mechanomyography

Test setup:

The evaluation aims to prove the general concept, and there is no comparative device that could act as a reference. Two measurements will be conducted, one without and one with the sensor material (soft intermediate plus normal sensor foil).

Material:

The MMG test setup consists of the introduced accelerometer (FXOS8700) of chapter 6.3 with a sensitivity of ± 2 g and 14 bit resolution. The integrated circuit is mounted on a breakout board from Adafruit (New York City, NY, USA) and thus wider than the desired final solution. The sensor was sewed in a neoprene ankle band and connected by an I²C interface to a joy-it mega 2560 microcontroller (Simac Electronics Handel GmbH, Neukirchen-Vluyn, Germany). The firmware was written in Arduino 1.8.9 (open-source) and is attached in 11.1. The resolution of the sensor provides 0.0024 m/s^2 as its smallest step width. The controller sampled all three axes with 200 Hz for 5 seconds. The orthogonal axis to the muscle was evaluated. The recorded values were raw signals with gravity distortion. The used sensor material was the normal sensor foil and the soft intermediate from figure 6.7. The materials are shown in figure 7.11.

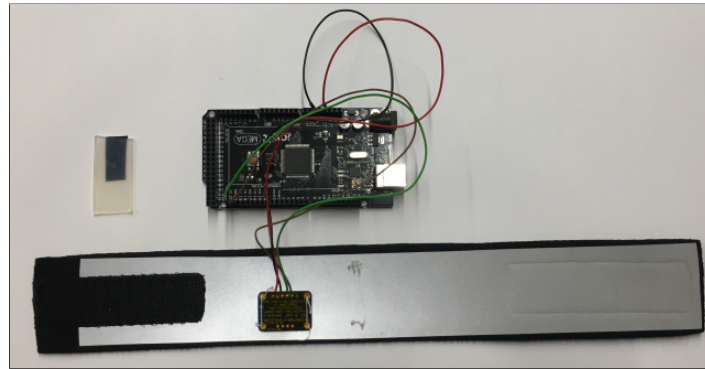


Figure 7.11: MMG-Setup: The breakout board is sewed into the band. The sensor material consists of the soft intermediate with the normal sensor foil.

Method:

The test protocol is described in the standardized protocol section 7.1. The sensor was placed on the muscle belly of the biceps, as researchers state it as the most prominent signal location MMG measurements (see chapter 5.3). The condition without the sensor material was obtained first. The second condition used the sensor material.

Data processing:

The data was acquired with the Arduino in-built serial monitor. A MATLAB 2018b (The MathWorks Inc., Natick, Massachusetts, USA) script was used for the pre-processing. The signal was 3rd order Butterworth band-pass filtered with cut-off frequencies at 5 and 99 Hz. The Root-Mean Square- and mean frequency value was calculated and averaged over the trials.

Results:

The results in figure 7.12 should be interpreted carefully, due to the sample size of one subject with 6 repetitions each. The resulting power spectral density shows that in between the loads, the spectrum mainly changes in its power. However, changes due to the applied sensor material are not obvious in the upper plot and better shown in the Root Mean Square (RMS) and Mean Frequency plot. The mean RMS and its standard deviation are higher with the applied sensor material. The Mean Frequency shows a systematic offset with applied sensor material. The standard deviation enlarges with an applied sensor material.

Both signals are showing a relationship between the increased load and the accelerations. The power density of the test with sensor material is shifted compared to the test without the sensor material. The classes 5 kg and 10 kg differ minorly, while the 15 kg load shows a clear rise in mean frequency.

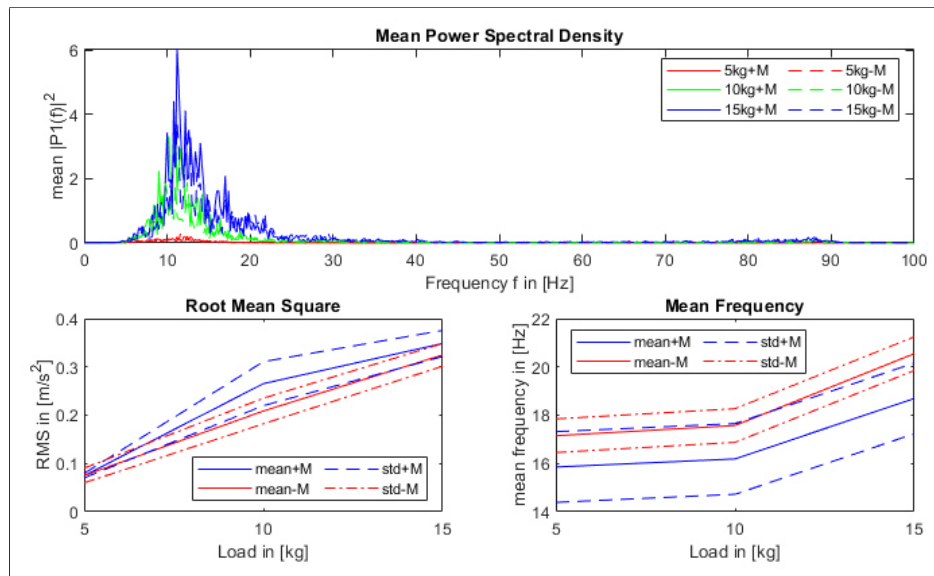


Figure 7.12: MMG Results: mean Power Spectral Density, RMS and Mean Frequency; band-pass filtered at 5-99 Hz; 5/10/15 kg load; 6 repetitions; 1 subject. +M= applied sensor material; -M= without sensor material

Discussion:

The results of the measured mechanomyographic parameters are comparable with the results in chapter 5.3. Due to the limitation that a maximal voluntary contraction was not obtained, it can not be clearly stated, that the frequency plateau between 5 and 10 kg is showing the signal between 0 to 40% torque from figure 5.11 (A). However, the amplitude increase and the PSD show similarities to the literature in figure 5.11 and figure 5.12. The amplitude changes could occur due to a different contact pressure after application. A score with RMS and mean frequency could benefit the classification by solving its drawbacks. The reduced mean frequency with the sensor material could show a low-pass filtering effect. However, the increased RMS would contradict the hypothesis of a high-pass filter effect due to a compliant intermediate material. In general, it can be concluded that mechanomyographic signals can be acquired with low-cost sensors like the FXOS8700. The parameters RMS and mean frequency verify a small correlation to the load, which should be further investigated in a larger study. Taken together, the application of a mechanomyographic sensor in a low-cost sensor matrix could be beneficial.

7.5 Conclusion

The test results showed promising results in all sensor modalities for one subject. The design of the sensor material should adapt to the results and provide higher sensitivity. However, the results of the foam proved the concept of force myographic information. The bare electromyographic PCB was able to provide myographic information to frequencies of up to $\approx 150\text{Hz}$ and outperformed the reference measurement in this case. The fixation of the sensor foil needs to be enhanced, and an application of the designed silver foil should be tested in a future evaluation with a larger sample size and statistical evidence. The mechanomyographic accelerometer was able to provide myographic information to distinguish in between the 3 loads. The future evaluation should embed the integrated circuit on a narrow PCB to also prove the effectiveness on a smaller board size. The comparison of the 2nd derivative of the FMG- and the MMG signal proves, that the MMG sensor is not obtaining redundant signals. In summary, the designed sensor modalities are proving the concept, and an evidence-based evaluation study can be conducted after adjusting the mentioned issues.

8 Sensor module

A sensor module is an arrangement of sensors embedded on a printed circuit board (PCB) with an interface to transfer data to a peripheral device. The central part of the module is a microcontroller which acquires data from the sensors connected to it. A sensor module can be used isolated or fused into a sensor matrix, which will be covered in chapter 9. Referring back to the pre-evaluation chapter 7, all modalities offer a possible amount of information about the current muscle activity. This chapter covers the design of a small set of different sensor modules which can be tested in a future case study.

A human-machine interface, introduced in chapter 2.1, aims to detect the intention of the user and predict them to control a device. To cover all target groups, the prediction should provide real-time capability as far as possible. Taking the motor pathway into account and the introduced electromechanical delay from chapter 4, EMG sensors are highly important to obtain a low latency and to detect an intention without major mechanical muscle contractions, e.g., with stroke patients. MMG and FMG sensors are delayed, but able to add further information to the prediction and its corresponding control task (see chapter 4). Thus a setup with a higher number of EMG sensors would be justifiable. One MMG sensor adds the board acceleration to the acquired set of information. A second MMG sensor would provide redundant information, due to the rigid PCB. The remaining space is filled with FMG sensors. FMG sensors are adding highly valuable and stable high-density information to the setup, which can be then used in a control scheme to re-adapt the first predicted movement, based on EMG, of the module (see figure 10.1).

Based on the design principles, a sensor module setup needs to fulfill different constraints, e.g., it should be easily exchangeable to be cost-efficient. The length of the sensor module should be taken into account, to not face lifting effects due to a local muscle bulge. The sensor module could be placed in a prosthetic socket or as a module in a wristband. An amputee aims for a higher reliability, and a teleoperated task may aim for a higher dexterity. Disabled persons may elicit a smaller degree of mechanical activation, which would decrease the signal to noise ration for MMG and FMG sensors and make an EMG sensor highly convenient.

To solve basic questions to better understand the used techniques, this thesis proposes raw

sensor modules for each modality and the already introduced multi-modal approach. The raw sensor modules enable a comparison between the three different sensor modalities and show how much accuracy each can achieve. The multi-modal approach can be used with all sensor modalities and decreased to one or two types of sensors; thus, the significance of the ignored sensor modality can be shown. Furthermore, the high-density grids can be clustered, and the amount of information is decreased; thus, overfitting problems can be solved in an algorithm. The impact of the mechanical delay can be investigated in detail with the desired multi-modal sensor module.

This thesis evaluated a bipolar setup due to the current limitations of sensor hardware in the German Aerospace Center for a monopolar setup. In general, the size constraints of a monopolar setup are smaller, unless they need a valid reference electrode. However, the development of a monopolar setup to decompose the signal should be treated as an independent question in future research (for decomposing, see chapter 2.4).

8.1 Microcontroller

Due to expertise in the German Aerospace Center, the LPC 845 (NXP Semiconductors, Eindhoven, Netherlands) was chosen as the controlling unit. The LPC 845 is a 32 bit microcontroller based on ARM Cortex-M0+ Cores. The controller runs on frequencies of up to 30 MHz. It includes two SPI controllers with SSP features and fully supports I²C-bus specification. The LPC 845 comprises one state configurable timer and a 12-bit ADC with 12 channels. To fulfill the size constraint, the HVQFN package with 5x5x0.85 mm was chosen. The controller is also capable of fulfilling the requirements for the upcoming trend of machine-learning on edge devices.

8.2 Components

The most important component for a data acquisition circuit is a low noise and constant voltage supply. The maximum noise amplitude must be lower than the smallest resolution of the analog to digital converter. A DC-DC converter is not recommended due to the switching nature along with a high noise ratio. A low dropout regulator is suited to provide the constant supply voltage with two stabilization capacitors to decrease the noise.

General components for each sensor modality differ and depend on the quantity of used sensors. EMG sensors footprint is large and needs to be shrunk to fit on the desired small printed circuit board. An integrated circuit instrumentation amplifier could save some space, e.g., ADS 1298 (Texas Instruments Incorporated., Dallas, Texas, USA) or AD8233 (Analog Devices, Norwood, MA, USA). In addition, resistors to adjust the gain of the amplifier and capacitors to filter the signal are necessary. The smallest SMD resistors and capacitors are 0.4 x 0.2 mm in size (SMD 01005). The force myographic setup consists of one resistor, and the mechanomyo-

graphic setup uses an integrated circuit (FXOS8700), which both ends up in a small footprint. An additional analog to digital converter like the ADS124S0x (Texas Instruments Incorporated., Dallas, Texas, USA) could add up to 12 channels with a resolution of 24 bits to our setup or an AD7490 (Analog Devices, Norwood, MA, USA) with 16 channels and 12 bit. The ADS124S0x and AD7490 have a package size of 5 x 5 mm, which fits on a narrow sensor module. A sample sensor module is designed in figure 8.1 and provides one EMG, one MMG and 42 FMG sensors.

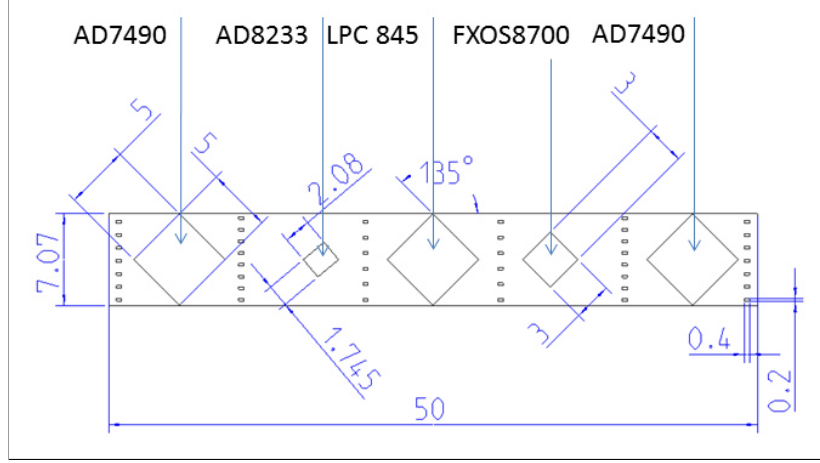


Figure 8.1: Sample sensor module components, the smallest footprints are SMD resistors; Dimensions in mm

8.3 Setups

This section shows sample printed circuit boards and how the sensors can be distributed to achieve a high density of sensors on a narrow board. The routing is not considered in this thesis; however, in the proposed FMG ring sensor setup, the board needs additional layers (see chapter 6.1). The sensor setup avoids the edge effect of a wide printed circuit board from which the Bielefeld Bracelet suffers. The electrodes from the force- and electromyographic sensors are located on the skin facing side and their components on the opposite side. Figure 8.2 (A) introduces a multi-modal sensor module using a tripolar EMG-sensor and 42 FMG-sensors, which results in 43 data channels. The maximum number of FMG-sensors on a 50 mm long and ≈ 7 mm wide PCB is 71, as shown in sketch (B). A monopolar sensor module, shown in sketch (c), could consist of 8 electrodes with an inter-electrode distance of 5 mm, and 33 FMG-sensors. To this end, an exchangeable module could consist of any desired electrode shape and size, which would highly benefit the research about optimal sensor parameters and sensor module compositions. The backside of the sensor consists of the described components in the last section. The routing is challenging and may decrease the maximal number of embedded sensors on a PCB.

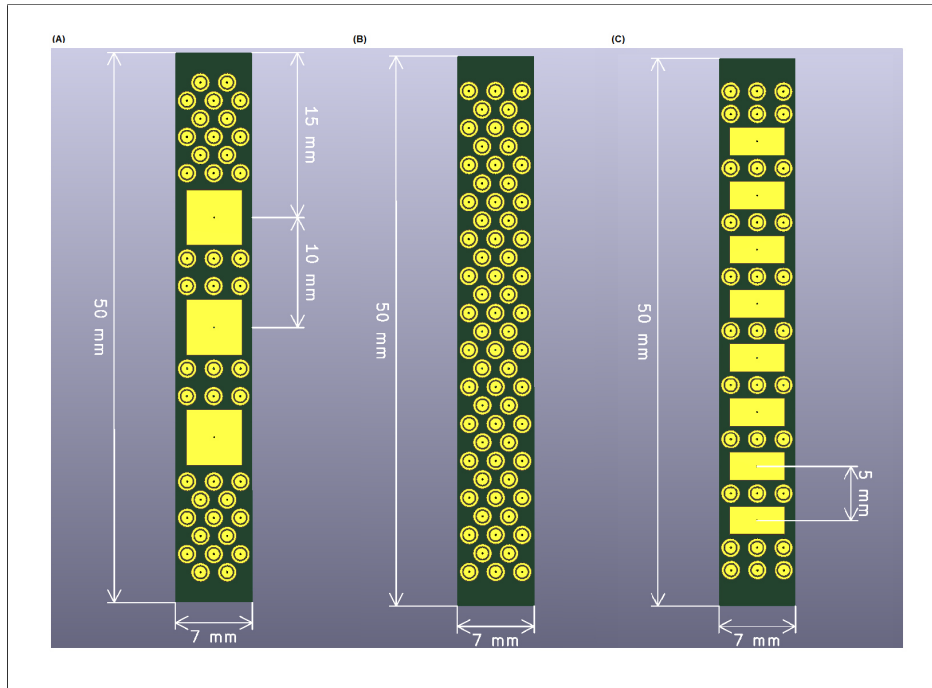


Figure 8.2: Sample sensor module setups, the design of the EMG-sensors is based on the proposed distances in chapter 6.2

8.4 Discussion

The LPC845 microcontroller provides a 12 bit analog to digital converter with 12 channels; thus, the controller can connect to a maximum of 12 FMG or EMG sensors until the circuit needs an external analog to digital converter. Aiming for a high density of sensors, one or more AD7490 could be used. An instrumentation amplifier can ensure the EMG-sensor quality and provide a high signal to noise ratio and attenuate DC noise. The controller's frequency of 30 MHz is sufficient for the desired tasks, and the two communication interfaces (I²C, SPI) can be used to connect to the MMG sensor and to offer data to a master device. The small footprint ensures the possible application on a narrow sensor module.

The small number of components for the FMG and MMG sensor modalities make them a perfect fit for the larger footprint of one EMG setup. The accelerometer for MMG measurements can be reduced to one DOF, which is orthogonal to the muscle belly. A tripolar EMG recording uses three electrodes and one ADC channel. A monopolar setup uses one electrode, a remote reference signal, a decreased EMG-processing setup and one analog to digital converter channel.

In summary, the sensor module has a powerful microcontroller that captures data from its analog to digital converter channels and communication interfaces. The aimed sensor matrix can use customized sensor module setups, which are based on someone's own design decisions.

The research field would highly benefit from exchangeable sensor modules and would be independent of fixed sensor setups, which may be outdated after some years. The SPI data interface should be generalized to ensure the possibility to easily exchange a sensor module, without the need to build up a full new setup.

9 Sensor Matrix

As already described in chapter 2.5, a sensor matrix is an arrangement of "n" sensor modules. The sensor modules provide local myographic information. A comprehensive sensor matrix can support the intention prediction for human-machine interactions, by unraveling the muscle activation regarding the intermuscular coordination (see chapter 4). Upcoming tasks for the sensor matrix design are providing a circular sensor module mounting, collection of data from each module, adding motion data, and sending of data to a peripheral computing device, e.g., PC, Tablet. The role model location of this thesis is the human forearm. However, extending the size of the sensor matrix can enable an application on the human thigh and other limb regions. An adjustable sensor matrix length can be achieved by adding modules to the setup. This approach satisfies the design principle of a modular sensor matrix. General ideas of how to ensure the proposed objectives are introduced in the following sections. The customized communication protocol is introduced, which ensures a data transmission with fewer traces/cables, compared to the "Bielefeld Bracelet". The connection of the Bracelet is shown in figure 2.5 (B).

9.1 Master Module

The master module is stacked on a sensor module or fixed at the outside of the sensor mounting. It embeds the "master" microcontroller and the communication interface to the "slave" microcontrollers of the modules. The master controller offers communication interfaces to peripheral or external devices. Furthermore, the master module comprises additional sensors to detect the motion to face the limb position effect. Due to frequent use at the German Aerospace Center, the LPC 1857 (NXP Semiconductors, Eindhoven, Netherlands) microcontroller was selected for this task. The LPC 1857 has a Cortex M3 core, capable of a maximum CPU frequency of 180 MHz and offers various interfaces, e.g., 4 SPI, 4 I²C busses and two high-speed USB-Interfaces. The footprint depends on the number of pins and can be as small as 9 x 9 mm.

Additional Sensors

As already introduced in chapter 5 and described in chapter 6.4 the additional motion tracking sensors are an IMU and a barometer. Both are suitable for tracking the limb position. The specs are already introduced in the mentioned chapters about the sensors, and a BNO055 and

BMP085 were selected. The higher prices are justifiable due to the decreased workload with an already implemented sensor fusion. Both sensors communicate with the main controller by an I²C protocol. The temperature sensor was not selected yet and is still an open decision.

9.2 Data Transfer

The data transfer between the main controller and the sensor modules should be capable of sending at high speed to provide real-time data. The basic Serial Peripheral Interface (SPI) protocol was chosen due to the high data bandwidth and small protocol overhead compared to other protocols. The SPI protocol requires four wires in total and can be operated in a bus system together with other sensors without addressing (see figure 9.1). The protocol has a serial clock line (SCK) to ensure synchronous data transmission, a Master-In-Slave-Out line (MISO) to "listen" with the master and send data from the slave device, a Master-Out-Slave-In line (MOSI) to send data to the slave device and a chip select (CS) line which enables the MISO line for one slave to avoid cross-talk from other slaves. Thus, a larger setup of 30 modules needs 33 SPI protocol lines. The large number of chip select lines makes the protocol inefficient for the sensor matrix. Nevertheless, the "Bielefeld Bracelet" used it successfully, but it decreases the comfort and robustness of the system due to the sensitive tiny cables and connectors [57]. Thus, the design aims for a customized SPI solution, using one chip select line as a bus system.

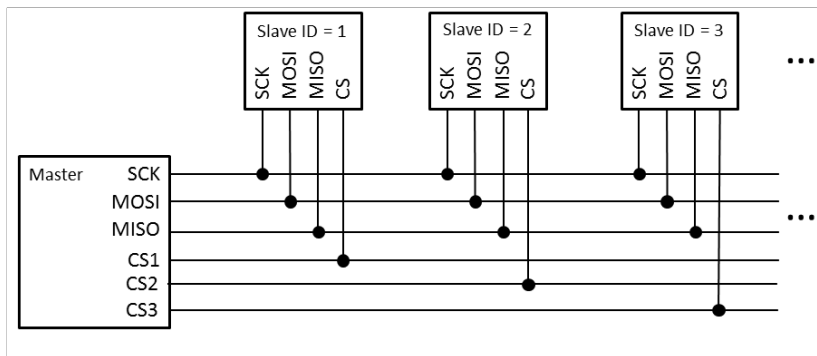


Figure 9.1: Standard SPI Protocol: SCK= Serial Clock, MOSI= Master Out Slave In, MISO= Master In Slave Out, CS= Chip Select

The general idea of the customized SPI protocol is to count the chip selects of the master device and send data at a preset condition. The customized architecture is shown in figure 9.2. To achieve a communication between the connected slaves and the master device, the slave needs preset conditions at which they should send data on the MOSI line. Thus, the slaves are introduced in a "welcome round" in which the master assigns IDs to every slave and sends general data, e.g., package sizes and the total number of slaves. Knowing about the quantity

of neighbors and their package size, a slave device can trigger its CS line with an interrupt once the previous slaves are finished with their data transmission based on past chip selects.

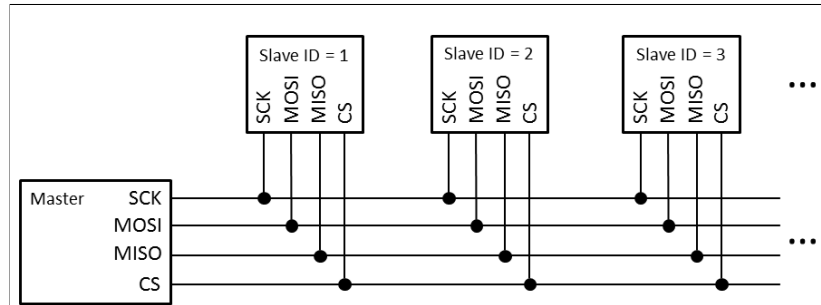


Figure 9.2: Customized SPI Protocol with 4 bus lines: SCK= Serial Clock, MOSI= Master Out Slave In, MISO= Master In Slave Out, CS= Chip Select

The principal idea of the customized SPI protocol was successfully implemented in the main loop of an LPC 1114 microcontroller. However, observing the CS line in the main loop in which other interrupts can occur can lead to miscounting. As the consistency is essential, and it would be hazardous for the communication if the setup fails, the thesis proposes an external counter, which throws an interrupt once it counted the preset number of chip selects for its chip select trigger. The external counter can be realized with a state configurable timer; this approach was not tested yet and is an open research question.

Using a SPI protocol adds a second constraint to the system. The protocol is not built to transfer data packages over longer distances, and a data loss could occur. Thus, the SPI protocol will be split into two independent systems which distribute in the two directions starting from the main controller.

The second communication protocol is used to connect the master controller with a peripheral device, e.g., a computer or tablet. Taking the design principles into account, the sensor matrix should aim for a wireless connection like Bluetooth or Wi-Fi. To the current state, a UART protocol was implemented. The first prototype matrix aims for a USB protocol to set up the system before extending the setup to a wireless protocol. The transferred data will consist of the raw values of the sensor.

Data volume

The data volume can be calculated using the designed parameters of 32 tripolar sensor modules with one mechanomyographic accelerometer on the back(see figure 8.2 (A)). Presupposing that the adjustments on the EMG sensor can ensure a myographic signal acquisition of up to 500 Hz, the sensor module should sample with 2000 Hz to achieve the four-time oversampling paradigm. The designed force myographic sensor has its vital signal in lower frequencies; thus, a sample rate of 20 Hz is sufficient. The vital mechanomyographic signal reaches up to 100 Hz;

thus, a sample rate of 400 Hz should be desired.

Using a 12 bit analog to digital converter for EMG and FMG signals and a 14 bit value for the MMG signal each sensor module acquires a data volume of ≈ 40 kbit/s. Consequently, using one customized SPI protocol for all 32 modules, the data volume is ≈ 1.28 Mbit/s, which is in the limits of the SPI protocol of the slave microcontroller and would be out of scope for an I²C interface [265].

9.3 Wristband/Bracelet

Taking the human forearm section and the cross-section image 4.8 into account, the human forearm is distributed by many muscles, i.e., 15 muscles in case of the considered cross-section image. Some of the muscles are small, and the signal might be difficult to distinguish from others, and others are deeper in the forearm and not accessible. The approach from figure 9.3 shows the challenge in this field; the density of electrodes is not large enough to cover all muscles of the human forearm. Thus, the design process was based on narrow sensor modules to achieve a high-density grid around the human forearm to avoid edge effects of the rigid PCB.

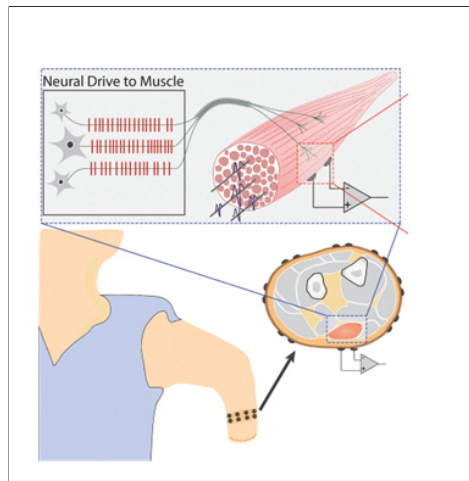


Figure 9.3: Sample image of a sensor arrangement based on electromyographic sensors modified from [84]

Having a self-measured circumference of ≈ 20 -30 cm around the human forearm, the sensor matrix could fit 28-50 sensor modules with a width of 6-7 mm. A small gap between the PCBs can not be prevented, which reduces the number of modules to ≈ 30 -35. However, the sensor matrix can assure a high spatial resolution which was never achieved with a multimodal wristband using active EMG recordings (see figure 9.4).

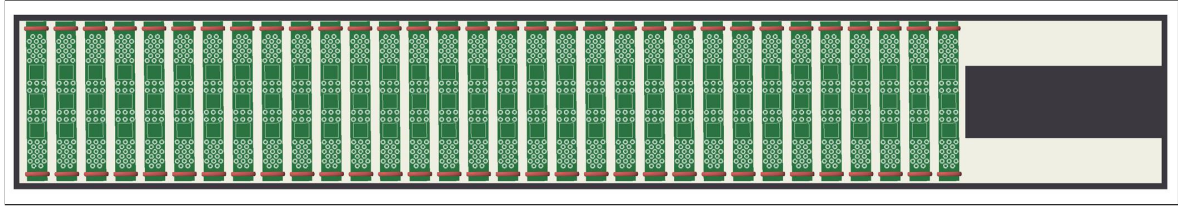


Figure 9.4: Designed sensor matrix, based on the designed multimodal, tripolar sensor module from chapter 8

The general idea is a modular, small and comfortable sensor wristband, which comprises the sensor modules, the master controller, the communication bus wires, a remote reference electrode wire, and a battery pack to comply the design principles of a wearable setup.

The pre-evaluation study was already conducted using a neoprene band as a mounting back-plane. The principle design is shown in figure 9.4. The neoprene band length can be adjusted with a velcro closing system. The components can be placed on the back of the printed circuit sensor board. The communication and remote reference wires are accessible from the backside of the neoprene band. The sensor module itself is held into the system by two elastic straps at the lateral sides of the PCB. Changing the module is easily possible by disconnecting the wires, slide out the old module, and slide the new module into the elastic straps. The master module is placed at the outside of the neoprene band and senses the motion of the user and collects the data from the sensor modules. Depending on the circumference of the recording site, the neoprene band can comprise a different number of sensors, which can be slid into elastic straps (see the red element in figure 9.5). Thus, one setup could be used with a different number of modules to ensure a high spatial recording.

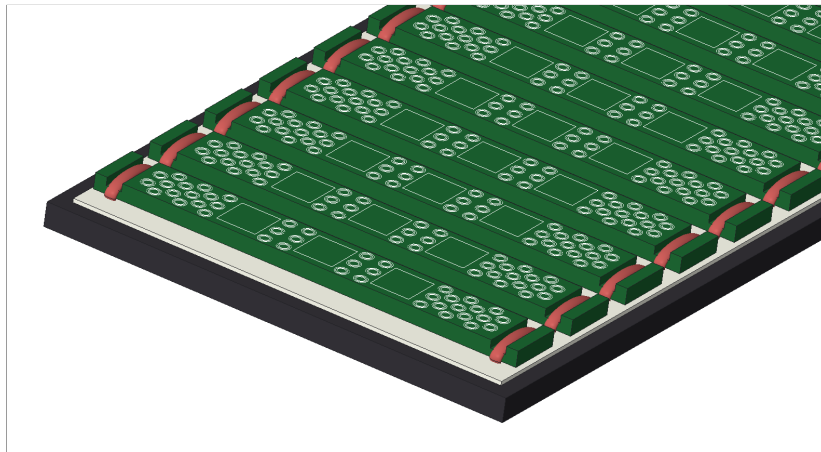


Figure 9.5: Designed sensor matrix with elastic straps to tight the sensor modules on the neopren band

9.4 Discussion

The design of a sensor matrix focuses on a high spatial resolution and aims to fulfill the proposed principles in chapter 3.1. The used microcontroller is powerful enough to provide the data acquisition and transmission for the sensor matrix. The additional motion detection sensors provide an already filtered and fused signal, which can be used to train the intent prediction algorithms with limb positions and current movement information. The bus architecture enables a robust data transmission, even if one sensor module breaks. Nevertheless, the controller needs to count the signals under a high computational load to avoid the break down of the full communication protocol. Thus, a state configurable timer should be set up in the master and slave devices to count externally of the main controller loop. The behavior of the module needs to be investigated in a long-term evaluation.

Research needs to be conducted to explore more sensor matrix mountings to compare them in real-life tasks. The proposed approach will be further investigated. Pitfalls in a sensor matrix design could be the placing of the master controller and the possible long distances for the SPI protocol. However, the general principle is feasible, and a prototype will be developed.

10 Discussion

The thesis proposes a low-cost sensor matrix for use in human-machine interactions on the basis of electromyographic, mechanomyographic, and force myographic information. The sensor matrix consists of low priced and small sensor modalities to fulfill the low cost and high spatial resolution constraint. The data transfer protocol between the sensor modules and the master module was designed and successfully tested in a short evaluation. The thesis proposes a state configurable timer to achieve a more robust solution. The modulated SPI protocol decreases the number of used data wires from 35 wires of 32 modules to 4 wires. A neoprene band mounting is proposed with exchangeable sensor modules. Thus, the sensor matrix is sustainable, and the modules can be adapted to personal or research preferences. The additional motion detection sensors need to be evaluated for their additional information. The designed sensor modules are ≈ 7 mm wide and 50 mm long; the width depends on the footprints of the necessary components. The narrow width of ≈ 7 mm should further avoid edge-effects of the sensor on the round limb, which was a problem with the Bielefeld Bracelet. The length is not based on any biomechanic parameter, and the influence of local muscle bulges on lateral sensors on the modules needs to be investigated to may adjust the width. Figure 8.2 shows sample modules on the basis of the desired sensor solutions. It is highly recommended that the sensor module comprises electromyographic sensors to achieve real-time capability. Based on the described forearm anatomy and electromyographic principle, a monopolar sensor setup should be further investigated. In principle, the three proposed sensor modalities EMG, MMG, FMG can be embedded together on the sensor module. The final components for each sensor modality need to be chosen to prototype the sensor module in the next step of the development process. A feedforward control scheme could be beneficial for the intention prediction to reduce the impact of the electromechanical delay (see figure 10.1). A future study should evaluate the sensor modalities in an upper limb control task against each other and determine the delay.

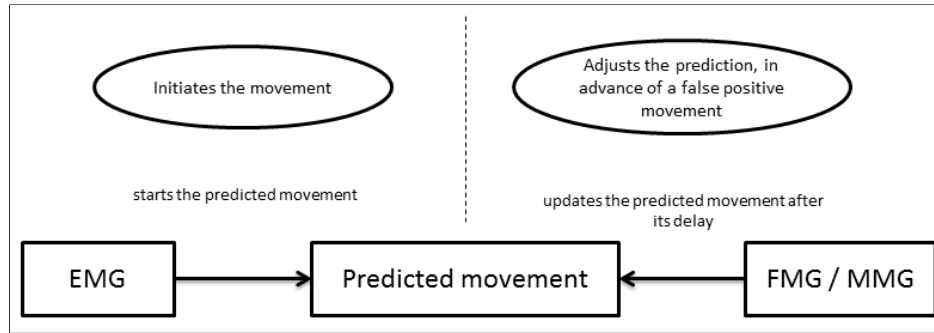


Figure 10.1: Control scheme to avoid a negative influence of the electromechanical delay

The pre-evaluation study proved the concept of electromyography, mechanomyography, and force myography and showed preliminary dependencies between the obtained sensor output and an increasing load at the biceps muscle. To proof, the concept for smaller muscles, a fully developed sensor matrix should compete against current solutions in an upper limb control task based on the introduced pattern recognition software in figure 2.3. The second force myographic test setup further showed the beneficial information of a mechanomyographic sensor in comparison to the 2nd derivation of the force myographic signal. The designed sensor material was not sensitive enough to measure the occurring forces at the human forearm and needs to be adjusted. Furthermore, the sensor material decreased the signal spectrum of the electromyographic sensor, which needs to be further investigated. A mechanical solution for a tight EMG skin interface is difficult, but a compliant sensor concept is shown in figure 10.2. The spring is mounted at the backside of the sensor material and pushes the electrode gently onto the user's skin. The concept or a similar approach would highly benefit the electromyographic signal. It should be taken into account that a mechanical solution decreases the space for sensor components. In total, the pre-evaluation chapter shows the necessary adjustments which need to be solved before conducting an evidence-based user study.

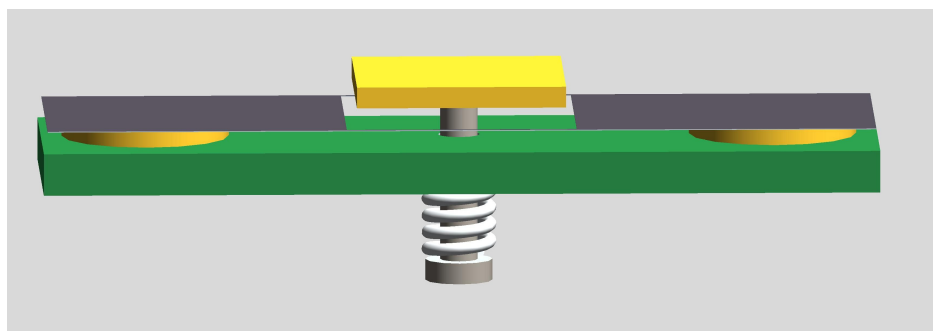


Figure 10.2: Sketch of a compliant electrode, the spring pushes the electrode towards the skin and is compliant to ensure a force myographic measurement

The proposed sensor solutions are focusing on the established design principles and the desired

phenomena. Each sensor modality was introduced and discussed in terms of applicability. Open positions were stated and should be researched with the designed sensor matrix to ensure the sensor quality in the desired parameters. The field of new sensor solutions for the introduced phenomena should be observed to adapt the sensor modules with emerging technologies. Especially the area of tomography would add essential information to the setup — for instance, a smaller ultrasound device or the upcoming technique of electrical impedance tomography.

A very promising method for monopolar recordings is the circular electrode shape from figure 6.14. The electrode shape shields the signal from surrounding cross-talk. The designed tree-shaped force myographic electrode may decrease the spatial resolution but enables a low-cost sensor solution. If the user desires a system without real-time capabilities, the electromyographic sensor can be ignored, and the sensor matrix can be potentially worn on top of clothes, which would enhance the user's comfort. Using force myographic sensors, the systematic error due to the force-length relationship needs to be considered. A possible solution for the issue is the application of two sensor matrices, one distal and one proximal of the joint. Thus, we can analyze the motion data of the master modules of each sensor matrix in order to deduce the joint angle of the user.

The myographic chapter adds general information about the origin of the underlying phenomena and the physiologic signal components. The features of machine-learning algorithms should take the provided knowledge about physiologic information in the signal into account. In addition, the stated open positions can be investigated with the modular sensor matrix to speed up the research in the field of myography and human intention detection.

The muscle architecture chapter links back to the introduced motor pathway and shows the underlying muscle physiology and processes. Thus, the reader can understand the sequence of obtainable phenomena and can deduce new myographic solutions with one of the introduced transducing techniques from table 2.1. Furthermore, the recording site of the human forearm is introduced to show that a generalized approach of a sensor matrix can limit the signal quality. The limitation is especially the case for bipolar and tripolar recordings on the arm, which are not always in fiber alignment and thus provide a signal mixture between activations of muscles with different mechanical effects. The chapter further propose the ulna bone as a promising reference signal site for the monopolar EMG setup.

Table 10.1 shows the established design principles from chapter 3 and their current status. It can be concluded, that the design concentrated on a prototype and a proof of concept for the desired myographic modalities. Having a first sensor matrix prototype, the open research positions should be solved. After fully understanding the determining parameters of the sensors, the sensor matrix should adapt to the required design principles.

Table 10.1: Design principles with their current status of the desired sensor matrix. Sorted by relevance and collected from [85, 58, 81, 84, 37, 38]

Nr.s	Design principle	Status
1	medical technology laws	pending
2	non-invasive	skin connection
3	robustness	multimodal, sensor fusion and motion sensors
4	latency	still capabilities with the used controllers
5	spatial resolution	very small, as small as the used ICs
6	delay/latency	sensor modality and prediction dependent
7	low cost	cheap modalities
8	modular	sensor modules are exchangeable
9	compact	small components due to modalities
10	free positioning	battery and wireless communication
11	safety	robust case
12	intuitive	pending
13	wearability	pending
14	durability	pending
15	feedback	pending
16	comfort	pending
17	calibration	pending
18	in-built power	pending
19	wireless	pending
20	resource friendly	exchangeable sensor modules
21	good looking	pending

The designed non-invasive low-cost sensor matrix can be used at different recording sites at the limb and includes amputees and non-amputees. The designed sensor matrix is potentially a step further to replace body-powered prostheses and enable the manifestation of robotic prostheses. The sensor modules are customized for a feature-based machine-learning algorithm. It needs to be proven that the high spatial resolution benefits the prediction and increases the human capabilities in an upper-limb control task. Using a control scheme to reduce the latency due to the electromechanical delay, the sensor matrix can achieve a low latency and a high spatial resolution with a robust prediction based on the force myographic information. The sensor matrix offers a higher spatial resolution to the introduced sensors matrices in chapter 2.5. The two activation related coordination types (intramuscular and intermuscular) were proven to be apparent (see 4). The most exciting intention prediction approach is based on neuromechanical knowledge and decomposes the signal before predicting the intention [159]. This auspicious approach should be investigated with the introduced circular electrodes

from Farina et al. (2001) in figure 6.14 [250] in terms of applicability in everyday tasks.

11 Conclusion/Outlook

The sensor matrix was successfully designed on the basis of a neuromechanical background, taking the human anatomy and physiology into account. It uses biological signals as an interface to obtain the human intention. The acquisition of myographic signals has real-time capabilities as well as a high spatial resolution compared to motion recordings and brain signal acquisition. The sensor matrix consists of three low-cost myographic sensors and measures the propagating motor unit action potential (EMG), lateral oscillations of the muscle fibers (MMG) and the isovolumetric behavior of the muscle (FMG). The EMG sensor was designed after the newest research innovations and offers a mono- and bipolar recording. The MMG sensor is a low-cost accelerometer with a small footprint on the board. The FMG sensor from Kõiva et al. (2015) was redesigned with a reduced size, different shape, and determinable sensor material. The proof of concept was conducted for all modalities, and adjustments will be made before a user study will compare the sensor modalities against each other. The proposed multimodal sensor matrix was designed, and the number of modules was increased from 16 (CTRL Kit, CTRL Lab) to 30-35 with the aim to obtain a higher spatial resolution of the forearm muscle activation. The modules are exchangeable to reduce the costs for the user and offer a sustainable product for the user. The thesis provides all necessary information about the signal origin and composition for a feature-based machine-learning algorithm.

The future design process should concentrate on the introduced neuromechanical background and investigate a sensor fusion with a nerve conduction wristband at the human wrist to obtain subtle finger activations. Closing the loop to the first chapter about human-machine interfaces, it is urgent to provide feedback for the user to achieve an embodiment and satisfy the user's independence. Regarding this, the finished sensor matrix will be adapted to fit into a modular prosthetic socket, to especially address the field of amputees. Merging knowledge from neuroscience studies, the possibility to use an electroencephalographic EEG cap for a reinforcement learning approach should be evaluated. The EEG cap can provide event-related potentials like error-related negativity or P300 to train the algorithm in a way like Kim et al. (2017) did [83]. These future ideas would provide a complete human-machine interface with a self-learning system based on biologic labeled datasets.

Appendix

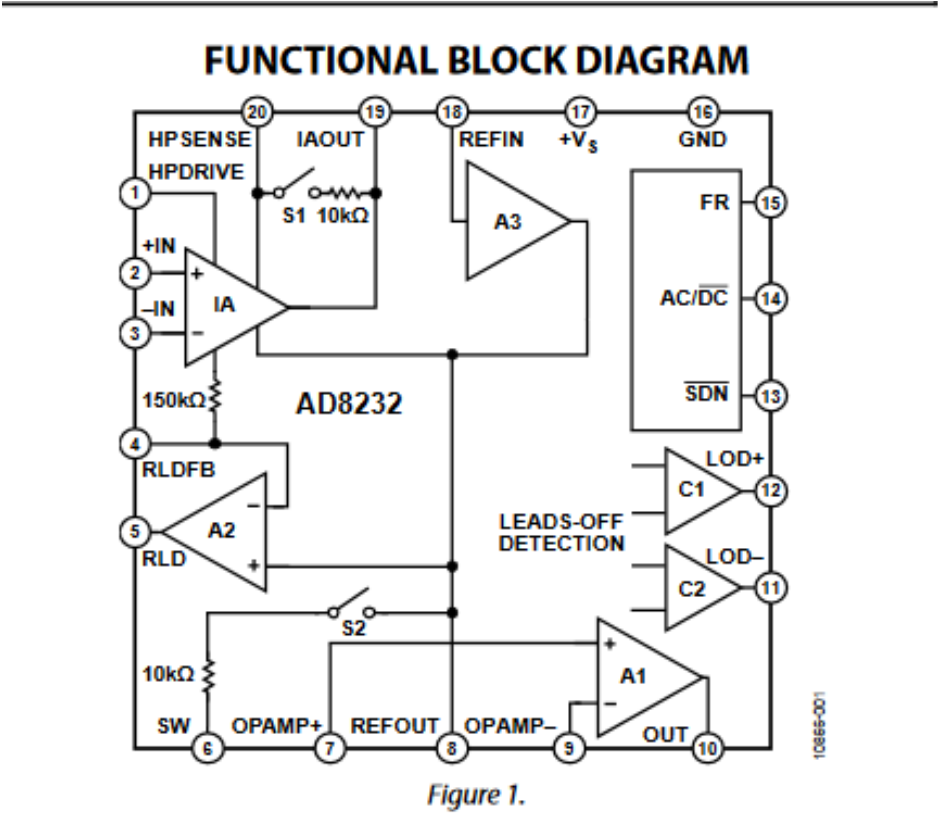


Figure 11.1: Functional Block Diagram SparkFun AD8232

Listing 11.1: Firmware MMG modified from [266]

```
1||#include <Wire.h>
```

```

2| #include <Adafruit_Sensor.h>
3| #include <Adafruit_FXOS8700.h>
4|
5| /* Assign a unique ID to this sensor at the same time */
6| Adafruit_FXOS8700 accelmag = Adafruit_FXOS8700(0x8700A, 0x8700B);
7|
8| int run = 0;
9| int samplerate = 200;
10| int seconds = 5;
11| int dof = 3;
12| const int Samples = seconds * samplerate * dof;
13| int16_t Buffer[3000];
14| unsigned long starttime = 0;
15| unsigned long stoptime = 0;
16|
17| void setup(void)
18| {
19|   Serial.begin(115200);
20|
21|   /* Wait for the Serial Monitor */
22|   while (!Serial) {
23|     delay(1);
24|   }
25|
26|
27|   /* Initialise the sensor */
28|   if (!accelmag.begin(ACCEL_RANGE_2G))
29|   {
30|     /* There was a problem detecting the FXOS8700 ... check your connections */
31|     Serial.println("Oops, no FXOS8700 detected ... Check your wiring!");
32|     while (1);
33|   }
34|
35| }
36|
37| void loop(void)
38| {
39|
40|   sensors_event_t aevent, mevent;
41|
42|   /* Get a new sensor event */
43|   accelmag.getEvent(&aevent, &mevent);
44|
45|
46|   Buffer[run] = aevent.acceleration.x * 1000;
47|   run++;
48|   Buffer[run] = aevent.acceleration.y * 1000;
49|   run++;
50|   Buffer[run] = aevent.acceleration.z * 1000;
51|
52|   //Check if Buffer is full
53|   if (run >= Samples)
54|   {
55|     stoptime = micros();
56|     Serial.println((stoptime - starttime));
57|

```

```
58 //send buffer values through serial interfaced
59 for (int iRun = 0; iRun < Samples - 1; iRun++)
60 {
61   Serial.print((float)Buffer[iRun] / 1000);
62   Serial.print(",");
63   Serial.print((float)Buffer[++iRun] / 1000);
64   Serial.print(",");
65   Serial.println((float)Buffer[++iRun] / 1000);
66 }
67 delay(5000);
68 run = 0;
69 starttime = micros();
70
71 }
72 else
73 {
74   //To achieve the desired samplerate, we need to subtract the runtime of the code of
       1859 microseconds
75   delayMicroseconds((1000000 / samplerate) - 1859);
76   run++;
77 }
78 }
79
80
```


Bibliography

- [1] Kurt Wagner. *Facebook to Buy Startup for Controlling Computers With Your Mind*. Website. Accessed: 2019-10-22. 2019. URL: <https://www.bloomberg.com/news/articles/2019-09-23/facebook-to-buy-startup-for-controlling-computers-with-your-mind>.
- [2] Mathilde Connan et al. “Assessment of a wearable force-and electromyography device and comparison of the related signals for myocontrol.” In: *Frontiers in neurorobotics* 10 (2016), p. 17.
- [3] Claudio Castellini et al. “Tactile myography: an off-line assessment on intact subjects and one upper-limb disabled.” In: *Technologies/SI: Assistive Robotics* 6.2 (2018).
- [4] Robert R Provine. “Illusions of intentionality, shared and unshared.” In: *Behavioral and Brain Sciences* 28.5 (2005), pp. 713–714.
- [5] I Scott MacKenzie. “Input devices and interaction techniques for advanced computing.” In: *Virtual environments and advanced interface design* (1995), pp. 437–470.
- [6] Michele René Tuga et al. “Co-Adaptives Lernen: Untersuchungen einer Mensch-Maschine-Schnittstelle mit anpassungsfähigem Systemverhalten.” In: *Proc.* Vol. 23. 2014, pp. 247–264.
- [7] Joan Lobo-Prat et al. “Non-invasive control interfaces for intention detection in active movement-assistive devices.” In: *Journal of neuroengineering and rehabilitation* 11.1 (2014), p. 168.
- [8] Eugenijus Kaniusas. *Biomedical signals and sensors I: Linking physiological phenomena and biosignals*. Springer Science & Business Media, 2012.
- [9] Florinel-Gabriel Banica. *Chemical sensors and biosensors: fundamentals and applications*. John Wiley & Sons, 2012.
- [10] Tyson Aflalo et al. “Decoding motor imagery from the posterior parietal cortex of a tetraplegic human.” In: *Science* 348.6237 (2015), pp. 906–910.
- [11] Tom Carlson and Jose del R Millan. “Brain-controlled wheelchairs: a robotic architecture.” In: *IEEE Robotics & Automation Magazine* 20.1 (2013), pp. 65–73.

- [12] Robert Leeb et al. “Self-paced (asynchronous) BCI control of a wheelchair in virtual environments: a case study with a tetraplegic.” In: *Computational intelligence and neuroscience* 2007 (2007).
- [13] SR Soekadar et al. “Hybrid EEG/EOG-based brain/neural hand exoskeleton restores fully independent daily living activities after quadriplegia.” In: *Science Robotics* 1.1 (2016), eaag3296–1.
- [14] Luke Osborn et al. “Targeted transcutaneous electrical nerve stimulation for phantom limb sensory feedback.” In: *2017 IEEE Biomedical Circuits and Systems Conference (BioCAS)*. IEEE. 2017, pp. 1–4.
- [15] Koen Cuyppers et al. “Long-term TENS treatment improves tactile sensitivity in MS patients.” In: *Neurorehabilitation and neural repair* 24.5 (2010), pp. 420–427.
- [16] Stanisa Raspopovic et al. “Restoring natural sensory feedback in real-time bidirectional hand prostheses.” In: *Science translational medicine* 6.222 (2014), 222ra19–222ra19.
- [17] Christian Antfolk et al. “Sensory feedback in upper limb prosthetics.” In: *Expert review of medical devices* 10.1 (2013), pp. 45–54.
- [18] Thomas (CTRL LAB) Reardon. *Cutting Edge Stage Live at CogX 2019 at 2:21:56 h.* 2019. URL: <https://www.youtube.com/watch?v=O9BQdi35Fp0> (visited on 09/05/2019).
- [19] Stephen G. Waxman. *Clinical Neuroanatomy, 28th Edition* -. 28 ed. New York: McGraw-Hill Education, 2016. ISBN: 978-0-071-84770-4.
- [20] Michel Desmurget and Scott Grafton. “Forward modeling allows feedback control for fast reaching movements.” In: *Trends in cognitive sciences* 4.11 (2000), pp. 423–431.
- [21] Gregory Allen Apker. “Influence of Sensorimotor Noise on the Planning and Control of Reaching in 3-dimensional Space.” PhD thesis. Arizona State University, 2012.
- [22] A Aldo Faisal, Luc PJ Selen, and Daniel M Wolpert. “Noise in the nervous system.” In: *Nature reviews neuroscience* 9.4 (2008), p. 292.
- [23] Michael SA Graziano, Charlotte SR Taylor, and Tirin Moore. “Complex movements evoked by microstimulation of precentral cortex.” In: *Neuron* 34.5 (2002), pp. 841–851.
- [24] GJ Romanes. “The motor pools of the spinal cord.” In: *Progress in brain research*. Vol. 11. Elsevier, 1964, pp. 93–119.
- [25] Elwood Henneman and Lorne M Mendell. “Functional organization of motoneuron pool and its inputs.” In: *Comprehensive Physiology* (2011), pp. 423–507.
- [26] Robert E Burke and V Reggie Edgerton. “Motor unit properties and selective involvement in movement.” In: *Exercise and sport sciences reviews* 3.1 (1975), pp. 31–82.

- [27] Gerd Hirzinger et al. “Sensor-based space robotics-ROTEX and its telerobotic features.” In: *IEEE Transactions on robotics and automation* 9.5 (1993), pp. 649–663.
- [28] J Artigas et al. “Force-feedback teleoperation of on-ground robots from the international space station in the frame of the” kontur-2” experiment,”” in: *Proceedings of” International Extreme Robotics Conference”, St. Petersburg, Russia.* 2016.
- [29] Neal Y Lii et al. “Toward Scalable Intuitive Teleoperation of Robots for Space Deployment with the METERON SUPVIS Justin Experiment.” In: *Proc. of the 14th Symposium on Advanced Space Technologies for Robotics and Automation (ASTRA).* 2017.
- [30] José Ribeiro et al. “Analysis of Man-Machine Interfaces in Upper-Limb Prosthesis: A Review.” In: *Robotics* 8.1 (2019), p. 16.
- [31] E Biddiss and T Chau. “Upper extremity prosthesis use and abandonment: A survey of the last 25 years.” In: *Prosthet Orthot Int* ().
- [32] Bartjan Maat et al. “Passive prosthetic hands and tools: A literature review.” In: *Prosthetics and orthotics international* 42.1 (2018), pp. 66–74.
- [33] Peter J Kyberd and Wendy Hill. “Survey of upper limb prosthesis users in Sweden, the United Kingdom and Canada.” In: *Prosthetics and orthotics international* 35.2 (2011), pp. 234–241.
- [34] Daniel R Merrill et al. “Development of an implantable myoelectric sensor for advanced prosthesis control.” In: *Artificial organs* 35.3 (2011), pp. 249–252.
- [35] Susannah M Engdahl et al. “Surveying the interest of individuals with upper limb loss in novel prosthetic control techniques.” In: *Journal of neuroengineering and rehabilitation* 12.1 (2015), p. 53.
- [36] Ning Jiang et al. “Myoelectric control of artificial limbs—is there a need to change focus?[In the spotlight].” In: *IEEE Signal Processing Magazine* 29.5 (2012), pp. 152–150.
- [37] Anders Fougner et al. “Resolving the limb position effect in myoelectric pattern recognition.” In: *IEEE Transactions on Neural Systems and Rehabilitation Engineering* 19.6 (2011), pp. 644–651.
- [38] Claudio Castellini et al. “Proceedings of the first workshop on Peripheral Machine Interfaces: going beyond traditional surface electromyography.” In: *Frontiers in Neurorobotics* 8 (2014), p. 22. ISSN: 1662-5218. DOI: 10.3389/fnbot.2014.00022. URL: <https://www.frontiersin.org/article/10.3389/fnbot.2014.00022>.
- [39] Bart Peerdeman et al. “Myoelectric forearm prostheses: state of the art from a user-centered perspective.” In: *Journal of Rehabilitation Research & Development* 48.6 (2011).

- [40] Archibald Vivian Hill. “The heat of shortening and the dynamic constants of muscle.” In: *Proceedings of the Royal Society of London. Series B-Biological Sciences* 126.843 (1938), pp. 136–195.
- [41] Andrew F Huxley. “Muscle structure and theories of contraction.” In: *Prog. Biophys. Biophys. Chem* 7 (1957), pp. 255–318.
- [42] J Luh, William Fisher, and R Paul. “Joint torque control by a direct feedback for industrial robots.” In: *IEEE Transactions on Automatic Control* 28.2 (1983), pp. 153–161.
- [43] Holger Urbanek and Patrick van der Smagt. “iEMG: imaging electromyography.” In: *Journal of Electromyography and Kinesiology* 27 (2016), pp. 1–9.
- [44] Carlo J De Luca et al. “Decomposition of surface EMG signals from cyclic dynamic contractions.” In: *Journal of neurophysiology* 113.6 (2014), pp. 1941–1951.
- [45] R. Douglas Fields. *Wristband Lets the Brain Control a Computer with a Thought and a Twitch*. Website. Accessed: 2019-10-22. 2018. URL: <https://www.scientificamerican.com/article/wristband-lets-the-brain-control-a-computer-with-a-thought-and-a-twitch/>.
- [46] Francesco Negro et al. “Multi-channel intramuscular and surface EMG decomposition by convolutive blind source separation.” In: *Journal of neural engineering* 13.2 (2016), p. 026027.
- [47] Rodolfo Bonnin. *Machine Learning for Developers: Uplift your regular applications with the power of statistics, analytics, and machine learning*. Packt Publishing Ltd, 2017.
- [48] Ulysse Côté-Allard et al. “Deep learning for electromyographic hand gesture signal classification using transfer learning.” In: *IEEE Transactions on Neural Systems and Rehabilitation Engineering* 27.4 (2019), pp. 760–771.
- [49] Manfredo Atzori, Matteo Cognolato, and Henning Müller. “Deep learning with convolutional neural networks applied to electromyography data: A resource for the classification of movements for prosthetic hands.” In: *Frontiers in neurorobotics* 10 (2016), p. 9.
- [50] Nurhazimah Nazmi et al. “A review of classification techniques of EMG signals during isotonic and isometric contractions.” In: *Sensors* 16.8 (2016), p. 1304.
- [51] Noémie Jaquier et al. “Combining electromyography and tactile myography to improve hand and wrist activity detection in prostheses.” In: *Technologies* 5.4 (2017), p. 64.
- [52] Arjan Gijsberts et al. “Stable myoelectric control of a hand prosthesis using non-linear incremental learning.” In: *Frontiers in neurorobotics* 8 (2014), p. 8.

- [53] Giacinto Luigi Cerone and Marco Gazzoni. “A wireless, minaturized multi-channel sEMG acquisition system for use in dynamic tasks.” In: *2017 IEEE Biomedical Circuits and Systems Conference (BioCAS)*. IEEE. 2017, pp. 1–4.
- [54] Monica Rojas-Martínez, Miguel A Mañanas, and Joan F Alonso. “High-density surface EMG maps from upper-arm and forearm muscles.” In: *Journal of neuroengineering and rehabilitation* 9.1 (2012), p. 85.
- [55] Erik Scheme and Kevin Englehart. “Electromyogram pattern recognition for control of powered upper-limb prostheses: state of the art and challenges for clinical use.” In: *Journal of Rehabilitation Research & Development* 48.6 (2011).
- [56] Anders Fougner et al. “Control of upper limb prostheses: Terminology and proportional myoelectric control—A review.” In: *IEEE Transactions on neural systems and rehabilitation engineering* 20.5 (2012), pp. 663–677.
- [57] Risto Koiva et al. “Shape conformable high spatial resolution tactile bracelet for detecting hand and wrist activity.” In: *2015 IEEE International Conference on Rehabilitation Robotics (ICORR)*. IEEE. 2015, pp. 157–162.
- [58] Markus Nowak, Thomas Eiband, and Claudio Castellini. “Multi-modal myocontrol: Testing combined force-and electromyography.” In: *2017 International Conference on Rehabilitation Robotics (ICORR)*. IEEE. 2017, pp. 1364–1368.
- [59] Paulette Campbell. *APL’s Modular Prosthetic Limb Reaches New Levels of Operability*. 2016. URL: <https://www.jhuapl.edu/PressRelease/160112> (visited on 09/10/2019).
- [60] Claudio Castellini. *VITA – Virtual Therapy Arm*. 2016. URL: <https://www.dlr.de/rm/desktopdefault.aspx/tabid-12023#gallery/29007> (visited on 09/10/2019).
- [61] Devin Coldewey. *SmartArm’s AI-powered prosthesis takes the prize at Microsoft’s Imagine Cup*. Website. Accessed: 2019-10-22. 2018. URL: <https://techcrunch.com/2018/07/25/smartarms-ai-powered-prosthesis-takes-the-prize-at-microsofts-imagine-cup/>.
- [62] Stephen Lake. *Ending Sales of Myo, Preparing for the Future*. Website. Accessed: 2019-10-22. 2018. URL: <https://medium.com/@srlake/ending-sales-of-myo-preparing-for-the-future-281af9bbcac2>.
- [63] Thalmic Labs Inc. *Myo Gesture Control Armband*. Website-Article. Accessed: 2019-11-26. 2018. URL: <https://web.archive.org/web/20180506091645/https://store.myo.com/>.
- [64] Cezar Morun and Stephen Lake. *Systems, articles, and methods for capacitive electromyography sensors*. US Patent App. 14/539,773. 2015.
- [65] Becky Stern. *Inside Myo*. 2016. URL: <https://learn.adafruit.com/myo-armband-teardown> (visited on 09/10/2019).
- [66] thalmiclabs. *myo-bluetooth*. <https://github.com/thalmiclabs/myo-bluetooth>. Accessed: 2019-10-22. 2015.

- [67] Stephen Lake and Matthew Bailey. *Systems, articles and methods for wearable electronic devices employing contact sensors*. US Patent App. 14/505,836. 2015.
- [68] Faeria. *Myo Armband Amazon.com Bracelet Gesture Wristband PNG*. Website. Accessed: 2019-10-22. 2018. URL: <https://imgbin.com/png/jx9X3pnA/myo-armband-amazon-com-bracelet-gesture-wristband-png>.
- [69] CTRL-labs. *CTRL-kit*. 2019. URL: <https://www.ctrl-labs.com/ctrl-kit/> (visited on 09/10/2019).
- [70] Patrick Kaifosh et al. *Adaptive system for deriving control signals from measurements of neuromuscular activity*. US Patent App. 15/659,487. 2018.
- [71] CTRL-labs. *CTRL-kit*. Website. Accessed: 2019-11-11. 2019. URL: <https://www.ctrl-labs.com/ctrl-kit/>.
- [72] Vikram Ravindra and Claudio Castellini. “A comparative analysis of three non-invasive human-machine interfaces for the disabled.” In: *Frontiers in neurorobotics* 8 (2014), p. 24.
- [73] Claudio Castellini et al. “Fine detection of grasp force and posture by amputees via surface electromyography.” In: *Journal of Physiology-Paris* 103.3-5 (2009), pp. 255–262.
- [74] Erina Cho et al. “Force myography to control robotic upper extremity prostheses: a feasibility study.” In: *Frontiers in bioengineering and biotechnology* 4 (2016), p. 18.
- [75] Agamemnon Krasoulis et al. “Improved prosthetic hand control with concurrent use of myoelectric and inertial measurements.” In: *Journal of neuroengineering and rehabilitation* 14.1 (2017), p. 71.
- [76] Zhen Gang Xiao and Carlo Menon. “A Review of Force Myography Research and Development.” In: *Sensors* 19.20 (2019), p. 4557.
- [77] Denton A. Cooley, Gregory Stewart, and Denton A. Cooley. *The Skeletal and Muscular Systems* -. Library Binding. New York: Chelsea House, 2004. ISBN: 978-0-791-07905-8.
- [78] Silvia Muceli, Ning Jiang, and Dario Farina. “Extracting signals robust to electrode number and shift for online simultaneous and proportional myoelectric control by factorization algorithms.” In: *IEEE Transactions on Neural Systems and Rehabilitation Engineering* 22.3 (2014), pp. 623–633.
- [79] Ning Jiang et al. “Is accurate mapping of EMG signals on kinematics needed for precise online myoelectric control?” In: *IEEE Transactions on Neural Systems and Rehabilitation Engineering* 22.3 (2014), pp. 549–558.
- [80] Agneta Gustus et al. “Human hand modelling: kinematics, dynamics, applications.” In: *Biological cybernetics* 106.11-12 (2012), pp. 741–755.

- [81] Kevin Englehart, Bernard Hudgins, et al. “A robust, real-time control scheme for multifunction myoelectric control.” In: *IEEE transactions on biomedical engineering* 50.7 (2003), pp. 848–854.
- [82] Todd R Farrell and Richard F Weir. “The optimal controller delay for myoelectric prostheses.” In: *IEEE Transactions on neural systems and rehabilitation engineering* 15.1 (2007), pp. 111–118.
- [83] Su Kyoung Kim et al. “Intrinsic interactive reinforcement learning—Using error-related potentials for real world human-robot interaction.” In: *Scientific reports* 7.1 (2017), p. 17562.
- [84] Dario Farina et al. “The extraction of neural information from the surface EMG for the control of upper-limb prostheses: emerging avenues and challenges.” In: *IEEE Transactions on Neural Systems and Rehabilitation Engineering* 22.4 (2014), pp. 797–809.
- [85] Daniele Esposito et al. “A Piezoresistive Sensor to Measure Muscle Contraction and Mechanomyography.” In: *Sensors* 18.8 (2018), p. 2553.
- [86] J Gordon Betts et al. “Anatomy and physiology.” In: (2014).
- [87] Daniel Wolpert. *The real reason for brains*. 2011. URL: https://www.ted.com/talks/daniel_wolpert_the_real_reason_for_brains (visited on 09/05/2019).
- [88] Fritz Buchthal, Christian Guld, and Poul Rosenfalck. “Innervation Zone and Propagation Velocity in Human Muscle. 1.” In: *Acta Physiologica Scandinavica* 35.2 (1955), pp. 174–190.
- [89] Dario Farina, Corrado Cescon, and Roberto Merletti. “Influence of anatomical, physical, and detection-system parameters on surface EMG.” In: *Biological cybernetics* 86.6 (2002), pp. 445–456.
- [90] B Bigland-Ritchie, EF Donovan, and CS Roussos. “Conduction velocity and EMG power spectrum changes in fatigue of sustained maximal efforts.” In: *Journal of applied physiology* 51.5 (1981), pp. 1300–1305.
- [91] OpenStax College. *Anatomy & physiology*. Houston, TX: OpenStax CNX, 2013. ISBN: 978-1-947172-04-3.
- [92] ERIC Kugelberg and Lars Edström. “Differential histochemical effects of muscle contractions on phosphorylase and glycogen in various types of fibres: relation to fatigue.” In: *Journal of neurology, neurosurgery, and psychiatry* 31.5 (1968), p. 415.
- [93] NA Rubinstein and AM Kelly. “The diversity of muscle fiber types and its origin during development.” In: *Myology* 1 (2004), pp. 87–108.

- [94] Eva Jansson, Bertil Sjödin, and Per Tesch. “Changes in muscle fibre type distribution in man after physical training: a sign of fibre type transformation?” In: *Acta Physiologica Scandinavica* 104.2 (1978), pp. 235–237.
- [95] Jacob M Wilson et al. “The effects of endurance, strength, and power training on muscle fiber type shifting.” In: *The Journal of Strength & Conditioning Research* 26.6 (2012), pp. 1724–1729.
- [96] Richard Wasicky et al. “Muscle fiber types of human extraocular muscles: a histochemical and immunohistochemical study.” In: *Investigative ophthalmology & visual science* 41.5 (2000), pp. 980–990.
- [97] V Reggie Edgerton, JL Smith, and DR Simpson. “Muscle fibre type populations of human leg muscles.” In: *The Histochemical Journal* 7.3 (1975), pp. 259–266.
- [98] Philip D Gollnick et al. “Human soleus muscle: a comparison of fiber composition and enzyme activities with other leg muscles.” In: *Pflügers Archiv* 348.3 (1974), pp. 247–255.
- [99] Cindy L Stanfield et al. *Principles of human physiology*. Benjamin Cummings, 2011.
- [100] Elwood Henneman, George Somjen, and David O Carpenter. “Functional significance of cell size in spinal motoneurons.” In: *Journal of neurophysiology* 28.3 (1965), pp. 560–580.
- [101] Stefano Schiaffino and Carlo Reggiani. “Fiber types in mammalian skeletal muscles.” In: *Physiological reviews* 91.4 (2011), pp. 1447–1531.
- [102] HS Milner-Brown, RB Stein, and R. Yemm. “The orderly recruitment of human motor units during voluntary isometric contractions.” In: *The Journal of physiology* 230.2 (1973), pp. 359–370.
- [103] Rune Hennig and Terje Lømo. “Firing patterns of motor units in normal rats.” In: *Nature* 314.6007 (1985), p. 164.
- [104] Terje Lømo. “Nerve–muscle interactions.” In: *Handbook of clinical neurophysiology*. Vol. 2. Elsevier, 2003, pp. 47–65.
- [105] Brent J Raiteri, Andrew G Cresswell, and Glen A Lichtwark. “Three-dimensional geometrical changes of the human tibialis anterior muscle and its central aponeurosis measured with three-dimensional ultrasound during isometric contractions.” In: *PeerJ* 4 (2016), e2260.
- [106] Hugh Esmor Huxley. “X-ray analysis and the problem of muscle.” In: *Proceedings of the Royal Society of London. Series B-Biological Sciences* 141.902 (1953), pp. 59–62.
- [107] GF Elliott, J Lowy, and CR Worthington. “An X-ray and light-diffraction study of the filament lattice of striated muscle in the living state and in rigor.” In: *Journal of molecular biology* 6.4 (1963), 295–IN9.

- [108] James M Wakeling and Avleen Randhawa. “Transverse strains in muscle fascicles during voluntary contraction: a 2D frequency decomposition of B-mode ultrasound images.” In: *Journal of Biomedical Imaging* 2014 (2014), p. 4.
- [109] Johann S. Schwegler. *Der Mensch - Anatomie und Physiologie ; Schritt für Schritt Zusammenhänge verstehen*. 4. Aufl. Stuttgart: Thieme, 2006. ISBN: 978-3-131-00154-2.
- [110] Daniel T Barry and Neil M Cole. “Muscle sounds are emitted at the resonant frequencies of skeletal muscle.” In: *IEEE transactions on biomedical engineering* 37.5 (1990), pp. 525–531.
- [111] Mihai T Tarata. “Mechanomyography versus electromyography, in monitoring the muscular fatigue.” In: *Biomedical engineering online* 2.1 (2003), p. 3.
- [112] Frederic H Martini, Judi L Nath, and Edwin F Bartholomew. “Fundamentals of Anatomy and Physiology. 2001.” In: *Pentice Hall: New Jersey* (2001), pp. 538–557.
- [113] PW Hodges et al. “Measurement of muscle contraction with ultrasound imaging.” In: *Muscle & Nerve: Official Journal of the American Association of Electrodiagnostic Medicine* 27.6 (2003), pp. 682–692.
- [114] Marco V Narici et al. “In vivo human gastrocnemius architecture with changing joint angle at rest and during graded isometric contraction.” In: *The Journal of physiology* 496.1 (1996), pp. 287–297.
- [115] E Azizi and Amber R Deslauriers. “Regional heterogeneity in muscle fiber strain: the role of fiber architecture.” In: *Frontiers in physiology* 5 (2014), p. 303.
- [116] Peter R Cavanagh and Paavo V Komi. “Electromechanical delay in human skeletal muscle under concentric and eccentric contractions.” In: *European journal of applied physiology and occupational physiology* 42.3 (1979), pp. 159–163.
- [117] Robert F. Schmidt, Florian Lang, and Gerhard Thews. *Physiologie des Menschen - mit Pathophysiologie*. 29. Aufl. Berlin Heidelberg New York: Springer-Verlag, 2005. ISBN: 978-3-540-26416-3.
- [118] Arthur F Reimann et al. “The palmaris longus muscle and tendon. A study of 1600 extremities.” In: *The Anatomical Record* 89.4 (1944), pp. 495–505.
- [119] JAMES L Fleckenstein et al. “Finger-specific flexor recruitment in humans: depiction by exercise-enhanced MRI.” In: *Journal of Applied Physiology* 72.5 (1992), pp. 1974–1977.
- [120] Henry Gray and WH Lewis. “Anatomy of the Human Body. Lea & Febiger, Philadelphia.” In: *From: Bartleby. com* (1918).
- [121] Holger Stefan Urbanek. “iEMG: Imaging Electromyography.” Dissertation. München: Technische Universität München, 2016.

- [122] IMAIOS SAS. *Visible Human Project: anatomy atlas of male cadaver*. 2019. URL: <https://www.imaios.com/en/e-Anatomy/Thorax-Abdomen-Pelvis/Visible-Human-Project> (visited on 09/17/2019).
- [123] Karen Burke Cynthia; Patrias. “Visible Human Project.” In: *Current bibliographies in medicine* (2007).
- [124] Basicmedical Key. *Anterior Forearm*. Website. Accessed: 2019-11-17. 2016. URL: <https://basicmedicalkey.com/anterior-forearm/>.
- [125] Merriam-Webster Online. “*Myogram*”. Website. Accessed: 2019-10-22. 2019. URL: <https://www.merriam-webster.com/medical/myograms>.
- [126] MEDIACC GmbH. § 23b of the Medical Devices Act (MPG) and Medical Device Regulation (MDR). Website. Accessed: 2019-11-18. 2019. URL: <https://mediacc.de/en/mediacc/news/ss-23b-of-the-medical-devices-act-mpg-and-mdr/>.
- [127] Europäisches Komitee für elektrotechnische Normung. “EN ISO 13485: 2016 Medical devices–Quality managementsystems–Requirements for regulatory purposes. 2016.” In: *Deutsche Fassung: Deutsches Institut für Normung e. V.: DIN EN ISO 13485* (), pp. 2016–08.
- [128] Yinfeng Fang et al. “Multi-modal sensing techniques for interfacing hand prostheses: a review.” In: *IEEE Sensors Journal* 15.11 (2015), pp. 6065–6076.
- [129] RH Edwards et al. “Fatigue of long duration in human skeletal muscle after exercise.” In: *The Journal of physiology* 272.3 (1977), pp. 769–778.
- [130] Matthew Cobb. “Exorcizing the animal spirits: Jan Swammerdam on nerve function.” In: *Nature Reviews Neuroscience* 3.5 (2002), p. 395.
- [131] Luigi Galvani. “D viribus electricitatis in motu musculari: Commentarius.” In: *Bologna: Tip. Istituto delle Scienze, 1791; 58 p.: 4 tavv. ft; in 4.; DCC. f. 70* (1791).
- [132] Edgar D Adrian and Detlev W Bronk. “The discharge of impulses in motor nerve fibres: Part II. The frequency of discharge in reflex and voluntary contractions.” In: *The Journal of physiology* 67.2 (1929), pp. 9–151.
- [133] Bruno Dubuc. *The Brain from Top to Bottom*. Website. Accessed: 2019-11-11. 2002. URL: https://thebrain.mcgill.ca/flash/i/i_06/i_06_m/i_06_m_mou/i_06_m_mou.html.
- [134] Clarissa Crone and Christian Krarup. “Neurophysiological approach to disorders of peripheral nerve.” In: *Handbook of clinical neurology*. Vol. 115. Elsevier, 2013, pp. 81–114.
- [135] R Merletti, Alberto Rainoldi, and D Farina. “Surface electromyography for noninvasive characterization of muscle.” In: *Exercise and sport sciences reviews* 29.1 (2001), pp. 20–25.

- [136] Fei Lu et al. “Review of stratum corneum impedance measurement in non-invasive penetration application.” In: *Biosensors* 8.2 (2018), p. 31.
- [137] Roberto Merletti et al. “Technology and instrumentation for detection and conditioning of the surface electromyographic signal: state of the art.” In: *Clinical biomechanics* 24.2 (2009), pp. 122–134.
- [138] JH Blok, DF Stegeman, and A Van Oosterom. “Three-layer volume conductor model and software package for applications in surface electromyography.” In: *Annals of biomedical engineering* 30.4 (2002), pp. 566–577.
- [139] Machiel J Zwarts and Dick F Stegeman. “Multichannel surface EMG: basic aspects and clinical utility.” In: *Muscle & Nerve: Official Journal of the American Association of Electrodiagnostic Medicine* 28.1 (2003), pp. 1–17.
- [140] Chen Chen et al. “Hand gesture recognition based on motor unit spike trains decoded from high-density electromyography.” In: *Biomedical Signal Processing and Control* 55 (2020), p. 101637.
- [141] N Amrutha and VH Arul. “A Review on Noises in EMG Signal and its Removal.” In: *Int. J. Sci. Res. Publ* 7 (2017), pp. 23–27.
- [142] Peter Konrad. “EMG-Fibel.” In: *Eine praxisorientierte Einführung in die kinesiologische Elektromyographie* (2011).
- [143] Carlo J De Luca et al. “Filtering the surface EMG signal: Movement artifact and baseline noise contamination.” In: *Journal of biomechanics* 43.8 (2010), pp. 1573–1579.
- [144] Dario Farina, Roberto Merletti, and Roger M Enoka. “The extraction of neural strategies from the surface EMG.” In: *Journal of applied physiology* 96.4 (2004), pp. 1486–1495.
- [145] Lara A Green, Anita Christie, and David A Gabriel. “Spike shape analysis for the surface and needle electromyographic interference pattern.” In: *Biomedical Signal Processing and Control* 36 (2017), pp. 1–10.
- [146] Stefano Pizzolato et al. “Comparison of six electromyography acquisition setups on hand movement classification tasks.” In: *PloS one* 12.10 (2017), e0186132.
- [147] Mamun Bin Ibne Reaz, MS Hussain, and Faisal Mohd-Yasin. “Techniques of EMG signal analysis: detection, processing, classification and applications.” In: *Biological procedures online* 8.1 (2006), p. 11.
- [148] John Edison Muñoz et al. “PhysioLab-a multivariate physiological computing toolbox for ECG, EMG and EDA signals: a case of study of cardiorespiratory fitness assessment in the elderly population.” In: *Multimedia Tools and Applications* 77.9 (2018), pp. 11521–11546.

- [149] Carlo J De Luca et al. “Inter-electrode spacing of surface EMG sensors: reduction of crosstalk contamination during voluntary contractions.” In: *Journal of biomechanics* 45.3 (2012), pp. 555–561.
- [150] Roberto Merletti et al. “Advances in surface EMG: recent progress in detection and processing techniques.” In: *Critical ReviewsTM in Biomedical Engineering* 38.4 (2010).
- [151] John V Basmajian and Carlo J De Luca. *Muscles alive: their functions revealed by electromyography*. Vol. 5. Williams & Wilkins Baltimore, 1985.
- [152] K Roeleveld et al. “The motor unit potential distribution over the skin surface and its use in estimating the motor unit location.” In: *Acta physiologica scandinavica* 161.4 (1997), pp. 465–472.
- [153] S Allouch et al. “Muscle force estimation using data fusion from high-density SEMG grid.” In: *2013 2nd International Conference on Advances in Biomedical Engineering*. IEEE. 2013, pp. 195–198.
- [154] Mariam Al Harrach et al. “Sensitivity evaluation of HOS parameters by data fusion from HD-sEMG grid.” In: *2013 2nd International Conference on Advances in Biomedical Engineering*. IEEE. 2013, pp. 97–100.
- [155] Manfredo Atzori et al. “Building the Ninapro database: A resource for the biorobotics community.” In: *2012 4th IEEE RAS & EMBS International Conference on Biomedical Robotics and Biomechatronics (BioRob)*. IEEE. 2012, pp. 1258–1265.
- [156] Lars Lindstrom. “Muscular fatigue and action potential conduction velocity changes studied with frequency analysis of EMG signals.” In: *Electromyography* 10.4 (1970), pp. 341–356.
- [157] Hatice Tankisi et al. “Standards of instrumentation of EMG.” In: *Clinical Neurophysiology* (2019).
- [158] Gaetano Gargiulo et al. “Wearable dry sensors with bluetooth connection for use in remote patient monitoring systems.” In: *Stud. Health Technol. Inform* 161 (2010), pp. 57–65.
- [159] Alessandro Del Vecchio and Dario Farina. “Interfacing the neural output of the spinal cord: robust and reliable longitudinal identification of motor neurons in humans.” In: *Journal of neural engineering* (2019).
- [160] LF Lucaccini, PK Kaiser, and J Lyman. “The French electric hand: Some observations and conclusions.” In: *Bull. Prosthet. Res* 10.6 (1966), pp. 31–51.
- [161] Sam L Phillips and William Craelius. “Residual kinetic imaging: a versatile interface for prosthetic control.” In: *Robotica* 23.3 (2005), pp. 277–282.

- [162] Paul Lukowicz et al. “Detecting and interpreting muscle activity with wearable force sensors.” In: *International Conference on Pervasive Computing*. Springer. 2006, pp. 101–116.
- [163] Michael Wininger, Nam-Hun Kim, and William Craelius. “Pressure signature of forearm as predictor of grip force.” In: *Journal of Rehabilitation Research & Development* 45.6 (2008).
- [164] JS Leedham and JJ Dowling. “Force-length, torque-angle and EMG-joint angle relationships of the human in vivo biceps brachii.” In: *European journal of applied physiology and occupational physiology* 70.5 (1995), pp. 421–426.
- [165] Emer P Doheny et al. “Effect of elbow joint angle on force–EMG relationships in human elbow flexor and extensor muscles.” In: *Journal of Electromyography and Kinesiology* 18.5 (2008), pp. 760–770.
- [166] Mahdi Rasouli et al. “Stable force-myographic control of a prosthetic hand using incremental learning.” In: *2015 37th Annual International Conference of the IEEE Engineering in Medicine and Biology Society (EMBC)*. IEEE. 2015, pp. 4828–4831.
- [167] Ashkan Radmand, Erik Scheme, and Kevin Englehart. “High-density force myography: A possible alternative for upper-limb prosthetic control.” In: *Journal of Rehabilitation Research & Development* 53.4 (2016).
- [168] Zhen Gang Xiao and Carlo Menon. “An Investigation on the Sampling Frequency of the Upper-Limb Force Myographic Signals.” In: *Sensors* 19.11 (2019), p. 2432.
- [169] Stefano Stassi et al. “Flexible tactile sensing based on piezoresistive composites: A review.” In: *Sensors* 14.3 (2014), pp. 5296–5332.
- [170] Mona Lisa Delva and Carlo Menon. “FSR based Force Myography (FMG) Stability Throughout Non-Stationary Upper Extremity Tasks.” In: *Proceedings of the Future Technologies Conference, Vancouver, BC, Canada*. 2017, pp. 29–30.
- [171] Claudio Castellini and Vikram Ravindra. “A wearable low-cost device based upon force-sensing resistors to detect single-finger forces.” In: *5th IEEE RAS/EMBS International Conference on Biomedical Robotics and Biomechatronics*. IEEE. 2014, pp. 199–203.
- [172] Karsten Weiß and Heinz Worn. “The working principle of resistive tactile sensor cells.” In: *IEEE International Conference Mechatronics and Automation, 2005*. Vol. 1. IEEE. 2005, pp. 471–476.
- [173] Carsten Schurmann, Robert Haschke, Helge Ritter, et al. “A modular high-speed tactile sensor for human manipulation research.” In: *2011 IEEE World Haptics Conference*. IEEE. 2011, pp. 339–344.

- [174] Wataru Fukui et al. “Hi-Speed Tactile Sensing for Array-type Tactile Sensor and Object Manipulation based on Tactile Information.” In: *Transactions of the Institute of Systems, Control and Information Engineers* 25.5 (2012), pp. 117–125.
- [175] Luke E Osborn et al. “Prosthesis with neuromorphic multilayered e-dermis perceives touch and pain.” In: *Science Robotics* 3.19 (2018), eaat3818.
- [176] Risto Kõiva et al. “Towards high-density barometer-based tactile sensor arrays.” In: *Workshop on New Advances in Tactile Sensation, Perception, and Learning in Robotics: Emerging Materials and Technologies for Manipulation (RoboTac 2019)*. 2019.
- [177] Don A Yungher et al. “Surface muscle pressure as a measure of active and passive behavior of muscles during gait.” In: *Medical engineering & physics* 33.4 (2011), pp. 464–471.
- [178] Hanna Yousef, Mehdi Boukallel, and Kaspar Althoefer. “Tactile sensing for dexterous in-hand manipulation in robotics—A review.” In: *Sensors and Actuators A: physical* 167.2 (2011), pp. 171–187.
- [179] F.M. Grimaldi. *Physico-mathesis de lumine, coloribus et iride aliisque annexis: libri duo*. Bernia, 1665. URL: <https://books.google.de/books?id=X3RvHQAACAAJ>.
- [180] William Hyde Wollaston. “I. The Croonian Lecture.” In: *Philosophical Transactions of the Royal Society of London* 100 (1810), pp. 1–15.
- [181] G Gordon and AHS Holbourn. “The sounds from single motor units in a contracting muscle.” In: *The Journal of physiology* 107.4 (1948), pp. 456–464.
- [182] Claudio Orizio. “Muscle sound: bases for the.” In: *Crit Rev Biomed Eng* 21.3 (1993), pp. 201–243.
- [183] Daniel T Barry, Steven R Geiringer, and Richard D Ball. “Acoustic myography: a noninvasive monitor of motor unit fatigue.” In: *Muscle & Nerve: Official Journal of the American Association of Electrodiagnostic Medicine* 8.3 (1985), pp. 189–194.
- [184] Thomas M Hemmerling et al. “Phonomyography and mechanomyography can be used interchangeably to measure neuromuscular block at the adductor pollicis muscle.” In: *Anesthesia & Analgesia* 98.2 (2004), pp. 377–381.
- [185] Y-T Zhang et al. “A comparative study of simultaneous vibromyography and electromyography with active human quadriceps.” In: *IEEE Transactions on Biomedical Engineering* 39.10 (1992), pp. 1045–1052.
- [186] Charles F Bolton et al. “Recording sound from human skeletal muscle: technical and physiological aspects.” In: *Muscle & Nerve: Official Journal of the American Association of Electrodiagnostic Medicine* 12.2 (1989), pp. 126–134.

- [187] Daniel T Barry, Timothy Hill, and Dukjin Im. “Muscle fatigue measured with evoked muscle vibrations.” In: *Muscle & Nerve: Official Journal of the American Association of Electrodiagnostic Medicine* 15.3 (1992), pp. 303–309.
- [188] Gerald Oster and Joshua S Jaffe. “Low frequency sounds from sustained contraction of human skeletal muscle.” In: *Biophysical journal* 30.1 (1980), pp. 119–127.
- [189] Mohamed Sarillee et al. “Non-invasive techniques to assess muscle fatigue using biosensors: A review.” In: *2014 IEEE 5th Control and System Graduate Research Colloquium*. IEEE. 2014, pp. 187–192.
- [190] Claudio Orizio et al. “Surface mechanomyogram reflects muscle fibres twitches summation.” In: *Journal of biomechanics* 29.4 (1996), pp. 475–481.
- [191] Travis W Beck et al. “Mechanomyographic amplitude and frequency responses during dynamic muscle actions: a comprehensive review.” In: *Biomedical engineering online* 4.1 (2005), p. 67.
- [192] Corrado Cescon, Pascal Madeleine, and Dario Farina. “Longitudinal and transverse propagation of surface mechanomyographic waves generated by single motor unit activity.” In: *Medical & biological engineering & computing* 46.9 (2008), p. 871.
- [193] John V Frangioni et al. “The mechanism of low-frequency sound production in muscle.” In: *Biophysical journal* 51.5 (1987), pp. 775–783.
- [194] Daqing Wang et al. “Estimation of Knee Extension Force Using Mechanomyography Signals Detected Through Clothing.” In: *International Conference on Intelligent Robotics and Applications*. Springer. 2019, pp. 3–14.
- [195] Travis W Beck et al. “Does the frequency content of the surface mechanomyographic signal reflect motor unit firing rates? A brief review.” In: *Journal of electromyography and kinesiology* 17.1 (2007), pp. 1–13.
- [196] Salvatore Fara et al. “Robust, ultra low-cost mmg system with brain-machine-interface applications.” In: *2013 6th International IEEE/EMBS Conference on Neural Engineering (NER)*. IEEE. 2013, pp. 723–726.
- [197] John Paul V Anders et al. “Inter-and Intra-Individual Differences in EMG and MMG during Maximal, Bilateral, Dynamic Leg Extensions.” In: *Sports* 7.7 (2019), p. 175.
- [198] Edyta Bichler. “Mechanomyograms recorded during evoked contractions of single motor units in the rat medial gastrocnemius muscle.” In: *European journal of applied physiology* 83.4-5 (2000), pp. 310–319.
- [199] Jared W Coburn et al. “Mechanomyographic time and frequency domain responses of the vastus medialis muscle during submaximal to maximal isometric and isokinetic muscle actions.” In: *Electromyography and clinical neurophysiology* 44.4 (2004), pp. 247–255.

- [200] Claudio Orizio et al. "Muscle sound and electromyogram spectrum analysis during exhausting contractions in man." In: *European journal of applied physiology and occupational physiology* 65.1 (1992), pp. 1–7.
- [201] Morufu Olusola Ibitoye et al. "Mechanomyography and muscle function assessment: A review of current state and prospects." In: *Clinical Biomechanics* 29.6 (2014), pp. 691–704.
- [202] M Tarata, A Spaepen, and R Puers. "The accelerometer MMG measurement approach, in monitoring the muscular fatigue." In: *Measurement Science Review* 1.1 (2001), pp. 47–50.
- [203] Kazuyuki Mito et al. "Effect of skin temperature on RMS amplitude of electromyogram and mechanomyogram during voluntary isometric contraction." In: *Electromyography and clinical neurophysiology* 47.3 (2007), pp. 153–160.
- [204] Tae-Kwang Kim et al. "Influence of force tremor on mechanomyographic signals recorded with an accelerometer and a condenser microphone during measurement of agonist and antagonist muscles in voluntary submaximal isometric contractions." In: *Journal of physiological anthropology* 27.1 (2008), pp. 33–42.
- [205] JH Allum, V Dietz, and HJ Freund. "Neuronal mechanisms underlying physiological tremor." In: *Journal of Neurophysiology* 41.3 (1978), pp. 557–571.
- [206] TG Smith and MJ Stokes. "Technical aspects of acoustic myography (AMG) of human skeletal muscle: contact pressure and force/AMG relationships." In: *Journal of neuroscience methods* 47.1-2 (1993), pp. 85–92.
- [207] M Watakabe et al. "Technical aspects of mechnomyography recording with piezoelectric contact sensor." In: *Medical and biological engineering and computing* 36.5 (1998), p. 557.
- [208] Anna Jaskólska et al. "A comparison between mechanomyographic condenser microphone and accelerometer measurements during submaximal isometric, concentric and eccentric contractions." In: *Journal of Electromyography and Kinesiology* 17.3 (2007), pp. 336–347.
- [209] Travis W Beck et al. "Comparison of a piezoelectric contact sensor and an accelerometer for examining mechanomyographic amplitude and mean power frequency versus torque relationships during isokinetic and isometric muscle actions of the biceps brachii." In: *Journal of Electromyography and Kinesiology* 16.4 (2006), pp. 324–335.
- [210] M Watakabe et al. "Mechanical behaviour of condenser microphone in mechanomyography." In: *Medical and biological engineering and computing* 39.2 (2001), pp. 195–201.

- [211] Tae-Kwang Kim et al. “Comparison of an accelerometer and a condenser microphone for mechanomyographic signals during measurement of agonist and antagonist muscles in sustained isometric muscle contractions.” In: *Journal of physiological anthropology* 27.3 (2008), pp. 121–131.
- [212] AO Posatskiy and Tom Chau. “The effects of motion artifact on mechanomyography: A comparative study of microphones and accelerometers.” In: *Journal of Electromyography and Kinesiology* 22.2 (2012), pp. 320–324.
- [213] Claudio Orizio et al. “Force and surface mechanomyogram relationship in cat gastrocnemius.” In: *Journal of electromyography and kinesiology* 9.2 (1999), pp. 131–140.
- [214] MyoDynamik ApS. *CURO.systems*. Website-Article. Accessed: 2019-11-27. 2019. URL: <http://www.curo.systems/>.
- [215] Eddy Krueger et al. “Advances and perspectives of mechanomyography.” In: *Revista Brasileira de Engenharia Biomédica* 30.4 (2014), pp. 384–401.
- [216] Jorge Silva and Tom Chau. “A mathematical model for source separation of MMG signals recorded with a coupled microphone-accelerometer sensor pair.” In: *IEEE transactions on biomedical engineering* 52.9 (2005), pp. 1493–1501.
- [217] B Gregori, E Galie, and N Accornero. “Surface electromyography and mechanomyography recording: a new differential composite probe.” In: *Medical and Biological Engineering and Computing* 41.6 (2003), pp. 665–669.
- [218] Jorge Silva, Winfried Heim, and Tom Chau. “MMG-based classification of muscle activity for prosthesis control.” In: *The 26th Annual International Conference of the IEEE Engineering in Medicine and Biology Society*. Vol. 1. IEEE. 2004, pp. 968–971.
- [219] Hong-Bo Xie, Yong-Ping Zheng, and Jing-Yi Guo. “Classification of the mechanomyogram signal using a wavelet packet transform and singular value decomposition for multifunction prosthesis control.” In: *Physiological measurement* 30.5 (2009), p. 441.
- [220] Haifeng Wu et al. “Real-time continuous recognition of knee motion using multi-channel mechanomyography signals detected on clothes.” In: *Journal of Electromyography and Kinesiology* 38 (2018), pp. 94–102.
- [221] Emiliano Cè et al. “Electromechanical delay components during relaxation after voluntary contraction: reliability and effects of fatigue.” In: *Muscle & nerve* 51.6 (2015), pp. 907–915.
- [222] Cabral LPA et al. “Time lag between the onset of electrical stimulation and the muscular response.” In: *XXIV Congress of the International Society of Biomechanics and XV Brazilian Congress of Biomechanics* (2013).

- [223] Weichao Guo et al. “Mechanomyography assisted myoelectric sensing for upper-extremity prostheses: A hybrid approach.” In: *IEEE Sensors Journal* 17.10 (2017), pp. 3100–3108.
- [224] Seward B Rutkove, Ronald Aaron, and Carl A Shiffman. “Localized bioimpedance analysis in the evaluation of neuromuscular disease.” In: *Muscle & nerve* 25.3 (2002), pp. 390–397.
- [225] Yang Zhang and Chris Harrison. “Tomo: Wearable, low-cost electrical impedance tomography for hand gesture recognition.” In: *Proceedings of the 28th Annual ACM Symposium on User Interface Software & Technology*. ACM. 2015, pp. 167–173.
- [226] Yang Zhang, Robert Xiao, and Chris Harrison. “Advancing hand gesture recognition with high resolution electrical impedance tomography.” In: *Proceedings of the 29th Annual Symposium on User Interface Software and Technology*. ACM. 2016, pp. 843–850.
- [227] Christian Gibas et al. “Investigation of necessary conditions for imaging cell analysis using EIT.” In: *Medical Imaging 2019: Biomedical Applications in Molecular, Structural, and Functional Imaging*. Vol. 10953. International Society for Optics and Photonics. 2019, 109532B.
- [228] Yu Wu et al. “Towards a high accuracy wearable hand gesture recognition system using EIT.” In: *2018 IEEE International Symposium on Circuits and Systems (ISCAS)*. IEEE. 2018, pp. 1–4.
- [229] Olavo L Silva et al. “A proposal to monitor muscle contraction through the change of electrical impedance inside a muscle.” In: *5th IEEE RAS/EMBS International Conference on Biomedical Robotics and Biomechatronics*. IEEE. 2014, pp. 763–767.
- [230] Alessandro Scano et al. “NIRS-EMG for Clinical Applications: A Systematic Review.” In: *Applied Sciences* 9.15 (2019), p. 2952.
- [231] DT Delpy and M Cope. “Quantification in tissue near-infrared spectroscopy.” In: *Philosophical Transactions of the Royal Society of London. Series B: Biological Sciences* 352.1354 (1997), pp. 649–659.
- [232] Stefan Herrmann and Klaus Buchenrieder. “Fusion of myoelectric and near-infrared signals for prostheses control.” In: *Proceedings of the 4th International Convention on Rehabilitation Engineering & Assistive Technology*. Singapore Therapeutic, Assistive & Rehabilitative Technologies (START) Centre. 2010, p. 54.
- [233] Luca Pollonini et al. “Integrated device for the measurement of systemic and local oxygen transport during physical exercise.” In: *2012 Annual International Conference of the IEEE Engineering in Medicine and Biology Society*. IEEE. 2012, pp. 3760–3763.
- [234] Yong-Ping Zheng et al. “Sonomyography: Monitoring morphological changes of forearm muscles in actions with the feasibility for the control of powered prosthesis.” In: *Medical engineering & physics* 28.5 (2006), pp. 405–415.

- [235] Claudio Castellini. “State of the art and perspectives of ultrasound imaging as a human-machine interface.” In: *Neuro-Robotics*. Springer, 2014, pp. 37–58.
- [236] Henricus L Journée and AndréB De Jonge. “Ultrasound myography: application in nerve conduction velocity assessment and muscle cooling.” In: *Ultrasound in medicine & biology* 19.7 (1993), pp. 561–566.
- [237] Jing-Yi Guo et al. “A comparative evaluation of sonomyography, electromyography, force, and wrist angle in a discrete tracking task.” In: *Ultrasound in medicine & biology* 37.6 (2011), pp. 884–891.
- [238] A Moncada-Torres et al. “Activity classification based on inertial and barometric pressure sensors at different anatomical locations.” In: *Physiological measurement* 35.7 (2014), p. 1245.
- [239] Rana Sadeghi Chegani and Carlo Menon. “Regressing grasping using force myography: an exploratory study.” In: *Biomedical engineering online* 17.1 (2018), p. 159.
- [240] OpenStax College. *College Physics for AP[®] Courses*. Houston, TX: OpenStax CNX, 2015. ISBN: 978-1-938168-93-3.
- [241] Jong-Shin Huang and LJ Gibson. “Creep of polymer foams.” In: *Journal of materials science* 26.3 (1991), pp. 637–647.
- [242] Nitish V Thakor. *Johns Hopkins School of Medicine, Biopotentials and Electrophysiology Measurement, The Measurement, Instrumentation and Sensors handbook, Editor John G, Webster*. 2000.
- [243] Delsys Incorporated. *Tiber - New generation wireless 64-channel HDsEMG biofeedback array system designed for mobility*. Website. Accessed: 2019-11-24. 2019. URL: <https://www.delsys.com/tiber/>.
- [244] Otto Bock Australia Pty. Ltd. *13E200 MyoBock electrode*. Website. Accessed: 2019-11-24. 2019. URL: <https://professionals.ottobock.com.au/Products/Prosthetics/Prosthetics-Upper-Limb/Adult-Terminal-Devices/13E200-MyoBock-electrode/p/13E200>.
- [245] Luke Dormehl. *The creator of Internet Explorer wants to read your mind with a bracelet*. Website-Article. Accessed: 2019-11-24. 2018. URL: <https://www.digitaltrends.com/cool-tech/ctrl-labs-mind-control-wearable/>.
- [246] Soundarapandian Karthik and Berarducci Mark. *Analog Front-End Design for ECG Systems Using Delta-Sigma ADCs*. Website/Datasheet. Accessed: 2019-11-22. 2010. URL: https://e2echina.ti.com/cfs-file/_key/telligent-evolution-components-attachments/00-58-01-00-00-22-60-03/Analog-Front_2D00_End-Design-for-ECG-Systems-Using-Delta_2D00_Sigma-ADCs.pdf.

- [247] MA Cavalcanti Garcia and TMM Vieira. “Surface electromyography: Why, when and how to use it.” In: *Revista andaluza de medicina del deporte* 4.1 (2011), pp. 17–28.
- [248] Sebastián Aced López. “Design and construction of an EMG multichannel acquisition system prototype.” In: *Politecnico di Torino* (2012).
- [249] Agarwal Vishal. *Does a capacitor by itself act as a high pass or low pass filter?* Website/Forum. Accessed: 2019-11-22. 2016. URL: <https://www.quora.com/Does-a-capacitor-by-itself-act-as-a-high-pass-or-low-pass-filter>.
- [250] Dario Farina and Corrado Cescon. “Concentric-ring electrode systems for noninvasive detection of single motor unit activity.” In: *IEEE transactions on biomedical engineering* 48.11 (2001), pp. 1326–1334.
- [251] Babak Afsharipour, S Soedirdjo, and Roberto Merletti. “Two-dimensional surface EMG: The effects of electrode size, interelectrode distance and image truncation.” In: *Biomedical Signal Processing and Control* 49 (2019), pp. 298–307.
- [252] Taian Martins Vieira et al. “Specificity of surface EMG recordings for gastrocnemius during upright standing.” In: *Scientific reports* 7.1 (2017), p. 13300.
- [253] Scott Day. “Important factors in surface EMG measurement.” In: *Bortec Biomedical Ltd publishers* (2002), pp. 1–17.
- [254] OpenStax College. *Chemistry 2e*. Houston, TX: OpenStax CNX, 2019. ISBN: 978-1-947172-62-3.
- [255] Gierad Laput, Robert Xiao, and Chris Harrison. “Viband: High-fidelity bio-acoustic sensing using commodity smartwatch accelerometers.” In: *Proceedings of the 29th Annual Symposium on User Interface Software and Technology*. ACM. 2016, pp. 321–333.
- [256] Riley Booth and Peter Goldsmith. “Detecting finger gestures with a wrist worn piezoelectric sensor array.” In: *2017 IEEE international conference on systems, man, and cybernetics (SMC)*. IEEE. 2017, pp. 3665–3670.
- [257] Eigenwald Holding ApS / Eigenwald. *MEDTECH: MyoDynamik ApS*. Website. Accessed: 2019-11-23. 2014. URL: <http://www.eigenwald.com/en/cases/medtech-myodynamik-aps.aspx>.
- [258] A Venkatanarayanan et al. “Review of Recent Developments in Sensing Materials.” In: (2014).
- [259] Corrado Cescon et al. “Effect of accelerometer location on mechanomyogram variables during voluntary, constant-force contractions in three human muscles.” In: *Medical and Biological Engineering and Computing* 42.1 (2004), pp. 121–127.
- [260] ANALOG DEVICES. *ADXL345*. Datasheet. Accessed: 2019-11-23. 2015. URL: <https://www.analog.com/media/en/technical-documentation/data-sheets/ADXL345.pdf>.

- [261] NXP Semiconductors. *FXOS8700CQ*. Datasheet. Accessed: 2019-11-23. 2016. URL: https://www.nxp.com/files-static/sensors/doc/data_sheet/FXOS8700CQ.pdf.
- [262] Ltd Hope Microelectronics co. *HP206C*. Datasheet. Accessed: 2019-11-12. 2013. URL: http://www.hoperf.de/upload/sensor/HP206C_Datasheet_v1.0.pdf.
- [263] Casey Kuhns. *AD8232 Heart Rate Monitor v10*. Website/Datasheet. Accessed: 2019-11-21. 2014. URL: https://cdn.sparkfun.com/datasheets/Sensors/Biometric/AD8232_Heart_Rate_Monitor_v10.pdf.
- [264] Angkoon Phinyomark et al. "The usefulness of mean and median frequencies in electromyography analysis." In: *Computational intelligence in electromyography analysis-A perspective on current applications and future challenges*. IntechOpen, 2012.
- [265] NXP Semiconductors. *LPC84x*. Datasheet. Accessed: 2019-11-27. 2019. URL: <https://www.nxp.com/docs/en/data-sheet/LPC84x.pdf>.
- [266] Kevin Townsend. *NXP Precision 9DoF Breakout*. Website. Accessed: 2019-11-16. 2017. URL: <https://learn.adafruit.com/nxp-precision-9dof-breakout/arduino-code>.